

University of Windsor

## Scholarship at UWindor

---

Electronic Theses and Dissertations

Theses, Dissertations, and Major Papers

---

2012

# Microstructure and Tensile Properties of Magnesium (AM60)/Aluminum Oxide Metal Matrix Composites with Varying Volume Fractions of Reinforcement

Xuezhi Zhang  
*University of Windsor*

Follow this and additional works at: <https://scholar.uwindsor.ca/etd>

---

### Recommended Citation

Zhang, Xuezhi, "Microstructure and Tensile Properties of Magnesium (AM60)/Aluminum Oxide Metal Matrix Composites with Varying Volume Fractions of Reinforcement" (2012). *Electronic Theses and Dissertations*. 5574.

<https://scholar.uwindsor.ca/etd/5574>

This online database contains the full-text of PhD dissertations and Masters' theses of University of Windsor students from 1954 forward. These documents are made available for personal study and research purposes only, in accordance with the Canadian Copyright Act and the Creative Commons license—CC BY-NC-ND (Attribution, Non-Commercial, No Derivative Works). Under this license, works must always be attributed to the copyright holder (original author), cannot be used for any commercial purposes, and may not be altered. Any other use would require the permission of the copyright holder. Students may inquire about withdrawing their dissertation and/or thesis from this database. For additional inquiries, please contact the repository administrator via email ([scholarship@uwindsor.ca](mailto:scholarship@uwindsor.ca)) or by telephone at 519-253-3000ext. 3208.

**Microstructure and Tensile Properties of Mg  
(AM60)/Al<sub>2</sub>O<sub>3</sub> Metal Matrix Composites with Varying  
Volume Fractions of Reinforcement**

By

Xuezhi Zhang

A Thesis  
Submitted to the  
Faculty of Graduate Students  
through Engineering Materials  
in Partial Fulfillment of the Requirements  
for the Degree of Master  
of Applied Science  
at the University of Windsor

Windsor, Ontario, Canada

2012

© 2012 Xuezhi Zhang

**Microstructure and Tensile Properties of Mg (AM60)/Al<sub>2</sub>O<sub>3</sub> Metal Matrix Composite with Varying Volume Fractions of Reinforcement**

By

Xuezhi Zhang

APPROVED BY:

---

Dr. Tirupati Bolisetti, Outside Program Reader  
Department of Civil and Environmental Engineering

---

Dr. Xueyuan Nie, Program Reader  
Department of Mechanical, Automotive and Materials Engineering

---

Dr. Henry Hu, Advisor  
Department of Mechanical, Automotive and Materials Engineering

---

Dr. Randy Bowers, Chair of Defense  
Department of Mechanical, Automotive and Materials Engineering

Sept. 10, 2012

## **DECLARATION OF ORIGINALITY**

I hereby certify that I am the sole author of this thesis and that no part of this thesis has been published or submitted for publication.

I certify that, to the best of my knowledge, my thesis does not infringe upon anyone's copyright nor violate any proprietary rights and that any ideas, techniques, quotations, or any other material from the work of other people included in my thesis, published or otherwise, are fully acknowledged in accordance with the standard referencing practices. Furthermore, to the extent that I have included copyrighted material that surpasses the bounds of fair dealing within the meaning of the Canada Copyright Act, I certify that I have obtained a written permission from the copyright owner(s) to include such material(s) in my thesis and have included copies of such copyright clearances to my appendix.

I declare that this is a true copy of my thesis, including any final revisions, as approved by my thesis committee and the Graduate Studies office, and that this thesis has not been submitted for a higher degree to any other University or Institution.

## **ABSTRACT**

Magnesium alloy AM60 matrix-based composite reinforced with 7%, 9%, 11%, 22% and 35% of  $\text{Al}_2\text{O}_3$  fibers were squeeze casted. The microstructure and mechanical properties were investigated in comparison with the matrix alloy AM60. The results of tensile testing indicated that the addition of  $\text{Al}_2\text{O}_3$  fibres to magnesium alloy AM60 led to a significant improvement in mechanical properties. As the fiber volume fraction increased, the strengths and moduli of the composites were enhanced considerably. However, the notably increase in strengths was at sacrifice in elongation. Microstructural analyses via Scanning Electron Microscopy (SEM) revealed that the grain size decreases with increasing volume fraction of reinforcement. The restriction of grain growth by the limited inter-fiber spacing could be the primary mechanism for a reduction in the grain size of the matrix alloy. The corrosion test showed an increasing in corrosion rates as fibers were added to the matrix alloy AM60.

## **DEDICATION**

I dedicate this thesis to my parents, my sister and my girlfriend. Their love and support, their encouragement and patience during my study in University of Windsor has given me the strength, and enabled me through those difficult times during the research period and finally complete this work.

Xuezhi Zhang

## **ACKNOWLEDGEMENTS**

First of all, I want to express my sincere gratitude to my supervisor Dr. Henry Hu for giving me the great opportunity to join the casting group in University of Windsor, for his excellent guidance, kindly suggesting, and great supervision for this research work.

Many thanks go to the program reader, Dr. Xueyuan Nie, and the outside program reader, Dr. Tirupati Bolisetti for taking the time for my proposal and research presentation, for their encouragement and great suggestion giving to this project.

Great thanks to the department technicians including Mr. Andy Jenner, Mr. David Tremblay for their help of cutting samples for the tensile test, and Mr. Gang Li's help of SEM training and sample preparation for the microstructure analysis, and also to classmates in the casting group including Zhizhong Sun, Meng Wang, Yanda Zou and Anindya Banerji, for their great help on the experiment and valuable discussions for this research work.

Many thanks to Dr. Xiaoping Niu (Chief Engineering Metallurgist at Cosma Promatek Research Center), for his great help on performing tensile tests.

I want to extend my appreciation to all my friends who help me in many ways to carry through this thesis.

Finally, my sincerest thanks to my family, especially my parents for the encouragement, understanding and support they place in me.

# TABLE OF CONTENTS

<b>DECLARATION OF ORIGINALITY .....</b>	<b>iii</b>
<b>ABSTRACT.....</b>	<b>iv</b>
<b>DEDICATION.....</b>	<b>v</b>
<b>ACKNOWLEDGEMENTS .....</b>	<b>vi</b>
<b>LIST OF FIGURES .....</b>	<b>xi</b>
<b>LIST OF TABLES .....</b>	<b>xvi</b>
<b>CHAPTER 1:.....</b>	<b>1</b>
<b>INTRODUCTION.....</b>	<b>1</b>
<b>1.1 Objectives of this study .....</b>	<b>2</b>
<b>1.2 Thesis layout .....</b>	<b>3</b>
<b>CHAPTER 2:.....</b>	<b>4</b>
<b>LITERATURE REVIEW .....</b>	<b>4</b>
<b>2.1 Metal matrix composite .....</b>	<b>5</b>
<b>2.2 Matrix.....</b>	<b>6</b>
2.2.1 Purpose of the matrix.....	6
2.2.2 Function of the matrix .....	7
2.2.3 Types of matrix.....	7
<b>2.3 Reinforcement.....</b>	<b>9</b>
2.3.1 Characteristics of reinforcement.....	12



<b>2.4 Fabrication of Metal Matrix Composites.....</b>	<b>16</b>
2.4.1 Powder metallurgy.....	17
2.4.2 Squeeze casting.....	18
<b>2.5 Wettability.....</b>	<b>21</b>
2.5.1 Contact angle .....	21
2.5.2 Wetting behaviour .....	22
2.5.3 Improving wettability .....	24
<b>2.6 MMCs mechanical properties .....</b>	<b>24</b>
2.6.1 Tensile strength.....	25
2.6.2 Ductility .....	28
2.6.3 Hardness .....	29
2.6.4 Young's modulus.....	29
2.6.5 Thermal expansion .....	29
<b>2.7 The applications of MMCs .....</b>	<b>31</b>
<b>2.8 Corrosion behavior of magnesium alloy and its composites .....</b>	<b>32</b>
2.8.1 Corrosion of magnesium in aqueous solutions.....	33
2.8.2 Corrosion by atmosphere and solutions.....	34
2.8.3 Corrosion in Al <sub>2</sub> O <sub>3</sub> reinforced composites .....	34
<b>2.9 Summary .....</b>	<b>35</b>
<b>CHAPTER 3:.....</b>	<b>36</b>
<b>EXPERIMENTAL PROCEDURE.....</b>	<b>36</b>
<b>3.1 Materials .....</b>	<b>37</b>
3.1.1 Saffil alumina fiber.....	37

3.1.2 Magnesium alloy .....	37
<b>3.2 Preform fabrication.....</b>	<b>38</b>
<b>3.3 Fabrication of composites.....</b>	<b>39</b>
<b>3.4 Tensile testing .....</b>	<b>43</b>
<b>3.5 Microstructure analysis .....</b>	<b>44</b>
<b>3.6 Heat treatment.....</b>	<b>45</b>
<b>3.7 DSC analysis .....</b>	<b>46</b>
<b>3.8 Corrosion test.....</b>	<b>47</b>
<b>CHAPTER 4:.....</b>	<b>48</b>
<b>EXPERIMENTAL RESULTS.....</b>	<b>48</b>
<b>4.1 Squeeze casting .....</b>	<b>48</b>
4.1.1 Casting parameters determination .....	48
4.1.2 Appearance of the preform .....	49
4.1.3 Appearance of cast composites.....	50
<b>4.2 Microstructure analysis .....</b>	<b>53</b>
4.2.1 Magnesium alloy AM60.....	53
4.2.2 Magnesium matrix composites .....	55
4.2.3 Grain structure .....	58
4.2.4 Solidification of magnesium matrix composites .....	63
<b>4.3 Mechanical properties of the composites .....</b>	<b>65</b>
4.3.1 Hardness .....	65
4.3.2 Tensile properties .....	66
<b>4.4 Fracture behavior.....</b>	<b>72</b>

<b>4.5 Corrosion test.....</b>	<b>81</b>
<b>4.6 Summary .....</b>	<b>83</b>
<b>CHAPTER 5:.....</b>	<b>85</b>
<b>CONCLUSIONS AND FUTURE WORK.....</b>	<b>85</b>
<b>5.1 Conclusions .....</b>	<b>85</b>
<b>5.2 Future work .....</b>	<b>87</b>
<b>REFERENCES.....</b>	<b>88</b>
<b>APPENDICES.....</b>	<b>95</b>
<b>VITA AUCTORIS .....</b>	<b>121</b>

## LIST OF FIGURES

Figure 2.1 Flow chart of a powder metallurgy process for fabrication of Metal Matrix Composite [20].	17
Figure 2.2 Flow chart of squeeze casting process for fabrication of composite [23].	18
Figure 2.3 Production of cast composite materials by (a) direct squeeze casting method, and (b) indirect squeeze casting method [23].	19
Figure 2.4 Definition of contact angle, $\theta$ [28].	21
Figure 2.5 Variation of wetting angle with addition of alloying elements of Cu and Mg for Al/SiC alloy system at 800°C for 5 minutes [27].	22
Figure 2.6 Comparison of the tensile strength of magnesium and alloys and their composites reinforced with Al <sub>2</sub> O <sub>3</sub> fiber [2].	25
Figure 2.7 Theoretically and experimentally obtained coefficient of thermal expansion values as function of weight percentage of SiC particulates in ZK60A magnesium alloy [40].	30
Figure 2.8 Partial short fiber reinforced light metal diesel pistons [39].	32
Figure 3.1 Fabrication and characterization of Mg based composite.	36
Figure 3.2 Procedure for alumina fiber preform fabrication a) blending fiber with binder, b) molding, and c) drying and baking.	39
Figure 3.3 a) A75-ton, vertical hydraulic press, and b) Electric furnace with SF <sub>6</sub> gas protection .	41

Figure 3.4 Schematic diagram of the squeeze casting procedure a) placing preform into the mold, b) pouring melt into the mold, c) applying pressure and d) composite is produced.....	42
Figure 3.5 Schematic illustration of tensile specimen. ....	43
Figure 3.6 INSTRON tensile machine (Model 8562).....	44
Figure 3.7 a) Scanning electron microscopy (JEOL Model JSM-5800LV), b) Buehler optical image analyzer model 2012. ....	45
Figure 3.8 A Differential Scanning Calorimetry-Thermogravimetric Analyzer (DSC-TGA Q600). ....	46
Figure 3.9 EC-LAB SP-150 electrochemical apparatus for corrosion test. ....	47
Figure 4.1 A preform with fiber volume fraction of 9%.....	50
Figure 4.2 Schematic description of preform deformation by squeeze casting, preform was preheated to 750°C before place into mold, a) before, b) after pressure infiltration. [D]: deformed height, [I]: original height. ....	51
Figure 4.3 A squeeze cast magnesium matrix composite (AM60/ Al <sub>2</sub> O <sub>3</sub> ). ....	51
Figure 4.4 Composite cross-sections showing the deformations of preforms under pressure, (a) composite with 7% fiber volume fraction, and (b) composite with 35% fiber volume fraction. ....	52
Figure 4.5 Optical (a) and SEM (b) micrographs of as-cast AM60.....	53
Figure 4.6 EDS analysis of the matrix alloy AM60, (a) primary $\alpha$ -Mg, and (b) Mg <sub>17</sub> Al <sub>12</sub> intermetallic. ....	54
Figure 4.7 Composite sample etched by (a) 10s, (b) 30s, (c) 50s, (d) 70s, (e) 90s, and (f) 110s. ....	56

Figure 4.8 SEM showing the orientation of the fiber before (a) and after (b) the infiltration. ....	56
Figure 4. 9 SEM showing the interface between the fiber and the matrix for the composite with fraction of 9 vol%. ....	57
Figure 4.10 Optical micrographs showing grain structure of, (a) unreinforced AM60 matrix alloy, (b) 7%, (c) 9%, (d) 11% and (e) 22% fiber reinforced composites (all are under T4 condition), respectively. ....	60
Figure 4.11 Measured grain size of the matrix alloy AM60 and it composite with fiber volume fraction of 7%, 9% and 11%. ....	61
Figure 4. 12 SEM micrograph showing the location of the alumina fibers for 11vol% composite. ....	62
Figure 4.13 DSC heat flow curves for magnesium matrix composite with fiber volume fraction of 7%, and 11% . ....	64
Figure 4. 14 Hardness variation as a function of fiber volume fraction for the composites. ....	66
Figure 4.15 Typical engineering stress vs. strain curves for AM60 alloy and 7%, 9%, 11%, 22% and 35% fiber reinforced composites. ....	67
Figure 4.16 UTS, YS and elongation of AM60 and its composites with fiber volume fraction of 7%, 9%, 11%, 22% and 35%. ....	69
Figure 4.17 Young's modulus of AM60 and its composites with fiber volume fraction of 7%, 9%, 11%, 22% and 35%. ....	69
Figure 4.18 Typical true stress vs. strain curves for AM60 alloy and composites with 7%, 9%, 11%,22% and 355 fiber volume fractions. ....	70

Figure 4.19 Strain-hardening rate vs. true plastic strain curves for unreinforced AM60 matrix alloy and composites with fiber volume fractions of 7%, 9%, 11%, 22% and 35%. .....	72
Figure 4.20 SEM fractographs of the unreinforced magnesium alloy AM60, (a) low and (b) high magnification.....	74
Figure 4.21 SEM fractographs of the 7% fiber reinforced composite, (a) low and (b) high magnification. ....	75
Figure 4.22 Fractographs of the 9% fiber reinforced composite, (a) low and (b) high magnification. ....	76
Figure 4.23 SEM fractographs of 11% fiber reinforced composite, (a) low and (b) high magnification. ....	77
Figure 4.24 Fractographs of 22% fiber reinforced composite, (a) low and (b) high magnification. ....	78
Figure 4.25 Fractographs of 35% fiber reinforced composite, (a) low and (b) high magnification. ....	79
Figure 4.26 SEM micrographs showing the, (a) debonding of the fiber and (b) the crack origin in the composite with fiber volume fraction of 22%. ....	81
Figure 4.27 Potentiodynamic polarization curves for the 7%, 9%, 11%, 22% and 35% Al <sub>2</sub> O <sub>3</sub> fiber reinforced composites in 3.5 wt% NaCl solution. ....	82
Figure Ap.1 Engineering stress vs. strain curves for the 7% fiber reinforced composite. .....	100
Figure Ap.2 Engineering stress vs. strain curves for the 9% fiber reinforced composite. .....	101

Figure Ap.3 Engineering stress vs. strain curves for the 11% fiber reinforced composite. .....	103
Figure Ap.4 Engineering stress vs. strain curves for the 22% fiber reinforced composite. .....	104
Figure Ap.5 Engineering stress vs. strain curves for the 35% fiber reinforced composite. .....	106
Figure Ap.6 SEM fractographs showing the fractured surfaces of composites with fiber volume fractions of 7%, 9%, 11%, 22% and 35% at the magnification of 1000X.....	109
Figure Ap.7 Fractured surfaces showing the fracture origin of 22% and 35% composites. .....	112
Figure Ap.8 Enlarged heat flow cure for 11% composite. ....	113



## LIST OF TABLES

Table 2.1 The effect of alloying elements in magnesium alloys .....	9
Table 2.2 MMCs combinations with different reinforcements.....	11
Table 2.3 Chemical composition of Saffil alumina fiber.....	14
Table 2.4 Physical and mechanical properties of Saffil fiber .....	15
Table 2.5 Property potential of different MMCs .....	15
Table 2.6 Contact angle between Al and AL <sub>2</sub> O <sub>3</sub> , Graphite and SiC ate different temperatures .....	23
Table 2.7 Tensile properties of some Mg alloys and their composites.....	26
Table 2.8 Elongation of Al7010 alloy and Al-5Mg Alloy and composites .....	28
Table 2.9 Potential technological applications of MMCs.....	31
Table 3.1 Thermophysical properties of magnesium alloy AM60 .....	38
Table 3.2 Density comparison of different gases.....	40
Table 4.1 A comparison between the measured grain size of the composites and the calculated inter-fiber spacing.....	63
Table 4.2 Calculated and measured heat absorption and the heat needed for melting AM60 for unreinforced matrix alloy and composites with fiber volume fractions of 7%, and 11% .....	65
Table Ap.1 Grain size measurement for matrix alloy and composites with different fiber volume fractions.....	96

Table Ap.2 Hardness measurement for matrix and composites with different fiber volume fractions..... 97

# CHAPTER 1:

## INTRODUCTION

Magnesium is one of the lightest engineering materials with a density of  $1.74 \text{ g/cm}^3$ . It is one-third lighter than aluminum, three-fourths lighter than zinc, and four-fifths lighter than steel. Magnesium is usually used with aluminum as an alloying element to improve the machinability and the corrosion resistance. Recently, the need of lightweight materials for fuel saving in automotive industry has led to extensive research in the development of magnesium alloys [1].

To further enhance the mechanical properties of magnesium alloys, metal matrix composites are introduced with the improvements in hardness, strength, toughness and wear resistance. In composites, magnesium alloy holds the reinforcement in position as a structural material to transfer of load to reinforcement. On the other hand, the reinforcement provides strengths to the matrix. The interface between the matrix and the reinforcement has significant influence on the final properties of the composites.

Basically, solid and liquid phase techniques are the two ways to fabricate metal matrix composites. Powder metallurgy is an example of solid phase technique which includes the process of powder blending and pressing, diffusion bonding of foils and physical vapor deposition. Squeeze casting is one of the fabrication processes that belong to liquid phase technique. Squeeze casting is a process that applying external pressure to infiltrate liquid metal into a preform. There is no need for surface treatment such as coating to improve the wetting

behavior like treatment done to the powder metallurgy technique. Cost effective and high efficiency are also the advantages of squeeze casting.

Two steps are involved to fabricate magnesium based composite by preform-squeeze casting technique. First, preform is made and pre-treated prior the infiltration of magnesium melt. The purpose and advantage of the preform is to uniformly and randomly distribute the reinforcement in order to achieve the desired mechanical properties. Second, pressure is applied to infiltrate the melt into the preform and the solidification process is under pressurized condition.

Recent studies have demonstrated that the preform and squeeze casting process was capable of producing porosity-free magnesium-based composites, which were reinforced with alumina fibers. However, in the open literature, there are almost no reports on the effect of volume fractions of alumina fibers as reinforcement on microstructure development and mechanical properties of magnesium matrix composites.

## **1.1 Objectives of this study**

The objectives of this project are:

1. To fabricate preforms with different fiber volume fractions by the modified process;
2. To fabricate the magnesium-based composites with different fiber volume fractions;
3. To analysis the effects of fiber volume fractions on the mechanical properties of the composites;
4. To study the solidification behaviour of the magnesium-based composites;
5. To analyze the microstructure of the magnesium-based composites;

6. To evaluate the influence of fiber volume fraction s on the corrosion behaviours of the magnesium-based composites.

## **1.2 Thesis layout**

There are five chapters included in this thesis. Chapter one provides an introduction on metal matrix composites and fabrication techniques. Chapter two reviews studies on composites processing, microstructure, corrosion behaviours and mechanical properties of magnesium-matrix composites. The detailed experimental procedures are described in chapter three. The experimental results and discussion on the microstructures, mechanical properties, corrosion behaviours, and fracture analysis are reported in chapter four. Chapter five summarized the present study along with calculations and made some recommendations for the future work.

## CHAPTER 2:

# LITERATURE REVIEW

Magnesium alloys have been increasingly grown in research community in recent years due to the extending areas of their applications. For the lightness and recyclability of magnesium alloys, researches have been done to explore the potential of magnesium and its alloy as a substitute of steel, aluminum and plastic in automotive industry. With the development of scientific and technological process, automobiles become more humanized. More and more electrical devices are installed in vehicles, for example, increasing size of Light-emitting Diode (LED) screen, satellite navigation system (GPS) and rear view camera etc. Obviously, the curb weight is increasing without substitute the materials. Reducing the automobile weight is critical in order to minimize fuel consumption and emission.

Magnesium is the lightest material with density of  $1.74 \text{ g/cm}^3$  among the metals for structural application, which is approximately  $2/3$  of aluminum,  $1/4$  of zinc and  $1/5$  of steel. It also has considerable low melting temperature of  $649 \text{ }^\circ\text{C}$ , slightly lower than aluminum. Magnesium alloys are much more workable at elevated temperatures than at room temperature [1]. The advantages of magnesium alloys are also demonstrated with their excellent castability, superior machinability and better damping capacity as compared to aluminum and cast iron. Also it is tougher than plastic, better electromagnetic interference (EMI) shielding than plastic and absorb vibration energy effectively and recyclability. However, magnesium alloys have relatively low absolute strength as compared to other structural materials, especially at elevated temperature [2].

Recently, Mg-Al system is the widely used for magnesium alloys. The temperature limit for applications is up to 120 °C. To expand the industrial application, it is essential to improve the high-temperature mechanical properties of magnesium alloys [3].

Development of magnesium matrix composites is one of the solutions for the need of high-performance and lightweight materials in some specific applications. For example, the magnesium matrix composite unidirectional reinforced with continuous carbon fiber provides 1000MPa in bending strength with the low density of 1.8 g/cm<sup>3</sup>. The superior mechanical properties can be retained at elevated temperature up to 400 °C. Based on the demand of application, the material properties can be tailored by changing the composite reinforced material. The potential application of magnesium composites in the automotive industry could include: disk rotor, piston head or piston ring grooves, gears, gearbox bearing, connecting rods, and shift forks [3, 4].

## **2.1 Metal matrix composite**

A metal matrix composite (MMC) is composite material composed at least two distinct phases. One is a metal and the other material can be a different metal or another material, such as a ceramic or organic compound. When at least three different materials are present, it is called hybrid composite. Many of common material such as metals, alloys or polymers mixed with additive also have a small amount of dispersed phases in their structure, however, they are not considered as composite material since their properties are similar to those of their base constituents. Thus, the phases in a composite material must have bulk properties significantly different from those of any of the constituents [4].

MMCs are fabricated by dispersing reinforcing material into a metal matrix. MMC offer unique combinations of properties. This group of materials becomes interesting for structural and functional applications where conventional materials no longer meet the requirements. MMCs have several advantages over the conventional material. The favourable properties are high strength and stiffness, low density, high electrical and thermal conductivity, high temperature stability, adjustable coefficients of thermal expansion, improved wear resistance etc.

## **2.2 Matrix**

### **2.2.1 Purpose of the matrix**

In a composite material, the matrix is a primary phase and having a continuous character. The matrix is usually more ductile and less hard phase that completely surrounds the reinforcement phase. The purpose of the matrix is [5]:

- To hold the reinforcement together and in the case of fibers;
- To transfer the load between the reinforcement form any external force;
- To provide the material its shape and give a rigid form to the composite;
- To control the electrical and chemical properties;
- To reduce stress concentrations by providing an elastic response and redistribute internal stress; and
- To prevent the damage of the reinforcement from the environment and handling.

Common matrixes include polymer, metal and ceramics. Typically, most common polymer based composite materials are fiberglass, carbon fiber and Kevlar, which includes at least two parts, the substrate and the resin. Ceramic matrices currently are mostly made of SiC or carbon



which can be provide wear and abrasion resistance or protect the fiber from oxidation and damage, and are used in aircraft system. Other examples are alumina reinforced cutting tools.

### **2.2.2 Function of the matrix**

Unlike the polymer and ceramic matrices, the metal matrix has great effect on the strength of the composite. Since the reinforcement is generally strong and stiff, the matrix is usually the weak link in the composite. Thus, the matrix serves only in a limited way to the carrying capacity of the tensile load in a composite structure. However, as a continuous phase, the selection of a matrix has significant influence on the interlaminar shear and the in-plane shear properties of the composite. The interlaminar shear strength is an important design consideration for structures under bending loads, whereas the in-plane shear strength is important for structures under torsional loads [6].

For the strength and damage of continuous fiber reinforced MMCs, Johnson [6] indicates that the failure models of MMCs can be grouped into four categories based on the relative fatigue behaviour of the fiber and matrix and the interface properties. The four categories are: (1) matrix dominated, (2) fiber dominated, (3) self-similar damage growth, and (4) fiber/ matrix interfacial failure. If the matrix material has a lower fatigue endurance strain range than the fiber, then matrix dominated damage could occur. The matrix cracks developed by this result would cause significant losses in stiffness in laminates with off-axis plies.

### **2.2.3 Types of matrix**

Aluminum, magnesium, titanium and copper, nickel-based super alloys, and stainless steel are currently used matrices. The first three matrices primarily serve as base alloys for automotive

and aerospace applications to reduce weight and remain their strength; for applications regarding to the thermal management and electrical contacts, copper-based matrix composites are mostly used; nickel-based and stainless steel matrix composites are suitable for high-temperature application ( $>500^{\circ}\text{C}$ ) [7].

Magnesium alloy developments have been driven by automotive and aerospace industries, which require lightweight materials to operate under increasing demanding conditions. Magnesium alloys have the characteristics of good manufacturability, which include casting, moulding, forging and also inert gas weldability [7, 8]. They also have excellent damping capacity compared to the same product from other metals, which makes the use of these alloys more attractive for increasing the life cycle of machines and equipment. Some other properties such as dent resistance due to the relatively low modulus of elasticity, good corrosion resistance to attack by alkali, chromic and hydrofluoric acids, and many organic chemicals extend applications of the alloys. Recently, the addition of strontium or calcium improved significantly the creep resistance with lower cost compared with the addition of the rare earth elements [9].

Magnesium alloys are mixture of magnesium with other metals, often aluminum, zinc, manganese, silicon, copper, rare earths and zirconium. They could be grouped as Mg-Al-Mn (with or without Zn), Mg-Zr, Mg-Zn-Zr (with or without rare earth), Mg-Ag-Zr (with rare earths or thorium). The addition of certain alloying elements has the effect of increasing the strength, corrosion resistance and high temperature properties. The effects of these elements are listed in Table 2.1 [8].

**Table 2.1** The effect of alloying elements in magnesium alloys [8]

Zn	Hardening agent, generally being used with aluminum and zirconium up to 6%.
Al	Increasing the alloy strength, provide a long freezing range which could cause casting porosity, commonly used up to 10% .
Mn	Improving the corrosion resistance with a slight influence on the strength of the alloy. Up to 2% is used alone, with considerably less in conjunction with Al and Zn.
Si	Improving the corrosion resistance with a slight influence on the strength of the alloy. Up to 2% is used alone, with considerably less in conjunction with Al and Zn.
Zr	Powerful grain refiner, consequently increase the strength, only slight solubility in magnesium.
Rare earths	Strengthening the alloys and improving the high temperature properties such as creep resistance.
Ag	Used with rare earth and zirconium alloys resulting in age hardening properties

### **2.3 Reinforcement**

MMCs require reinforcement to achieve their manifold demand. The choices of the reinforcements are determined by production and processing and by the matrix alloy of the composite material. Generally, the applicable demands are include, i.e. low density, thermal stability, mechanical compatibility, chemical compatibility, high Young's modulus, high compression and tensile strength, good processability and economic efficiency [10]. To achieve

these demands, non-metal inorganic reinforcement components are used. MMCs generally are categorized based on the type of reinforcement. In particular, the composites can be separated into two categories:

- Continuous reinforcement: fiber or filaments;
- Discontinuous reinforcement: short fiber, whiskers or particles.

Continuous fibers offer the composite highly anisotropic properties because of the high aspect ratio (length to the cross sectional dimensions, diameter or thickness). The mechanical properties are strongly influenced by the orientation of the fiber, i.e., the composite reaches its highest level of mechanical properties when all fibers are aligned along the primary loading direction for a given fiber volume fraction [11, 12]. The continuous reinforcement has the advantages, as the excellent wear resistance, lower coefficient of thermal expansion and higher thermal conductivity. On the other hand, discontinuous fiber or particles give good specific stiffness and strength, it has positive effect on the hardness, wear resistance, fatigue resistance and compression resistance. MMCs reinforced with discontinuous fiber have wide range of applications due to their ease of manufacturing, excellent thermal and electrical properties. One of the biggest advantages of the discontinuous fiber reinforced composites is the possibility to work with the usual techniques of rolling, extrusion and forging. However, MMCs reinforced with discontinuous fiber require diamond tools for cutting due to fast tool wear caused by the hard second phase [11].

The purpose of the matrix is to hold together the fibers or other type of reinforcement. It is increasingly clear that the microstructure of the matrix alloy has great influences on the overall performance of the composite. Aluminum, magnesium, titanium and copper mostly are chosen

for the matrix due to their excellent resistance at high temperature. The combination of MMC can be summarized in Table 2.2 [13].

**Table 2.2** MMCs combinations with different reinforcements [13]

	Aluminum	Magnesium	Titanium	Copper
Long fiber	Boron (B), silicon carbide (SiC), alumina ( $Al_2O_3$ ), graphite (C)	Alumina ( $Al_2O_3$ ), graphite(C)	Silicon carbide (SiC)	Silicon carbide (SiC), graphite (C)
Short fiber	Alumina ( $Al_2O_3$ ), alumina-silicon ( $Al_2O_3+SiO_2$ )	Alumina ( $Al_2O_3$ )		
Whiskers	Silicon carbide (SiC)	Silicon carbide (SiC)	Titanium carbide (TiC)	
Particles	Silicon carbide (SiC), boron carbide ( $B_4C$ )	Silicon carbide (SiC), boron carbide ( $B_4C$ )		Titanium carbide (TiC), silicon carbide (SiC), boron carbide ( $B_4C$ )

## 2.3.1 Characteristics of reinforcement

### 2.3.1.1 Carbon fiber

Among all kinds of composites, carbon fibers are the most developed fiber group. Carbon fiber is popular in advanced composites in aerospace, transportation, and the military industry and it the first used in recreational equipment. The reason for this is their excellent property profile [10]:

- Low density
- High strength
- High Young's modulus
- High stability to molten mass in various metal system
- Possible large variation in property profiles
- Low coefficient of thermal expansion
- Good thermal and electrical conductivity
- High availability
- Cost effectiveness

Carbon fiber is more amenable to large-scale production than other advanced fibers. Carbon fiber is also chemical inert except in strongly oxidizing environments or in contact with certain molten metals and has exceptional thermophysical properties and excellent damping characteristics. These engineering properties can be translated into usable physical and mechanical properties. Besides, graphite fiber is in the carbon fiber family with a special form which is obtained after heating to a temperature greater than 2400 °C (a process called *graphitization*). Graphitization results in highly oriented, layered crystallographic structure,

which leads to significantly different chemical and physical properties than non-graphitic forms of carbon .

### ***2.3.1.2 Boron fiber***

Boron, like carbon, has high strength and stiffness. It is another elemental fiber, commonly made by chemical vapor deposition (CVD) on a substrate such as carbon or tungsten. Boron fiber is the first high-performance monofilament reinforcement in composite. Due to its great mechanical properties, thermal stability and reduced reactivity with the matrix, boron fiber is still being used today, but cannot be compete with carbon fiber [14].

### ***2.3.1.3 Silicon carbide***

Silicon carbide (SiC) is used as reinforcement in composites by means of fiber, whisker or particulate form. SiC is the most important monoxide ceramic fiber available commercially. Commercially, the two main varieties of this fiber available are large diameter fiber made by chemical vapor deposition (CVD) and small diameter fiber made by controlled pyrolysis of a polymer [15]. In whisker form, the diameter range is from 0.01-0.3  $\mu\text{m}$  and the lengths from 8-100  $\mu\text{m}$ . In particulate form, SiC provides a ready commercial source, which is related to the abrasives industry and helps to lower the cost. Commercially available products are green and black SiC. Green SiC provide better strength and thermal conductivity than black SiC. Typical grain size used are between F-600 (mean size between 8.3 to 1.3 $\mu\text{m}$ ) and F-1200 (mean size between 2.3 to 3.5  $\mu\text{m}$ ) [15, 16]. The most use of composite material reinforced both by SiC whiskers and powders are based on magnesium alloy, because magnesium forms no stable carbides, i.e. SiC is stable in pure magnesium. However, a reaction takes place with sufficient contact time if it is applied in magnesium alloys which contain significant amounts of aluminum.

### 2.3.1.4 Alumina fiber

**Table 2.3** Chemical composition of Saffil alumina fiber [17]

Chemical composition	Content, wt%
Al <sub>2</sub> O <sub>3</sub>	96-97
SiO <sub>2</sub>	3-4
Fe	0.040
Cr	0.006
Ni	0.014
Na	0.088
Mg	0.013
Ca	0.053
Chloride (total)	0.008
Chloride (leachable)	0.0005

Alumina fiber is a cost effective reinforcement, and it still keeps the excellent properties, such as the strength, stiffness and thermal resistance. A short fiber, in the allotropic form of  $\delta$ -alumina (96%) is available commercially, manufactured by Saffil. Saffil alumina fiber was produced in the early 1970s and has been involved in the development of MMCs application since the 1980s. The chemical composition and some important properties provided by the manufacturer are listed in Tables 2.3 and 2.4 [17], respectively. MMC reinforced discontinuously have the best conditions for reaching the development goals. The alumina short fiber is cost effective and mass production is possible. MMCs reinforced with short alumina fiber has further advantages over the long-fiber continuous reinforced material, such as the relatively high isotropy of the



properties, and the possibility of processing composites by cutting and forming engineering.

Table 2.5 provide an overview of possible property profiles of different types of MMCs [18].

**Table 2.4** Physical and mechanical properties of Saffil fiber [17]

Physical Properties	Main crystal phase	$\delta$ -Al <sub>2</sub> O <sub>3</sub>
	Density (g/cm <sup>3</sup> )	3.3
	Melting point (°C)	2000
	Maximum useful temperature (°C)	1600
	Coefficient of linear thermal expansion (K <sup>-1</sup> )	$8 \times 10^{-6}$
Mechanical Properties	Tensile strength (MPa)	2000
	Elastic modulus (GPa)	300
	Strain to failure (%)	0.67
	Hardness (Mohs' scale)	7

**Table 2.5** Property potential of different MMCs [18]

MMC types	Properties strength	Young's modulus	High temperature properties	Wear	Expansion coefficient	Costs
Discontinuous reinforced MMC	**	**	*	***	**	Low
Long fiber reinforced MMC	**	**	**	*	***	High
Mineral wool: MMC	*	*	**	**	*	Medium
Other fibers	***	***	***	*	**	High

**Note:** \* good, \*\* very good, \*\*\* excellent

## **2.4 Fabrication of Metal Matrix Composites**

To fabricate the Metal Matrix Composite, different kinds of techniques can be applied. The selection of the suitable process is depended on the distribution and quantity of the reinforcement, (i.e. fiber and particle), the matrix alloy and the application. The convenient and versatile way to fabricate MMC is the mixing of metallic powder and ceramic fibers or particulates, which provide excellent controlling over the ceramic content across the complete range. MMCs can be produced by conventional metalworking equipment. Two common ways to produce magnesium matrix composites are powder metallurgy and casting.

The challenge in the processing of composites is to homogeneously distribute the reinforcement in the matrix alloy to reach a defect-free microstructure. In the powder metallurgy process, the composition of the matrix and reinforcement are independent of one another. It can be difficult to achieve a homogeneous mixture during the process of blending, especially for fibers and fine particles. For squeeze casting, preform is used which is made of fiber or/and particles. The preform is placed in a pre-heated mould, which is later filled with the liquid metal before applying pressure. The pressure creates an intimate link between the reinforcement and the matrix alloy in molten state. Since, magnesium is very active, the other casting technique, i.e., stir casting, in which fibers or particles are exposed to a high temperature for long period, is not good as squeeze casting or powder metallurgy process. In the following sections, the process of powder metallurgy and squeeze casting for the production of magnesium composites are explained [19].

### 2.4.1 Powder metallurgy

By applying powder metallurgy process, magnesium alloys are first atomized and then mixed with the reinforcement, then pressed, degassed and sintered at certain temperature in a controlled atmosphere (vacuum). In present, a variety of magnesium based composites are being fabricated by apply this process, for example, SiC/AZ91, TiO<sub>2</sub>/AZ91, ZrO<sub>2</sub>/AZ91, SiC/QE22, AND B<sub>4</sub>C/AZ80. Powder metallurgy has its own advantage, which has the capability to produce composite with high volume fraction of reinforcement (fiber/particle). However, this technique involves the atomization process, which is complicated and expensive for bulk material production. Thus, powder metallurgy might not suitable for mass production of MMCs. Figure 2.1 [20] shows the flow chart of the powder metallurgy processing.

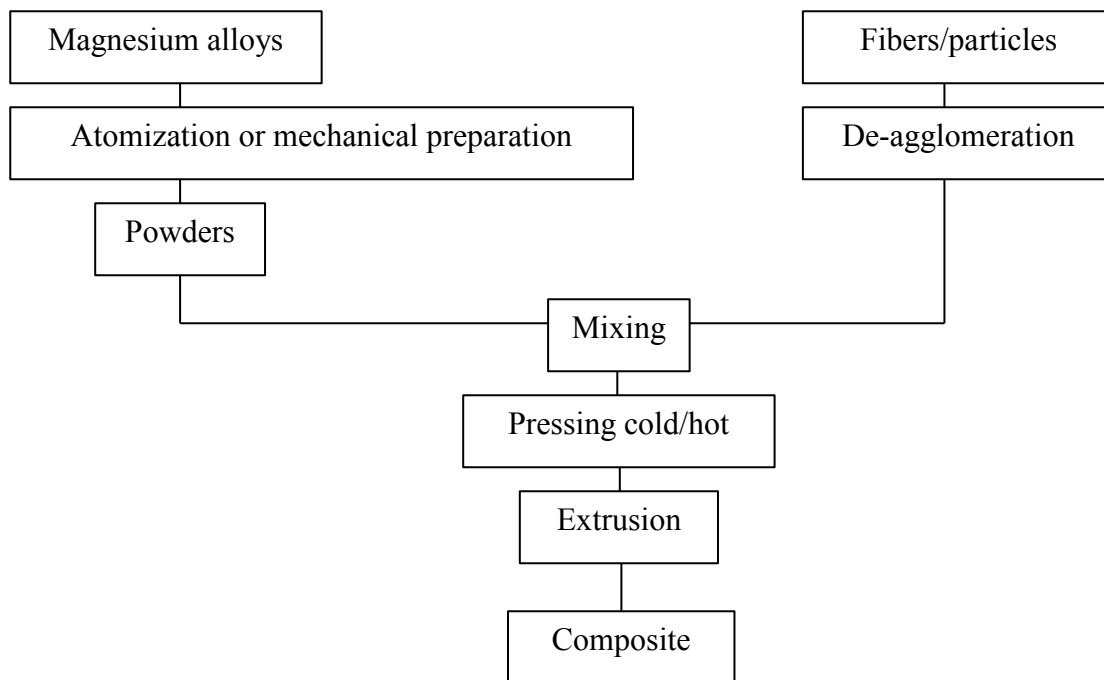


**Figure 2.1** Flow chart of a powder metallurgy process for fabrication of Metal Matrix Composite [20].

### 2.4.2 Squeeze casting

Squeeze casting is the most common fabrication process of MMCs. Not only does it can fabricate contours with a smooth surface finish, but also the heavy or thick walled parts can be obtained by this technique. Figure 2.2 shows the process of squeeze casting process for manufacturing composites [21]. Generally, the liquid metal is slowly filled into the mold and the melt solidifies under very high pressure, which provides a fine-grained structure. The squeeze casted parts have less or no gas inclusion in comparison with die casted parts. Squeeze casting can be direct or indirect. With direct squeeze casting the die is part of the mold and the pressure is applied directly to the melt to infiltrate into the preform [22]. However, with the indirect process, the volume of the liquid metal must be exactly predetermined, since there is no gate present and the quality of melt determines the size of the cast construction unit. Figure 2.3 shows [23] the squeeze casting processes with direct and indirect methods.

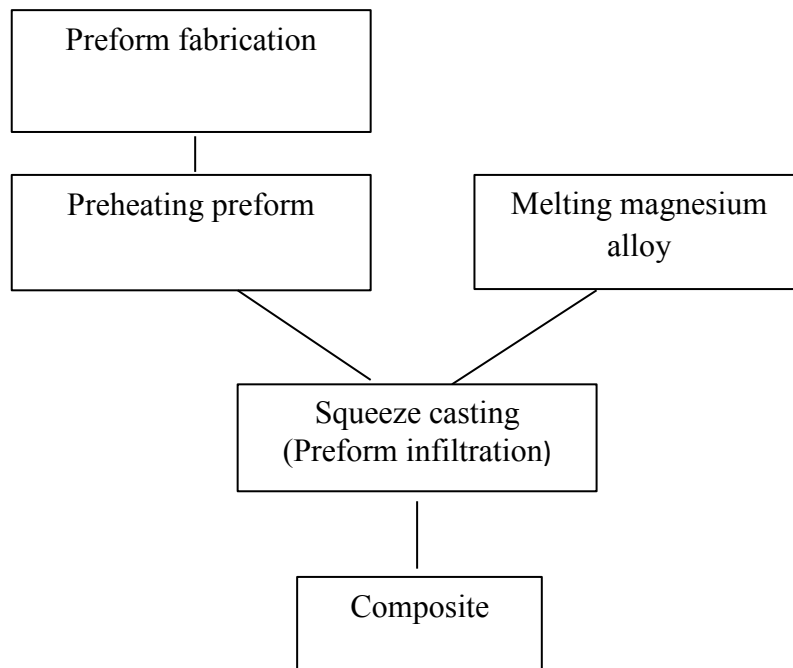


**Figure 2.2** Flow chart of squeeze casting process for fabrication of composite [23].

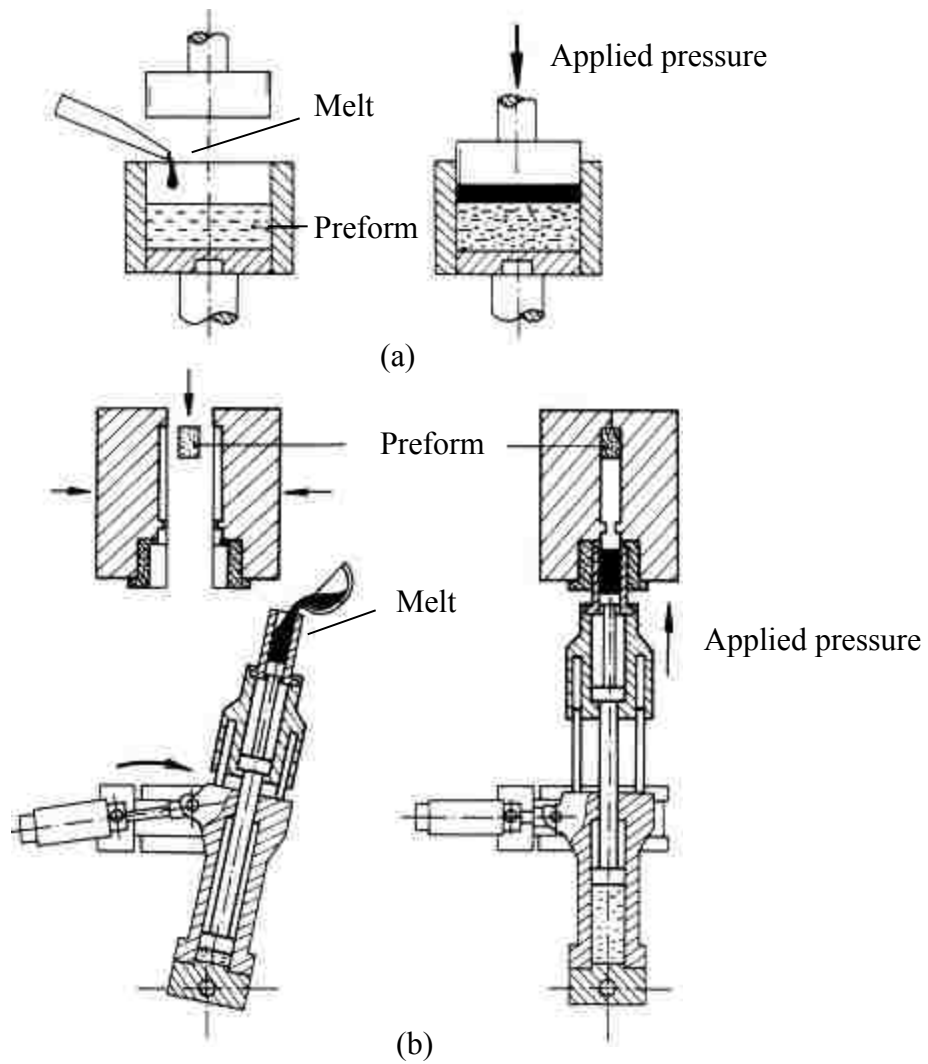


**Figure 2.3** Production of cast composite materials by (a) direct squeeze casting method, and (b) indirect squeeze casting method [23].

In the process of squeeze casting, the reinforcements (fibers, particles or whiskers) are usually in the form of a preform and then placed into the casting mold (direct squeeze casting process). Following this, a very high pressure is applied to infiltrate the melt into the preform. The applied pressure can significantly influence the mechanical properties and the microstructure of the castings. During the solidification process, several phenomena take place under the high-applied pressure. Firstly, freezing temperature can be shifted. The Clausius-Clapeyron equation [24],

$$\frac{dT}{dP} = \frac{T_f(V_s - V_l)}{L_f} \quad \text{Eq. 2.1}$$

where  $T_f$  is the equilibrium freezing temperature of the material

$V_l$ : the specific volume of liquid,       $V_s$ : the specific volume of solid,

$L_f$ : the latent heat of solidification.

shows that the solidification temperature of the material depends on the applied pressure and the solidification latent heat. Secondly, the enhanced heat transfer by apply the high-pressure causes the cooling rate to increase due to the firm contact between the solidifying melt and mold walls. Besides, the applied high pressure can effectively compensate the solidification contraction. As a result, the casting can be produced with finer grain and higher density, which bring the great mechanical properties for the casting. For instance, the ultimate tensile strength (UTS) of a squeeze cast Mg-4.2% Zn-RE alloy were improved by 15-40% over those manufactured by permanent mold casting process [25]. Squeeze casting process also can improve the casting yield due to the elimination of the risers in comparison to the gravity casting technique. However, the pressure for squeeze casting has to be carefully controlled. The excess pressure can produce turbulent flow of the molten metal, consequently gas might entrapped in the casting. Also, the excess pressure can damage the reinforcements during infiltration, especially for fibers. As a result, the mechanical properties of the composite can be significantly decreased [26].

## 2.5 Wettability

The infiltration of the liquid metal and the bonding between the reinforcement and matrix alloys are mainly influenced by wetting. The sufficient infiltration and excellent bonding give the composite higher standards of mechanical properties. For a non-wettable system, the liquid metal can flow into the channels first, and a pressure is necessary to push the melt into the capillaries. For this situation, the interfacial reactions tend to be the most active mechanism to reach good bonding between the melt and the reinforcement. As a result, the inadequate wetting of the reinforcement by the liquid metal and/or the excessive interaction between the reinforcement and the liquid metal will probably reduce the mechanical properties of the composite [27]. However, for a wettable system, the melt touches the surface of the reinforcement with a high surface activity, the melt flows into both of the preform channels and small capillaries easily and sufficiently in order to receive better mechanical properties of the composite.

### 2.5.1 Contact angle

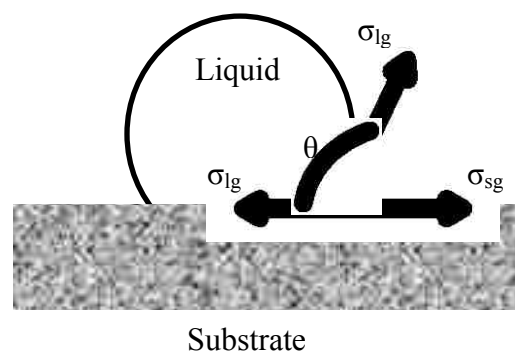


**Figure 2.4** Definition of contact angle,  $\theta$  [28].

The term of contact angle characterizes the wettability of a solid (prefom) by a liquid (melt); this can be defined in Figure 2.4 [28]. From measuring the contact angle, the wetting preference can be determined. The contact angle,  $\theta$ , can be obtained by apply equation 2.2, Yong's equation [27], by balancing the interfacial tensions.

$$\sigma_{lg} \cos \theta + \sigma_{ls} = \sigma_{sg} \quad \text{Eq 2.2}$$

where  $\sigma_{lg}$ ,  $\sigma_{ls}$ , and  $\sigma_{sg}$  are the interfacial tension between liquid (l), solid (s) and gas (g). If the contact angle,  $\theta$ , is less than  $90^\circ$ , then the solid is wetted by the liquid. On the other hand, if the contact angle is greater than  $90^\circ$ , the solid will not be wetted and if the contact angle approaches to  $180^\circ$ , it indicated that the solid is complete nonwetting.

### 2.5.2 Wetting behaviour

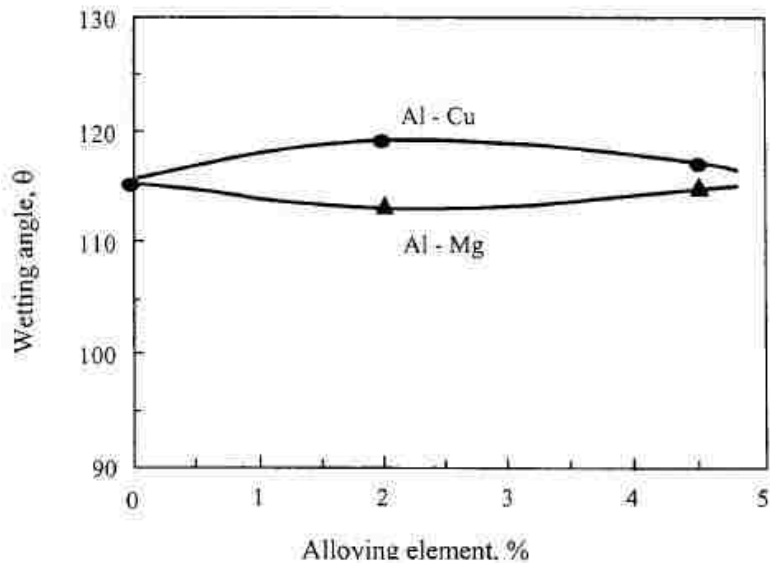


**Figure 2.5** Variation of wetting angle with addition of alloying elements of Cu and Mg for Al/SiC alloy system at  $800^\circ\text{C}$  for 5 minutes [27].



**Table 2.6** Contact angle between Al and Al<sub>2</sub>O<sub>3</sub>, Graphite and SiC at different temperatures [29]

	T (°)	Θ (°)
Al <sub>2</sub> O <sub>3</sub>	660	103
	700	150
	870	139
	900	120
	1100	86
	1500	60
Graphite	800	157
	700	150
	1200	39
SiC	700	125
	900	60

The temperature, time and alloying element can influence the wettability of the liquid metal on the reinforcement. Table 2.6 shows the contact angle between aluminum melt and ceramic substrate under different temperatures [29]. As shown in Table 2.6, the wetting is very poor for the contact angle range of 150° to 700° to less than 60° at 1500° between aluminum and Al<sub>2</sub>O<sub>3</sub>. The similar phenomenon is observed for aluminum melt and SiC. The contact angle changes from 125° to 60° and indicates a strong temperature dependence behavior. The use of magnesium alloy will improve the wettability of SiC by reducing the surface tension of aluminum, in which it will react with oxygen and generate a reaction product. Figure 2.5 illustrates the changing of wetting angle with addition of alloying elements, copper and magnesium [27]. The previous

study has found that a good wettability was in the Mg-C system. The initial contact angles of liquid magnesium on carbon and porous graphite at 973K were 80° and 74°, respectively.

### **2.5.3 Improving wettability**

#### *Mechanical enhancement*

It can be pressurized to improve the wettability which includes squeeze casting, liquid metal processing, vacuum infiltration and pressure-assisted network infiltration. The capillary action can be effectively improved by apply a force on the interface [30].

#### *Chemical enhancement*

For this procedure the wettability can be either improved by depositing a suitable coating on the surface of the substrate or by adding surface active alloy elements to the metal. According to the study of Rohatgi [31], the contact angle on graphite particles in molten Al changes from 157° to 60° when the surface is coated with nickel. Besides, the variation in wettability with alloying can changes the surface energy, interfacial reaction, or the electronic structures of the surface atoms, with regard to the effect of alloying element.

## **2.6 MMCs mechanical properties**

The first study on the strength of discontinuously reinforced Al alloys was by McDanel [32]. The reinforcement used was SiC whisker and particle. The results of his experiments showed that there was a 60% increase on the yield and ultimate tensile strength, depending on different volume fraction of the reinforcement and the types of the alloy. In comparison with the melt processed composite, the powder processed material tends to provide higher strength. The presence of the particles improves the modulus at high temperatures, but the high temperature

strength is not improved significantly. The reported experiment data shows and high degree of scatter and it somewhat reflects the quality of the material and differences in processing.

### 2.6.1 Tensile strength

In general, the stiffness, hardness, tensile strength, and wear resistance (due to the high hardness) of the composite increase with the addition of a reinforcement phase (fiber/particle), in comparison with the unreinforced alloys. The properties of the magnesium based composites show the same tendency as the aluminum matrix composites, no matter the fabrication process are squeeze casting or powder metallurgy. If the low density is taken into account, magnesium matrix composites can compete well with aluminum ones, as shown in Figure 2.6 [2].

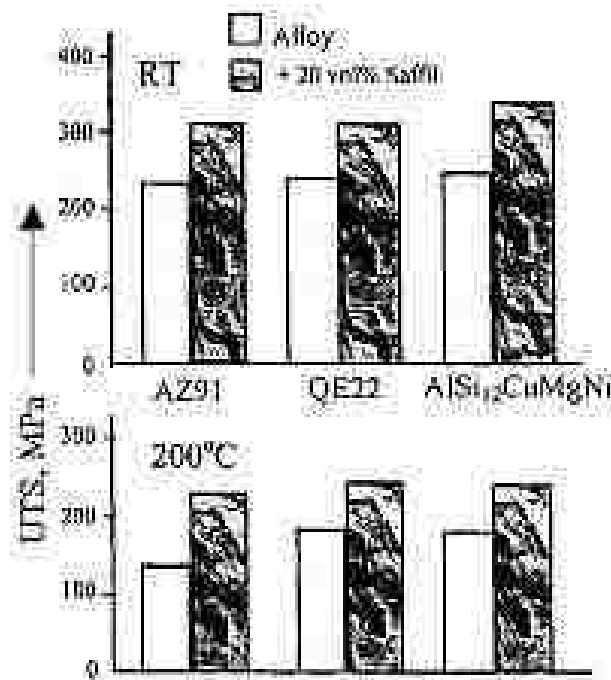


**Figure 2.6** Comparison of the tensile strength of magnesium and alloys and their composites reinforced with Al<sub>2</sub>O<sub>3</sub> fiber [2].

General speaking, as the volume fraction of the reinforcement increases, the yield strength and the elastic modulus of the Mg MMCs increase linearly, but it is only within a certain range. The main strengthening mechanisms for magnesium based composites are the work hardening, load transfer, particle strengthening and grain refinement by the reinforcement phases. The presence of the fibers or particles in the matrix blocks the movement of dislocations and thus strengthens the material. When the matrix is strained, the work hardening takes place. The strain mismatch between the matrix and the reinforcement generates high density of dislocations around the reinforcement and then strengthens the material. For the fiber reinforced composite, the load transfer is a significant strengthening mechanism. If the bonding between the fiber and matrix is strong enough, the applied stress can be transferred from the matrix to the fiber. Table 2.7 [25] shows the typical properties of commercially available Mg MMCs reinforced by SiC and the unreinforced magnesium alloys.

**Table 2.7** Tensile properties of some Mg alloys and their composites [25]

Alloy Composite	YS (MPa)	UTS (MPa)	El (%)	Elastic modulus (GPa)
AZ61	157	198	3.0	38
AZ61/20%SiC <sub>p</sub>	260	328	2.5	80
AZ91	168	311	21	49
AZ91/9.4%SiC <sub>p</sub>	191	236	2	47.5
AZ91/15.1%SiC <sub>p</sub>	208	236	1	54

The cracking of the reinforcement in the composite can relax the stress built up by the applied load. For example, in a fractured Mg-SiC composite, the SiC particles fractures was observed to

be the predominant form of localized damage under tensile loading. The fracture of the reinforcing particles leads to the cacking of the magnesium matrix composite. The final fracture occurred as a result of the crack propagation through the matrix alloy. The size, as well as the volume fraction of the reinforcement can significantly influence the tensile properties of the composite. A finer secondary phase can produce more cooperated deformation within the matrix. It has found that in a 10 vol% SiC magnesium matrix composite, the matrix around the SiC particles (2  $\mu\text{m}$ ) had fine grains and strong bondings after high strain deformation. In contrast, cavities were found around the bigger SiC pariticles (5  $\mu\text{m}$ ), due to the stress built up around the particles when the load is applied [33].

The stress built up in the MMCs could also be relaxed by debonding between the reinforcement and the matix alloy. When the interface between the reinforcement and the matrix was weak, the composite might fail prematurely at the interface when a load was applied. A study on an AZ91 reinforced with 15 vol% SiC showed that the decreasing in tensile strength was attributed to the excessive chemical reactions, different powder size distribution of the reinforcement. Besides, the strength of the interfaces between the matrix and the reinforcement was temperature dependent. The tensile behaviours of AZ91 based composite reinforced with randomly oriented short carbon fibers revealed that the failure mode of the composite changed form fiber/MgO interface failure to the MgO/matrix interface as the temperature increased from room temperature to 200 °C [34].

### 2.6.2 Ductility

For the application of both of the aluminum and magnesium based composites, the major limitation in the mechanical properties was the ductility. The elongation dropped while the tensile strength was improved. For both of the fiber and particle reinforced MMCs, the elongation decreased rapidly with the addition of reinforcement phases. Musson and Yue's work showed [35] that the ductility decreased as the addition of the Saffil alumina fiber increased in an aluminum alloy based composite, as shown in Table 2.8.

**Table 2.8** Elongation of Al7010 alloy and Al-5Mg Alloy and composites [35]

	7010 alloy	Al-5Mg alloy
Matrix alloy	10.5	13.8
15 vol% alumina fiber	0.2	2.0

In contrast to the ceramic reinforced composites, the elemental metallic powder reinforced composite showed better ductility due to the reduced possibility of breaking the reinforcement and interface bond. The decreasing in the ductility was also evident in the interactions between the reinforcement and dislocations. Since the resistance to the dislocation motion of the reinforcement reduced the ductility of the composites. The previous work examined the super-plastic behaviour of fine-grained (2  $\mu\text{m}$ ) WE43 magnesium alloy containing spherical precipitates (200 nm) within grains, which had an elongation to failure of over 1000% at 400 °C [36]. Within the grain, the dislocation tended to interact with the particles. The existence of intra-granular particles diminished the super plastic flow. However, the composite reinforced with high brittleness reinforcement did not mean the composite had to show a low ductility. The grain

refinement by the reinforcement could result in super-plasticity in magnesium matrix composite, even with higher brittle secondary phases. For instance, a ZK60A magnesium alloy reinforced with 17 vol% SiC particles showed an elongation of 200-350% at temperature range of 350-500 °C [37].

### **2.6.3 Hardness**

The addition of Al<sub>2</sub>O<sub>3</sub> short fiber in the composite could increase the hardness of 70-80% in comparison with the unreinforced matrix alloy, indicated by Kainer's experiment with AZ91 and MSR (2.5%Al, 2% rare earth, and 0.6% Zr) [38]. Yong and Clegg [36] showed that the hardness of the Mg-4.2% Zn-RE reinforced with 14 Vol% Al<sub>2</sub>O<sub>3</sub> short fiber was as twice as the unreinforced gravity die casting specimens. The reason was that the low solidification rate of the gravity die casting generated coarse grains. But, the grain refinement resulting from the introduction of Al<sub>2</sub>O<sub>3</sub> fiber led to a significant increase in the matrix hardness.

### **2.6.4 Young's modulus**

By squeeze casting, a wide range of mechanical properties could be achieved, such as strength, hardness and Young's modulus. Schwartz reported that [37] there was a significant increase in Young's modulus, from 45 GPa for the unreinforced Mg to 77 GPa for the hybrid reinforced composite (10 Vol% fibers and 15 Vol% particles). Kainer also reported an increase in Young's modulus from 43 GPa of QE22 to 88GPa with 20 Vol% Al<sub>2</sub>O<sub>3</sub> platelets [39].

### **2.6.5 Thermal expansion**

Thermal expansion has been extensively studied due to its significant effect on the mechanical properties of the MMCs. For example, brake drum components and engine turbine blades are

potential applications of MMCs. The thermal damage could be expected to be worse than that of unreinforced metals. In the design of composites, the stability for a long period of time use is a great concern. Geometrical change and mechanical property variation are the two main aspects to describe the stability. The coefficient of thermal expansion plays an important role in the former case. The mismatch of the thermal expansion coefficient between the matrix and reinforcement has a dominant effect. The coefficient of thermal expansion can be obtained either by experiment or predicted by analytical models. Lim's experiment found that [40] the experimental values followed a similar trend to the theoretically computed values and were also close to the predictions made by the Kerner model, as shown in Figure 2.7.

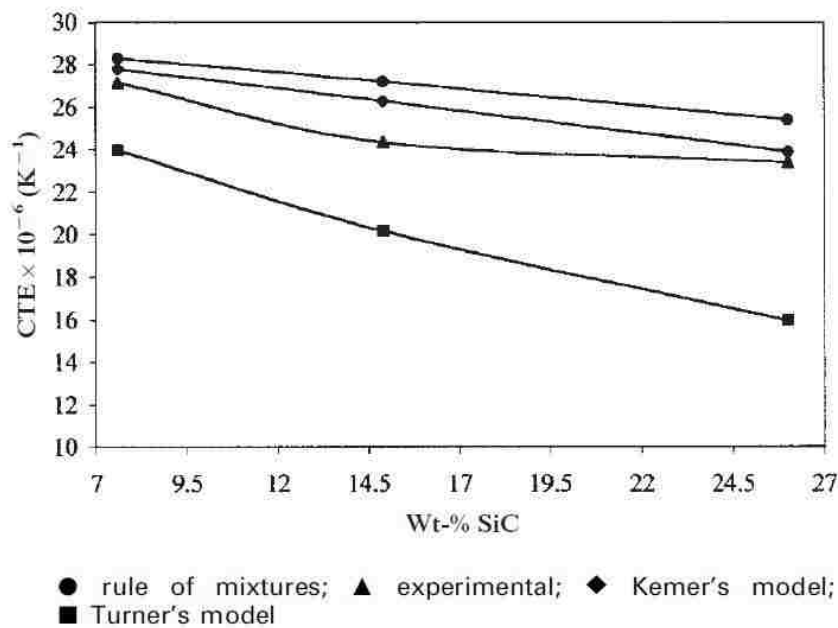


**Figure 2.7** Theoretically and experimentally obtained coefficient of thermal expansion values as function of weight percentage of SiC particulates in ZK60A magnesium alloy [40].



## 2.7 The applications of MMCs

MMCs could generally applied in automotive and aerospace industries. Parts can use MMCs are required higher properties, for example, high specific strength and stiffness, temperature stability, low thermal expansion, wear resistance and low thermal conductivity. Table 2.9 shows the potential applications of MMCs in both of automotive and aerospace industries [41].

**Table 2.9** Potential technological applications of MMCs [41]

Application	Material	Fabrication method
<u>Vehicles</u> Brake disk, piston pins, connecting rod, stiffeners, retainer and drive shaft	Al-Al <sub>2</sub> O <sub>3</sub> , Al-SiC, Mg-SiC and Mg-Al <sub>2</sub> O <sub>3</sub> (discontinuous reinforcements)	Squeeze casting, gravity die casting, melt infiltration, extrusion, forging
<u>Aircraft</u> Gear boxes, stiffeners, wings, compressor blades, turbine blade and supporting tubes	Ti-SiC, Al-Al <sub>2</sub> O <sub>3</sub> , Mg-Al <sub>2</sub> O <sub>3</sub> , Al-SiC, and Al-B (continuous and discontinuous reinforcements)	Squeeze casting, extrusion, diffusion welding and soldering, hot pressing, melt infiltration
<u>Space</u> Stiffeners, antennas, joins and frames	Al-SiC, Al-B, Al-C, Al-Al <sub>2</sub> O <sub>3</sub> , Mg-Al <sub>2</sub> O <sub>3</sub> (continuous and discontinuous reinforcements)	Melt infiltration, extrusion, diffusion bonding and joining

DuPont USA has changed the diesel engine connecting rods to Al-based MMC for the conventional forged steel rods. Figure 2.8 illustrate a piston that is partially reinforced with alumina short fiber. Besides, Toyota also used composite for the engine pistons, by using Al alloy as the matrix and Kawool (alumina-silicate) and Saffil (alumina) fibers for the reinforcement [39].



**Figure 2.8** Partial short fiber reinforced light metal diesel pistons [39].

## **2.8 Corrosion behavior of magnesium alloy and its composites**

In the automotive industry and other engineering applications, not only the strength but also the corrosion resistance can limit the application of the magnesium matrix composite. For pure magnesium, the limit of its applications is mainly from the shortcomings, such as high reactivity in the molten state and poor corrosion resistance [42]. The main challenges of using magnesium are to overcome its poor corrosion resistance particularly for outdoor applications. Magnesium and its alloys are extremely susceptible to galvanic corrosion which can attack the metals to reduce their mechanical stability and lead to an unattractive appearance.

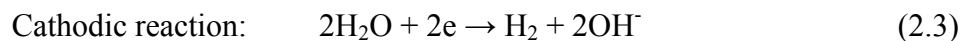
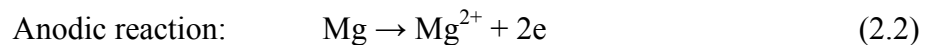
The corrosion resistance of material varies with environments. There is no such material that shows high corrosion resistance in all kinds of environments. For example, magnesium and its alloys are stable in basic solutions and dissolve at high rate in neutral and acidic media [43]. In contrast, aluminum alloys are usually stable in neutral media and unstable in both basic and acidic solutions.

### 2.8.1 Corrosion of magnesium in aqueous solutions

With some exceptions, pure magnesium has no appreciable corrosion at room temperature unless water is present. The dissolution of magnesium in water usually proceeds by an electrochemical reaction with water to generate magnesium hydroxide and hydrogen gas. Such a mechanism is relatively insensitive to the oxygen concentration, even though the oxygen is a major factor in atmospheric corrosion. [44]. Reaction 2.1 describes the probable over reaction:



This net reaction could be expressed as a sum of the following partial reactions:



The reduction process of hydrogen ions and the hydrogen overvoltage of the cathode play an important role in the corrosion of magnesium. Low overvoltage cathodes facilitate hydrogen evolution, causing a substantial corrosion rate.

### 2.8.2 Corrosion by atmosphere and solutions

The corrosion behaviours of magnesium alloys are similar to the pure magnesium, as shown in reactions 2.1 ~ 2.4. Basically, magnesium alloy has better corrosion resistance than pure magnesium. When magnesium alloying with Al, Mn or Zn that are exposed to the atmosphere, an analysis of films formed which shows an enrichment of the secondary constituents. It was suggested that air-formed oxide on Mg-Al alloys has a layered structure composed of MgO/Mg-Al-oxide/substrate, with the Mg-rich oxide becoming thinner with increasing in aluminum content. It is likely that this benefit of aluminum is related to the strong tendency for aluminum to form a stable passive film [44].

Lindstrom [45] studied the effect of NaCl and CO<sub>2</sub> on the atmospheric corrosion of magnesium alloy AZ91. The combination of high humidity and NaCl solution was a significant effect on the corrosion behaviour of AZ91. However, CO<sub>2</sub> inhibited atmospheric corrosion in the situation of with or without the presence of NaCl. In the absence of CO<sub>2</sub>, the main product was Mg(OH)<sub>2</sub> by localizing NaCl-induced corrosion. On the other hand, magnesium alloy AZ91 would suffer from general corrosion if CO<sub>2</sub> was presented and the carbonate-containing products would be formed. Mg<sub>5</sub>(CO<sub>3</sub>)<sub>4</sub>(OH)<sub>2</sub> was detected by XRD when NaCl was presented. It was suggested that a decrease in PH in the surface electrolyte and stabilizing alumina in passive film could cause the inhibitive effect of CO<sub>2</sub> [46].

### 2.8.3 Corrosion in Al<sub>2</sub>O<sub>3</sub> reinforced composites

The addition of an reinforcement into a magnesium alloy matrix could significantly improve the physical and mechanical properties, but a deterioration in the corrosion resistance could be raised.

Based on Hihara's study [47, 48], there were three possible reasons that could deteriorate the corrosion resistance of the MMCs:

1. Galvanic coupling of the reinforcement constituent and matrix alloy;
2. Formation of the interfacial phase between the matrix alloy and the reinforcement; and
3. Microstructure changes during the fabrication of MMCs.

Generally, the corrosion rates of the composite were higher than the matrix alloy. Also it has been found that 20% alumina fiber reinforced magnesium AZ91C based composite exhibited more susceptibility to corrosion in solutions containing chloride, in comparison with matrix alloy. The corrosion current density ( $I_{\text{corr}}$ ) of the composite was almost the same as the matrix alloy in low chloride-concentration solutions. However, the  $I_{\text{corr}}$  of the composite increased almost three times than the matrix alloy when the concentration of chloride was increased up to 3.5% NaCl.

## **2.9 Summary**

Metal matrix composites have been developed by applying the techniques of powder metallurgy, squeeze casting and stir casting. Most published studies are focused on aluminum based composites, reinforcing with either  $\text{Al}_2\text{O}_3$  fibers or other particles. However, limited work has been done on  $\text{Al}_2\text{O}_3$  fiber-reinforced magnesium-based composites. There is no published systematic study, to date, disclosing the effects of fiber volume fraction on microstructure development, tensile properties and corrosion resistance of Mg-based composites reinforced with  $\text{Al}_2\text{O}_3$  fibers.

# CHAPTER 3:

## EXPERIMENTAL PROCEDURE

The experimented work included three main steps: the first part was to fabricate the alumina fiber preform. The second step involves pressure infiltration of magnesium alloy (AM60) by applying squeeze casting technique. Finally, mechanical property and microstructure evaluation were carried out. Figure 3.1 illustrates the general procedure for the experiment. The details of the experiment are discussed in the following sections.

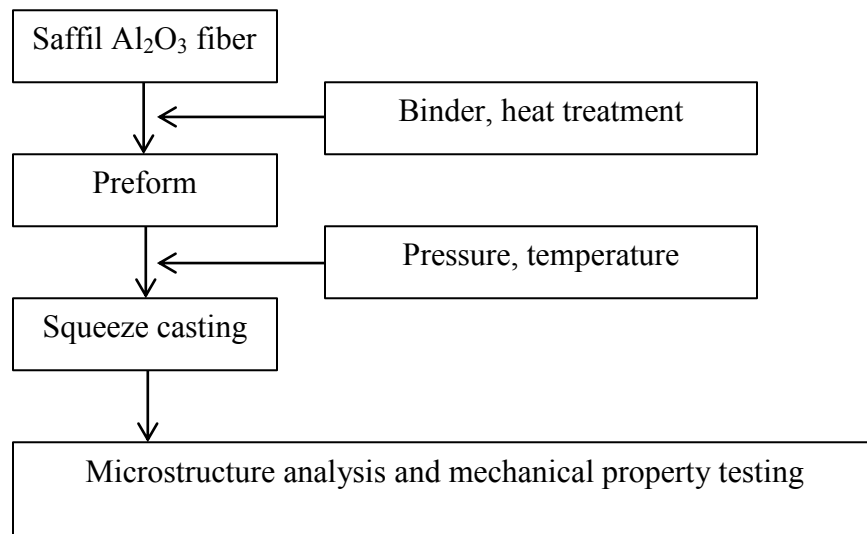


**Figure 3.1** Fabrication and characterization of Mg based composite.

## **3.1 Materials**

### **3.1.1 Saffil alumina fiber**

The material used to fabricate the preform was the Saffil<sup>®</sup> Al<sub>2</sub>O<sub>3</sub> short fiber due to its low cost and adequate properties. The fiber was characterized for their high purity polycrystallinity with an average diameter of 3.0 μm and length of 100 μm. The chemical composition and properties are shown in Tables 2.3 and 2.4, respectively. According to the physical property of the Al<sub>2</sub>O<sub>3</sub> fiber, the δ-Al<sub>2</sub>O<sub>3</sub> crystal structure was stabilized against transformation to α-Al<sub>2</sub>O<sub>3</sub> due to the presence of about 3~4% of SiO<sub>2</sub> [49]. The purpose of the SiO<sub>2</sub> was to inhibit grain coarsening of the fine Al<sub>2</sub>O<sub>3</sub> crystallites. Fiber volume fraction of 7, 11, 22, and 35% were selected for the composite fabrication. There was a high-speed blender process involved to release the aggregation of the fiber.

### **3.1.2 Magnesium alloy**

The matrix alloy was magnesium alloy AM60 with the chemical composition (wt.%) of 6.0Al-0.22Zn-0.4Mn-0.1Si-0.01Cu-0.004Fe-0.002Ni-Mg due to its wide usage in the automotive industry and excellent ductility. The thermophysical properties of the matrix alloy (AM60) are listed in Table 3.1.

**Table 3.1** Thermophysical properties of magnesium alloy AM60

Material	AM60
Elasticity modulus (GPa)	35-44
Density (g/cm <sup>3</sup> )	1.74
Heat expansion coefficient (10 <sup>-6</sup> k <sup>-1</sup> )	45
Specific heat (J Kg <sup>-1</sup> k <sup>-1</sup> )	1250
Thermal conductivity (W m <sup>-1</sup> k <sup>-1</sup> )	85

### 3.2 Preform fabrication

Preform fabrication is the first and important step of squeeze casting technique to achieve the final composite. The preform method can reach to a wide volume fraction and with no agglomeration of the reinforcement during casting, in comparison to the particulate reinforcement. The process of making preforms with different fiber volume fraction was developed. Five different preforms were chosen to develop the composites with 7, 9, 11, 22, and 35 Vol%. Figure 3.2 shows a schematic illustration of the preform fabrication procedure. The required amount of fibers for different volume fractions was accurately weighed and dispersed in water with the help of low speed stirring. The mixture of fiber and binders were then poured in a container and the excessive water was filtered pressure. The rest of the content was then put into a cylindrical mold to shape the preform under pressure. The preforms were dried for 24 hours in air before being put in an oven for heat treatment to achieve the maximum possible strength. The dimensions of the preforms were of  $\varnothing$  100x 25mm.



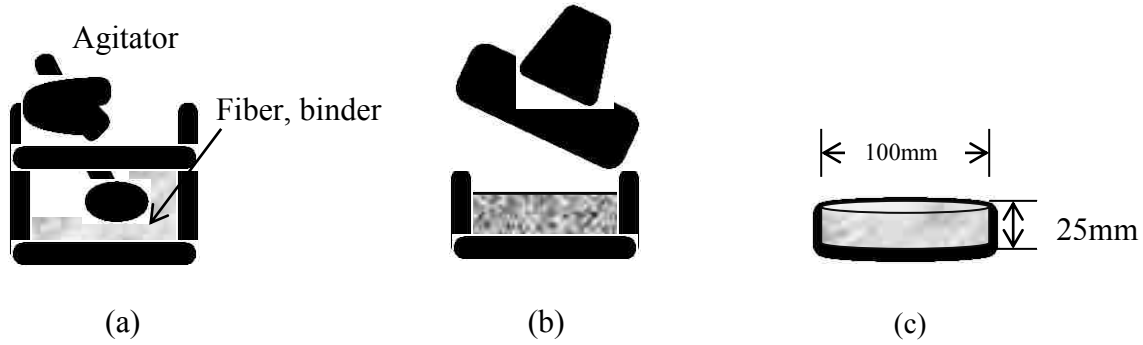


**Figure 3.2** Procedure for alumina fiber preform fabrication a) blending fiber with binder, b) molding, and c) drying and baking.

To reach the desired fiber volume fraction of the preform, the porosity of the preform was calculated based on the following equation [50]:

$$\rho_p = 1 - \frac{\rho_f}{\rho_m} \quad (\text{Eq 3.1})$$

where  $\rho_p$  is the porosity of the preform,  $\rho_f$  is the density of the preform (weight of reinforcement/preform volume), and  $\rho_m$  is the density of the reinforcement material ( $\text{Al}_2\text{O}_3$  fiber). To achieve the desired the volume fraction, as the volume of the preform was fixed, the key was to control the weight of the fiber.

### 3.3 Fabrication of composites

The previous study pointed out [51] that the capillary force could not ensure complete elimination of void with an array of fiber, even when a ceramic was perfectly wetted with zero contact angles. The application of external pressure (squeeze casting) is thus necessary for liquid metal to infiltrate into the preform. All the squeeze casting experiments, including both of the composites and magnesium alloy AM60, were carried out on a 75-ton, vertical hydraulic press as

shown in Figure 3.3 (a). The alloy melting was performed in an electrical resistance furnace, which was protected by gas system, Figure 3.3 (b). The use of the protective gas mixture was to prevent the melt from oxidation and burning. The gas mixture employed was the Sulfur Hexafluoride (SF<sub>6</sub>) 0.5% +CO<sub>2</sub> in balance. SF<sub>6</sub> is a high-density gas mixture which was much higher than air and oxygen. It can entirely cover the melt and separate the melt from air to avoid oxidization. Table 3.2 lists the density of SF<sub>6</sub> in comparison with other gases such as CO, air, O<sub>2</sub>, CO<sub>2</sub> and argon. The flow rate of the gas was set to the range of 0.8-1.0 L/min with the outlet pressure of 20~25 psi during the alloy melting.

All tools, such as skimming rods, crucible handle were preheated before contacting with the magnesium melt. The purpose of preheating was to eliminate the moisture to avoid a reaction between the moisture and the molten magnesium.

**Table 3.2** Density comparison of different gases

Gas	Carbon monoxide	Air	Oxygen	Argon	Carbon dioxide	SF <sub>6</sub>
Density (Kg/m <sup>3</sup> )	1.25	1.29	1.31	1.784	1.80	6.27



(a)



(b)

**Figure 3.3** a) A75-ton, vertical hydraulic press, and b) Electric furnace with SF<sub>6</sub> gas protection .

During casting, the safety procedures must be followed since magnesium alloys are very active. It can easily react with water or concentrated chemical reagents and initiate a chemical reaction that produces hydrogen gas and create hazardous explosion in the present of a heat source or an open flame. The moisture in the tools can be transformed into high-temperature and high-pressure vapor that might cause explosion. To minimize the possibility of injury from the possible hazard, the following safety procedures must be followed at all times:

1. Ventilation system in the lab is ON;
2. Protection gas on the melt is ON;
3. Safety hats with full face shield, safety shoes, lab coat and leather gloves must be worn at all times;
4. Tools must be preheated;

5. Fire extinguisher must be easily accessed; and
6. At least two trained student in the lab when conduct an experiment.

During squeeze casting the upper and lower molds were preheated to 300 °C. Before placing the preform into mold, the preform was preheated to 750 °C. Then, the molten matrix alloy AM60 with temperature of 760 °C was infiltrated into the preheated preform under an applied pressure of 90 MPa. The pressure was hold for 25 seconds. The heater for the mold was quickly turned off after the pressure withdrawal in order to cool the mold as soon as possible. After solidification, a cylindrical composite coupon was ejected. All of the 7, 11, 22 and 35 vol% composites were fabricated in the same procedure. Figure 3.4 illustrates the fabrication process of the fiber-reinforced composite by using the squeeze casting technique.

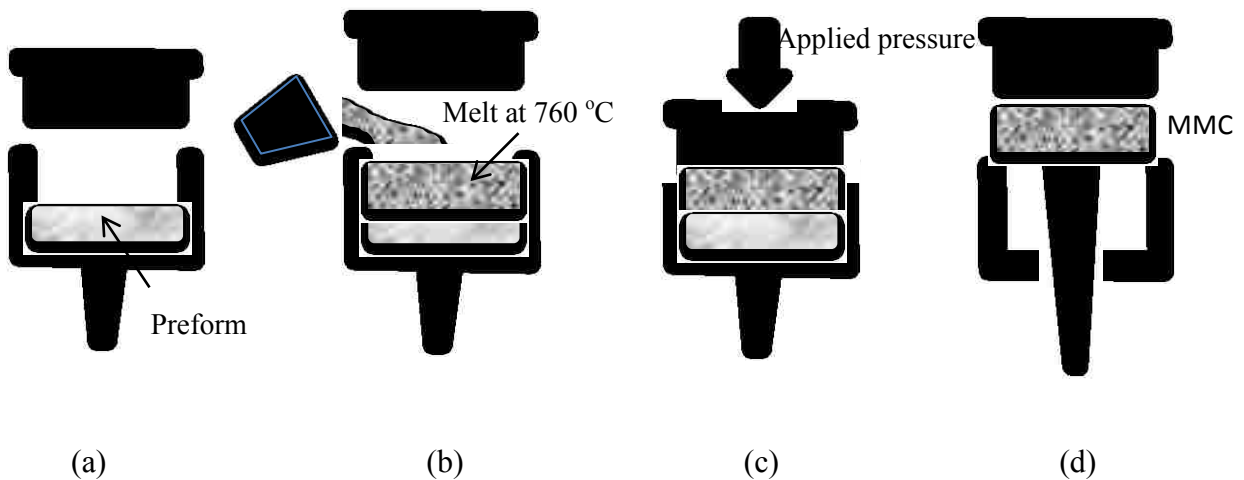
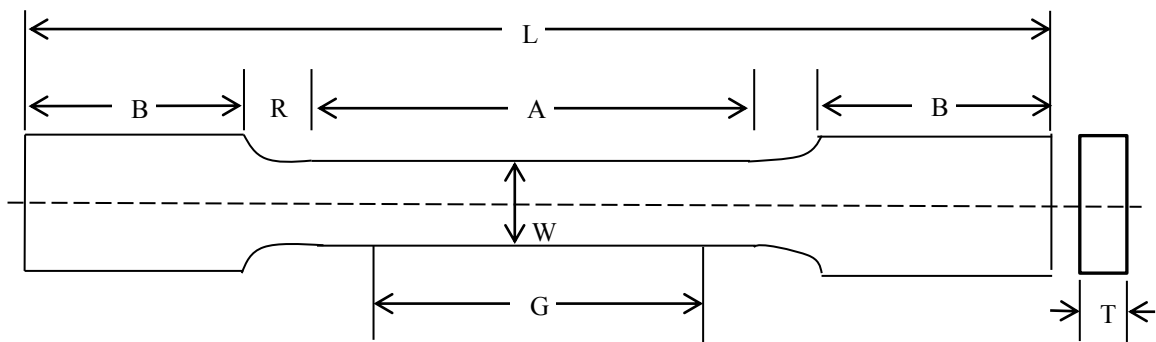


**Figure 3.4** Schematic diagram of the squeeze casting procedure a) placing preform into the mold, b) pouring melt into the mold, c) applying pressure and d) composite is produced.

### 3.4 Tensile testing

Tensile testing was carried out to evaluate the mechanical properties of the composites. The testing was performed on an INSTRON machine equipped with a computer data acquisition system, at room temperature. The tensile specimens were machined according to ASTM B557 [52], as shown in Figure 3.5. Total four tensile specimens can be cut from each composite coupon. The tensile bars were 25 mm in gage length, 6 mm in width, and 10 mm in thickness. The tensile properties, including yield strength (YS), ultimate tensile strength (UTS), and elongation to failure ( $E_f$ ), were obtained. There were four tensile specimens cut from each composite coupon with different fiber volume fractions. The final tensile results were calculated from the average of these four results for each composite. Figures 3.5 and 3.6 show the tensile specimen and the INSTRON tensile machine, respectively.



**G:** gage length  $25 \pm 0.1$  mm

**W:** width  $6 \pm 0.1$  mm

**T:** thickness  $6 \pm 0.1$  mm

**R:** radius of fillet, 6mm

**L:** overall length 100mm

**A:** length of reduced section 32 mm

**B:** length of grip section 30mm

**Figure 3.5** Schematic illustration of tensile specimen.



**Figure 3.6** INSTRON tensile machine (Model 8562).

### **3.5 Microstructure analysis**

To characterize the fiber-matrix interface and the alloy structure of the composite, optical and scanning electron microscopic (SEM) observation were performed, as shown in Figure 3.7. A Buehler optical image analyzer 2002 system was used for determining the primary characteristics of the composite. The detailed features including intermetallic phase morphology, composite fiber-matrix interface and fracture behaviors, were characterized at higher magnification by JSM-5800LV SEM, which had a maximum resolution of 100 nm in a backscattered mode and maximum useful magnification of 30,000X. Before placing the samples into the SEM, they were coated with Au and a copper tape was used on the surfaces to enhance the sample conductivity to eliminate the surface charging.



(a)



(b)

**Figure 3.7** a) Scanning electron microscopy (JEOL Model JSM-5800LV), b) Buehler optical image analyzer model 2012.

Samples were mounted and ground by 240, 400 and 600 grit paper, followed by polishing with 1 and 0.5 micron diamond solution, which was alcohol-based. During polishing, water was avoided because magnesium and its alloys are susceptible to corrosion by contacting with water. To ease microstructural observations of composite samples under SEM, an etchant was applied to the polished specimens, which was 5% Nitric acid ( $\text{HNO}_3$ ).

### 3.6 Heat treatment

The type of heat treatment, T4, was conducted on both of the unreinforced alloy AM60 and fiber reinforce composite to evaluate the behavior of changing in grain size. T4 is designated as solution heat treatment and it is a common heat treatment for magnesium castings and wrought products. The heat treatment was conducted in an electric furnace. To prevent the samples oxidized when exposed to air, there were two methods carried out. One way was to add an inert gas ( $\text{SF}_6$ ) directly into the furnace. Another way was to place the samples in a steel cup and cover the samples with sand and preventing the sample exposing to air.

### 3.7 DSC analysis



**Figure 3.8** A Differential Scanning Calorimetry-Thermogravimetric Analyzer (DSC-TGA Q600).

Differential Scanning Calorimetry-Thermogravimetric Analyzer (DSC-TGA Q600) was used for thermal analysis as shown in Figure 3.8. Before running the experiment, the alumina sample cup (crucible) was preheated to eliminate the moisture and the residue left on the surface. During the experiment, argon gas was used at flow rate of 100 ml/min to prevent specimens' contamination from the measurement beams and also prevent the oxidation. The heating and cooling rate for all DSC tests were set to be 20 °C/min and over the temperature range of 50–800 °C. After the heating cycle, the samples were air cooled by nitrogen gas. To ensure the accurate running, the SDT Q600 TA Instrument was calibrated for TGA weight, DTA baseline, temperature, and DSC heat flow. Beside the alumina cup with specimens, there was an empty reference cup. Before or after each DSC tests, a baseline run was necessary by running a separate test with two empty and clean alumina cups on the sample and reference beams. The DSC trace was then calibrated by subtracting the baseline.



### 3.8 Corrosion test

Electrochemical tests were carried out by using EC-LAB SP-150 electrochemical apparatus with corrosion analysis EC-lab software, as shown in Figure 3.9. A three-electrode cell was used for all tests. The prepared samples were set to be the working electrode, Ag/AgCl/sat'd KCL electrode as a reference electrode and Pt metal electrode as counter-electrode. For all of the experiment, 3.5% NaCl solution was prepared (salt mixing with deionized water). At the beginning of the test, samples were immersing into the salt solution to allow the open circuit potential to settle to a constant value. Potentiodynamic polarization scans were conducted at a rate of 10mv/s form  $-0.5\text{v}$  versus open circuit potential in a more noble direction up to  $0.5\text{v}$  versus the reference electrode. All samples for corrosion tests were cut from the center of the coupon. All samples were ground by using silicon carbide papers with grades 240, 600 and 2500 grits. Then the samples were cleaned in acetone, rinsed with deionized water and dried before the potentiodynamic polarization.



**Figure 3.9** EC-LAB SP-150 electrochemical apparatus for corrosion test.

# CHAPTER 4:

## EXPERIMENTAL RESULTS

### 4.1 Squeeze casting

#### 4.1.1 Casting parameters determination

Studies on squeeze casting of magnesium alloys are mainly focus on the most common magnesium alloy AZ91. The alloy AM60 has similarities with AZ91 that both belong to Mg-Al series, which provides the basis to determine the casting parameters. However, the parameters have to be modified to obtain fiber reinforced composites.

There are some important casting parameters that have the greatest influence on the microstructure and mechanical properties, which include the alloy melting temperature, pouring temperature, the mold temperature, preform temperature and the pressure. When the melt is poured into the mold, the alloy is superheated above its melting point. The superheat temperature is necessary because the time to transfer the melt from the furnace to the mold and the total solidification time need to be considered. It is very critical to determine the superheated temperature. If the temperature is too low, it may cause inadequate fluidity of the melt. On the other hand, if the temperature is too high, it probably increases the risk of the melt oxidation. The experiment showed that the melt temperature dropped immediately after pouring into the mold when the melt temperature, mold temperature, and preform preheated temperature were set at 720 °C, 300 °C, and 400 °C, respectively. The infiltration under a semi-solid state was

incomplete and the preform was destroyed. Basically, the normal superheat temperature for the magnesium alloys were 30~140 °C above the melting temperature of the alloy. Changing the temperature of the mold and the preform was an alternative way to ensure the complete infiltration in the liquid state. When the temperature of the preform was 400 °C much lower than the alloy melt temperature, the alloy solidified rapidly and it was difficult for a semi-solid to reach to the bottom of the preform. Thus, the preform temperature was adjusted to the 750 °C that was slightly higher than the melt temperature, 720 °C. However, the temperature of the mold cannot be higher than 400 °C because it has been reported that a very high mold temperature (>400 °C) caused hot spots and shrinkage pores in the casting [53].

For complete infiltration, a minimum pressure of 70~105 MPa was required to eliminate the gas porosity and shrinkage for the simple shaped nonferrous metals. For other complex shapes and thin sections, the pressure of 140~210 MPa was necessary. However, a successful fabrication of MMCs with the pressure of 30 MPa was also reported [54]. Raising the pressure can provide the benefits of grain refinement and improved mechanical properties. On the other hand, the added benefits have to be weighed against the high costs due to the application of high pressures and high temperatures. By considering the facts given above, the magnesium matrix composites were casted under the conditions of 720 °C, 750 °C and 90 MPa for the melt temperature, preform temperature and pressure, respectively.

#### **4.1.2 Appearance of the preform**

The preform fabrication procedure is critical and the quality of the preform directly influences the properties of the composite. The preform fabrication procedure was optimized from Qiang's work [55]. However, there was a modification when fabricating the preform with low fiber

volume fraction of 7%. A fugitive corn flour was mixed with the fibers during agitation. The purpose of this additive was to achieve the desired thickness of the preform during the shaping procedure. Then, the corn flour was burned out without leaving any residues as the preform was fired. Figure 4.1 illustrates a preform with a fiber volume fraction of 9%.

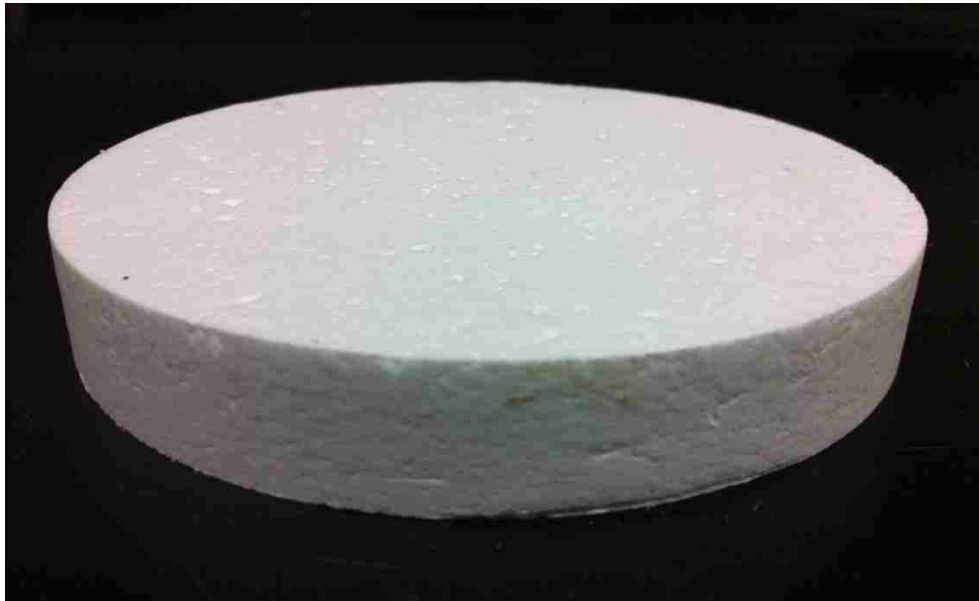


**Figure 4.1** A preform with fiber volume fraction of 9%.

#### **4.1.3 Appearance of cast composites**

Figures 4.2 and 4.3 illustrates the infiltration process and a squeeze cast sample of the composite, respectively. By observing the appearance of the sample, it can be conclude that the preform deformed due to compression. The vertical cross sections of the alumina fiber reinforced composite are shown in Figure 4.2. The height of the preform was 25mm before the infiltration as shown in Figure 4.2 (a). The height of the composite was divided into two areas after infiltration took place, as shown in Figure 4.2 (b). The area around the edge of the preform decreased. However, the height at the central area remained to be 25mm.

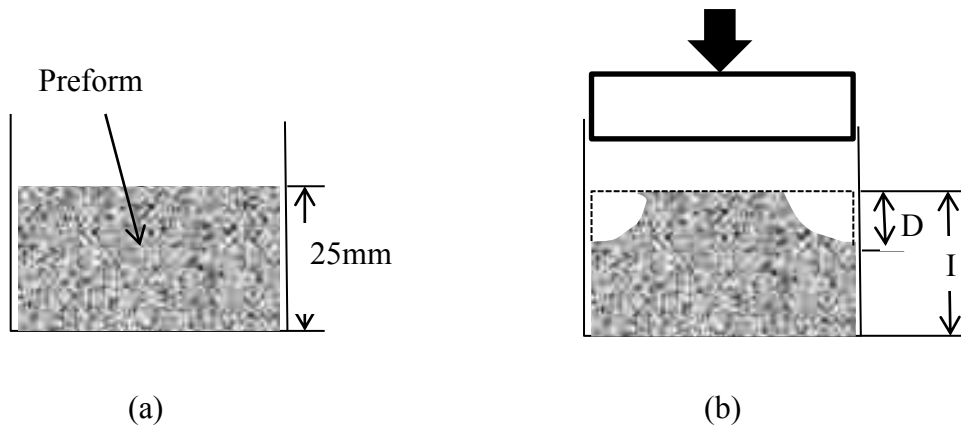


**Figure 4.2** Schematic description of preform deformation by squeeze casting, preform was preheated to 750°C before place into mold, a) before, b) after pressure infiltration. [D]: deformed height, [I]: original height.



**Figure 4.3** A squeeze cast magnesium matrix composite (AM60/ Al<sub>2</sub>O<sub>3</sub>).

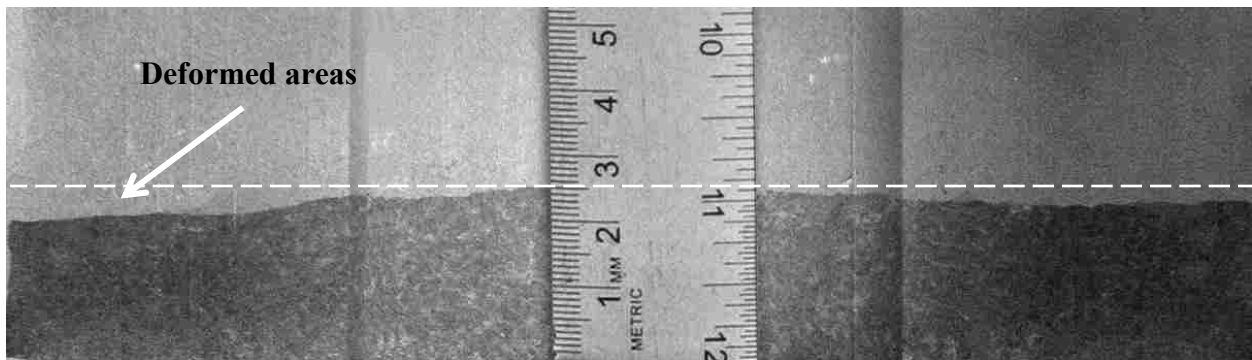
It can be seen from Figure 4.2 that the height around edge was decreased, in comparison with the central area. However, it was determined that the preform deformation under compression was

unavoidable. It has been shown [56] that compressive deformation occurs if the applied pressure is high than the compressive strength of the preform.

The degree of the deformation depends on the applied pressure, the pressure holding time, the viscosity of the melt, and the strength of the preform. In comparison between the preforms with 7, 9, 11, 22 and 35% fiber volume fraction, the 7vol% preform deformed more than 35 vol%. This may be explained by the strength of the preform. The fibers served as the supporting frame in the preform. As the amount of fiber increased, the strength required to overcome the compression increased. Figure 4.4 shows the cross-sections of the composites with fiber volume fractions of 7% and 35%, respectively.



(a)



(b)

**Figure 4.4** Composite cross-sections showing the deformations of preforms under pressure, (a) composite with 7% fiber volume fraction, and (b) composite with 35% fiber volume fraction.

## 4.2 Microstructure analysis

### 4.2.1 Magnesium alloy AM60

In the as-cast condition, there were no noticeable casting defects on the surface of the casting by visual observation, as shown in Figure 4.5 (a) which was taken by the optical microscope. A closer observation by SEM combined with EDS showed that the microstructure consisted of primary  $\alpha$ -Mg (A) with divorced intermetallic eutectic phase  $\beta$ -Mg<sub>17</sub>-Al<sub>12</sub> (B), as shown in Figure 4.5 (b). The precipitates were hard and brittle which had certain contribution to the hardness of the alloy. Figure 4.6 shows the EDS analysis of the phases of the alloy that were indicated by the letter A and B in Figure 4.4 (b).

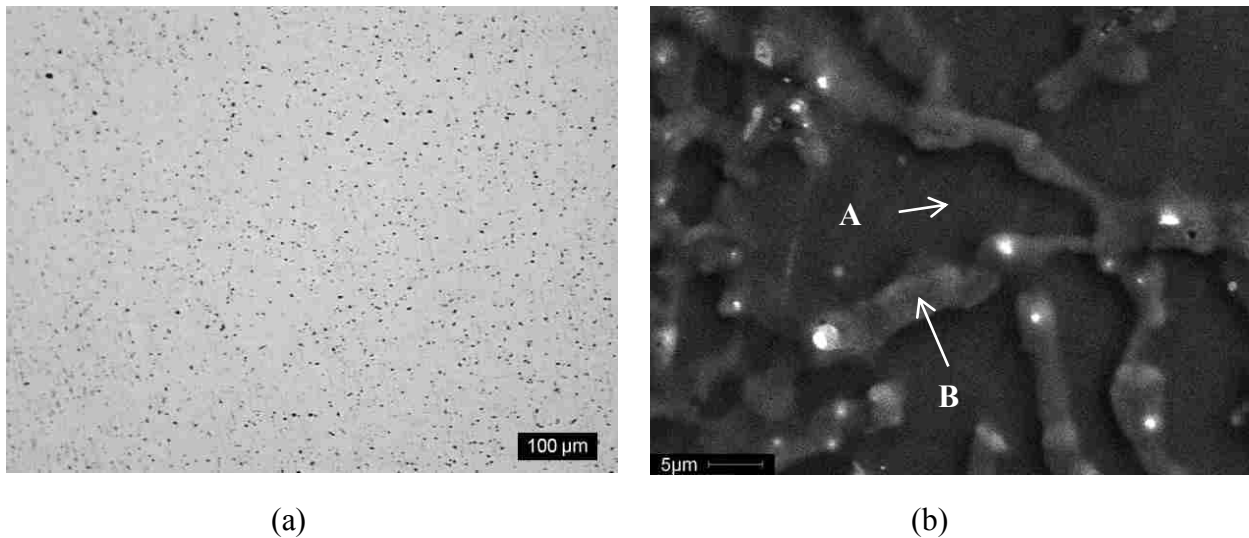
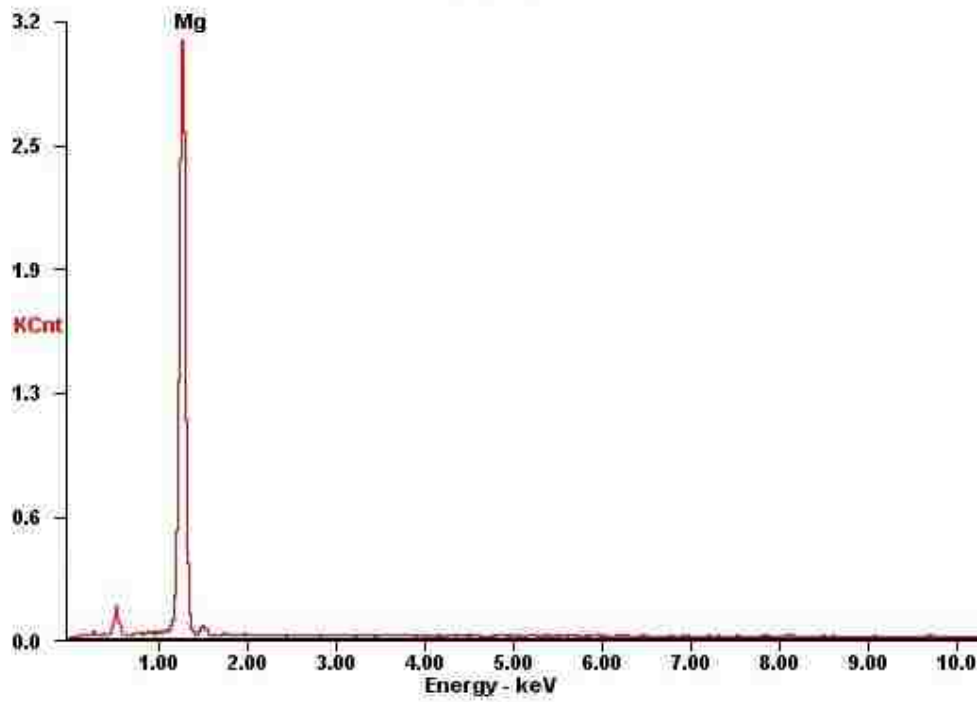
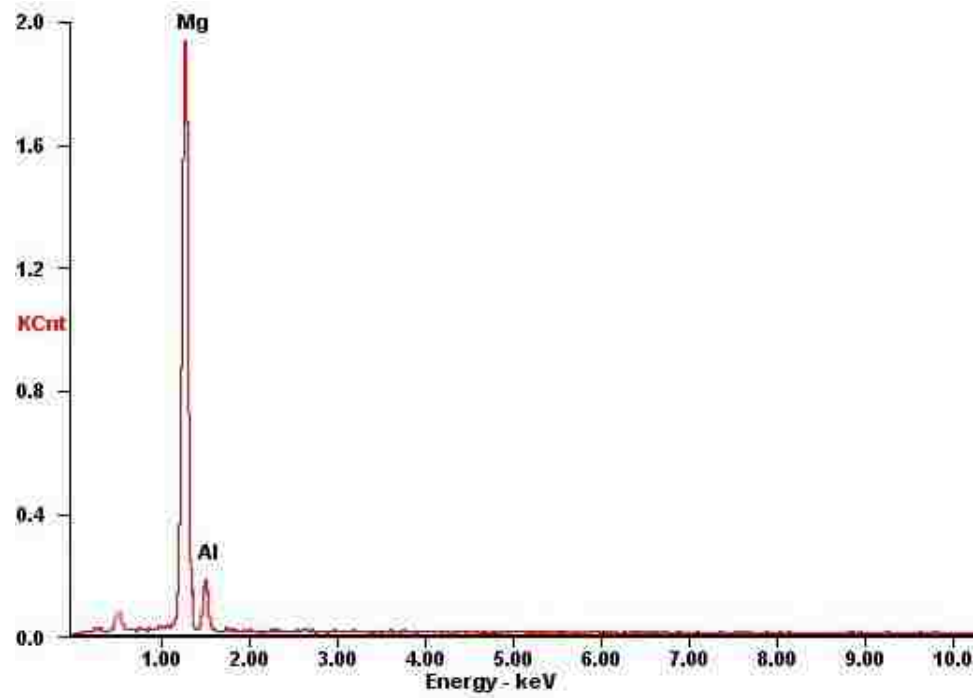


**Figure 4.5** Optical (a) and SEM (b) micrographs of as-cast AM60.



(a)



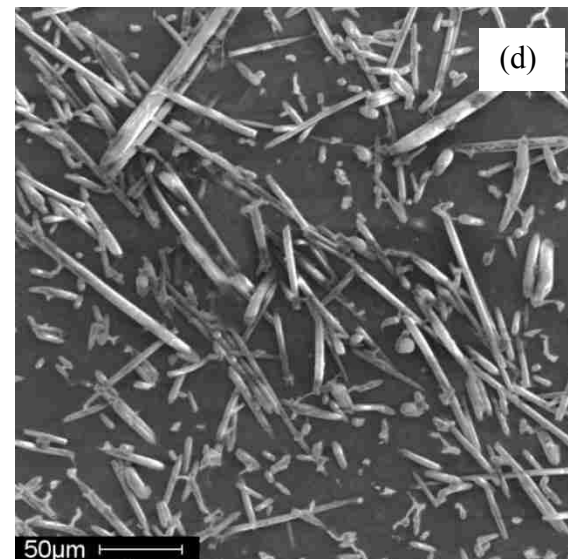
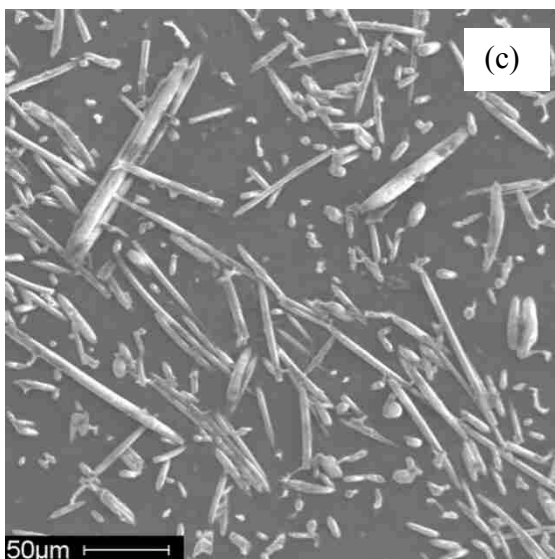
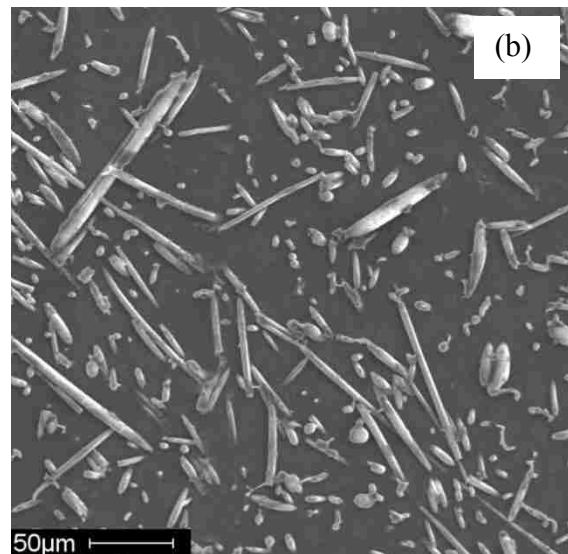
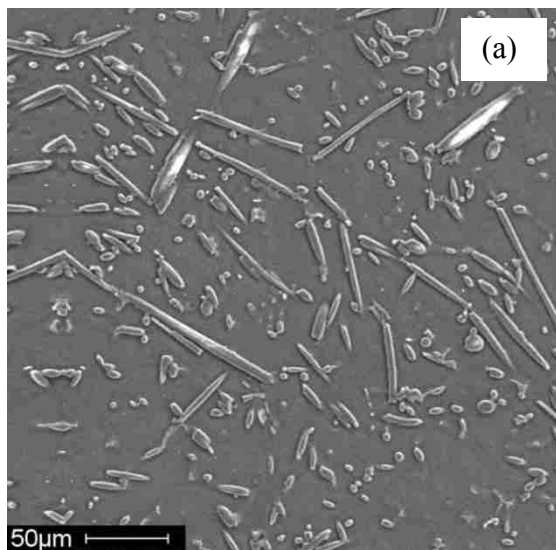
(b)

**Figure 4.6** EDS analysis of the matrix alloy AM60, (a) primary  $\alpha$ -Mg, and (b)  $Mg_{17}Al_{12}$  intermetallic.



#### 4.2.2 Magnesium matrix composites

Squeeze casting of the composites with the reinforcement of 7%, 9%, 11%, 22% and 35% fiber volume fractions was conducted under the same condition as the AM60 to investigate the variation in microstructure and mechanical properties with different fiber volume fractions. To ensure the fibers were uniformly distributed in the composite, the composites samples were etched at the different time periods to allow the fibers to reveal their distribution at different depths of the composites, as shown in Fig 4.7.



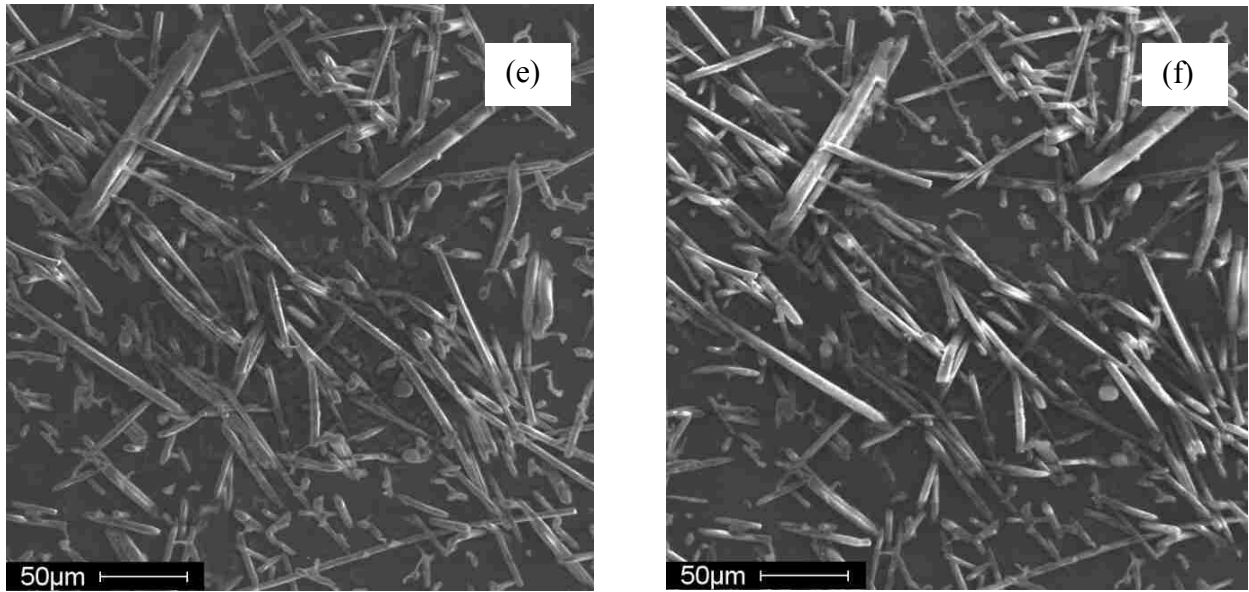


**Figure 4.7** Composite sample etched by (a) 10s, (b) 30s, (c) 50s, (d) 70s, (e) 90s, and (f) 110s.

As shown in Figure 4.7, the fibers were distributed in a random and isotropic orientation and no agglomeration observed. This uniformity of the fiber distribution provided great contribution to the mechanical properties of the magnesium matrix composite. Figure 4.8 shows the orientation of the fiber before and after the infiltration. As illustrated, the orientations of the fibers were unchanged and fibers were not deformed even after the application of the high pressure.

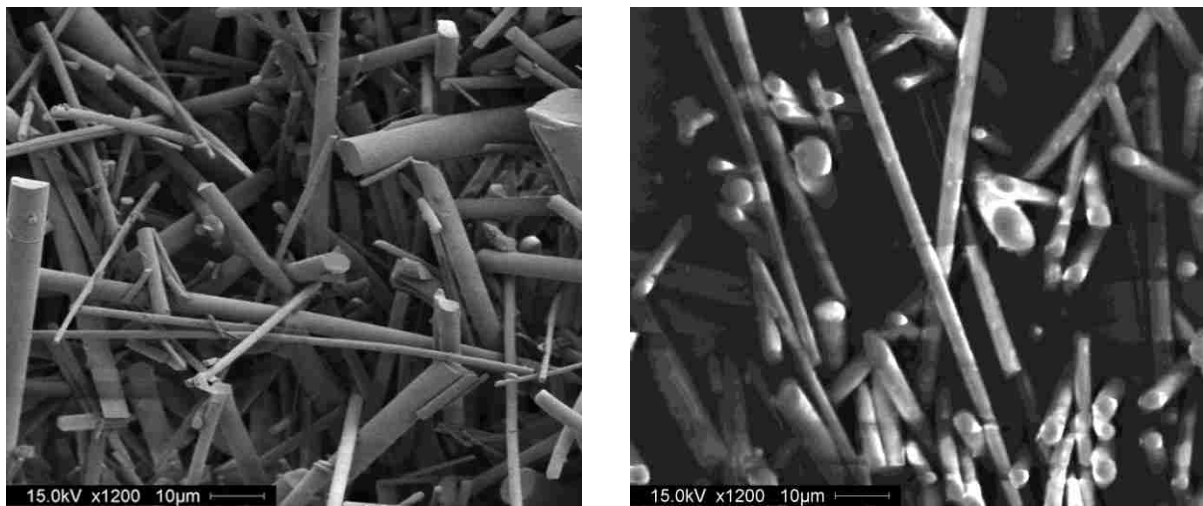


**Figure 4.8** SEM showing the orientation of the fiber before (a) and after (b) the infiltration.

#### 4.2.2.1 Fiber/matrix interface

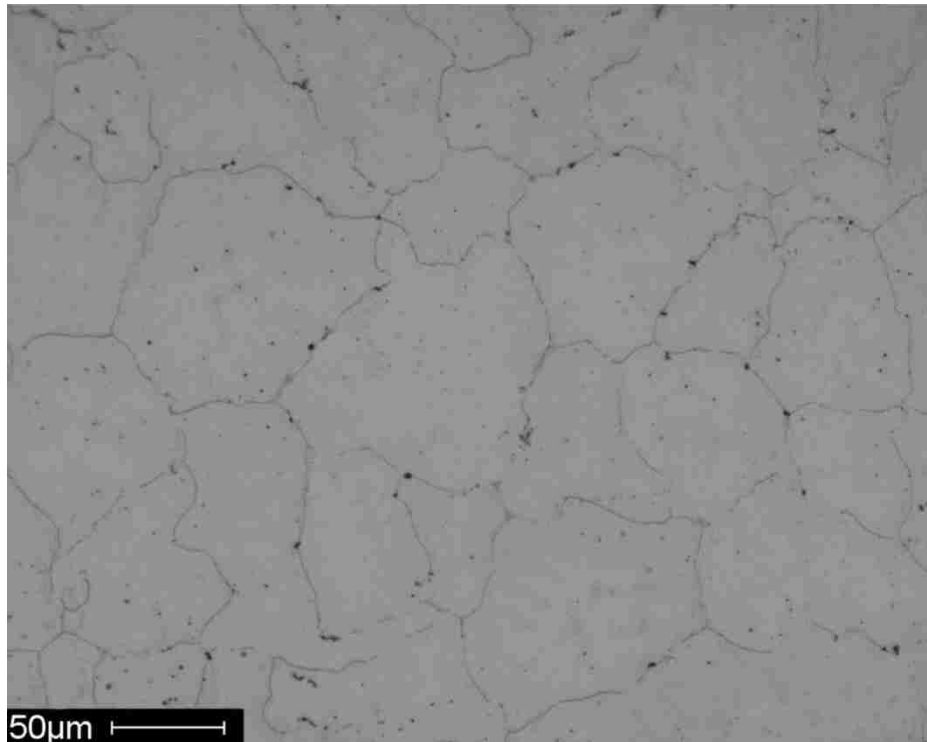
The interface formed between the fiber and the liquid metal can be mechanical bonding and physical adsorption [57, 58]. They are mainly from the mechanical interlocking between the matrix and fiber network. Also, chemical reactions could occur to form chemical bonding at the fiber/matrix interface. The interface has a strong influence to the properties of the composites. The interface of the matrix and the fiber was investigated with SEM. Figure 4.9 shows the high magnification SEM photograph that illustrated good bonding between the fiber and the matrix. The interface was sharp and clean without any visible interaction zone. Also, there was no void observed around the interface. It was indicated by Cappelman [58] that the only and most likely reaction on the interface was the formation of MgO, which could occur when the melt infiltrated into the preform and oxygen might be entrapped in the melt.



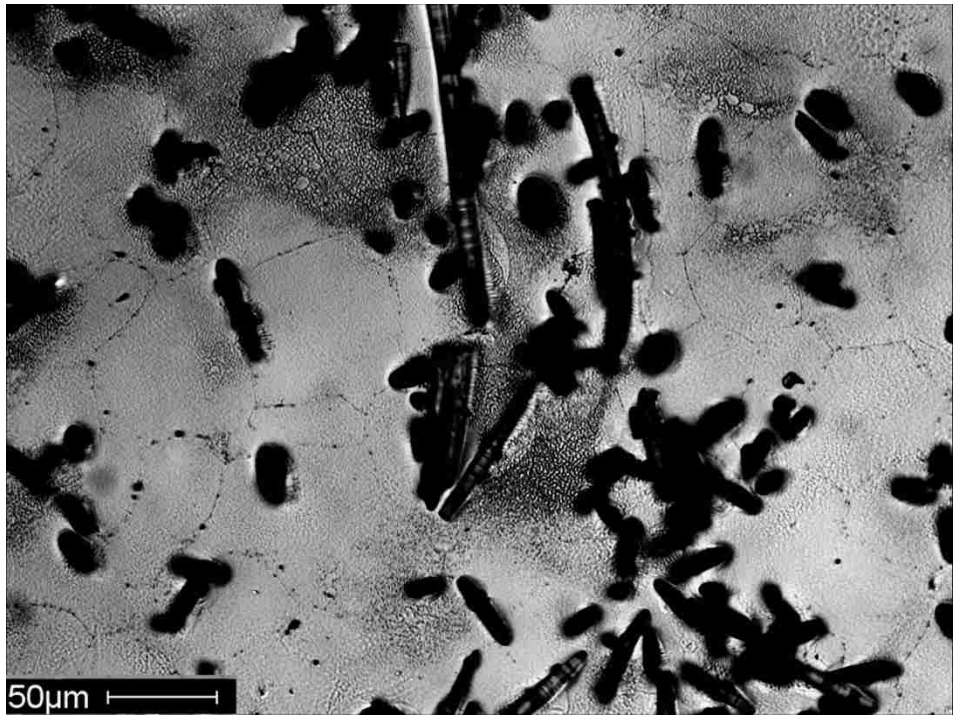
**Figure 4. 9** SEM showing the interface between the fiber and the matrix for the composite with fraction of 9 vol%.

### 4.2.3 Grain structure

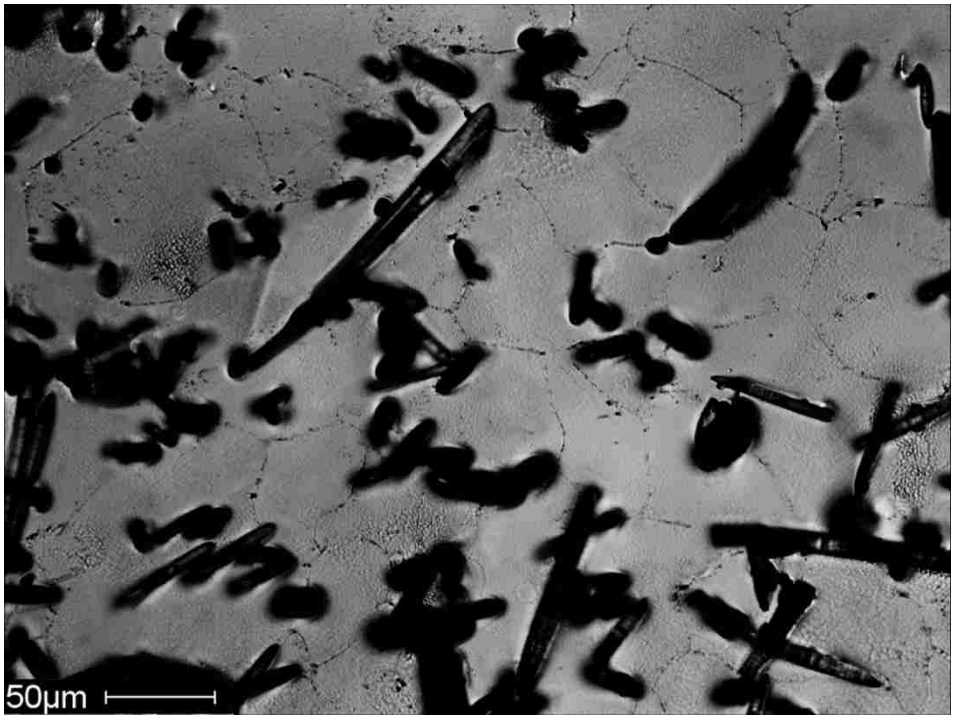
An evident difference in grain sizes was found, in comparison between the unreinforced alloy and the composites with the fiber volume fractions of 7%, 9%, 11%, and 22%. The change in grain size implies that the addition of fibers led to a finer grain structure in the composites. Figure 4.10 shows the grain structure of the unreinforced alloy AM60 and the composites reinforced with the fibers of the volume fractions of 7%, 9%, 11% and 22%. The grain size measurement for unreinforced alloy AM60 and its composites reinforced with different volume fractions of fibers are given in Figure 4.11. It can be seen from the Figure 4.10 (e) that the grains in the composites with 22% of fibers were mostly covered by the fiber, which made the grain size measurement impossible on a base of statistics.



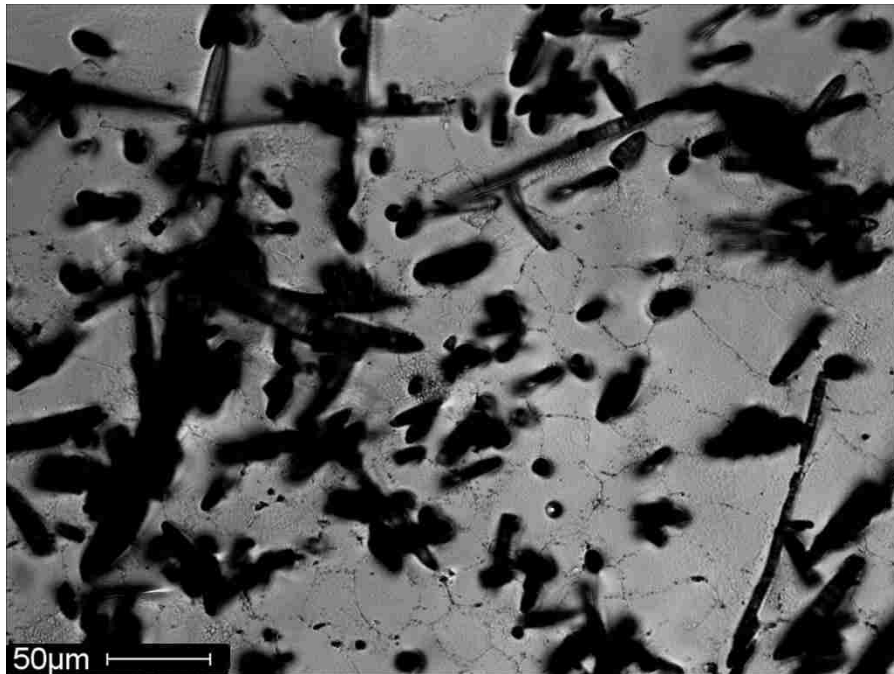
(a)



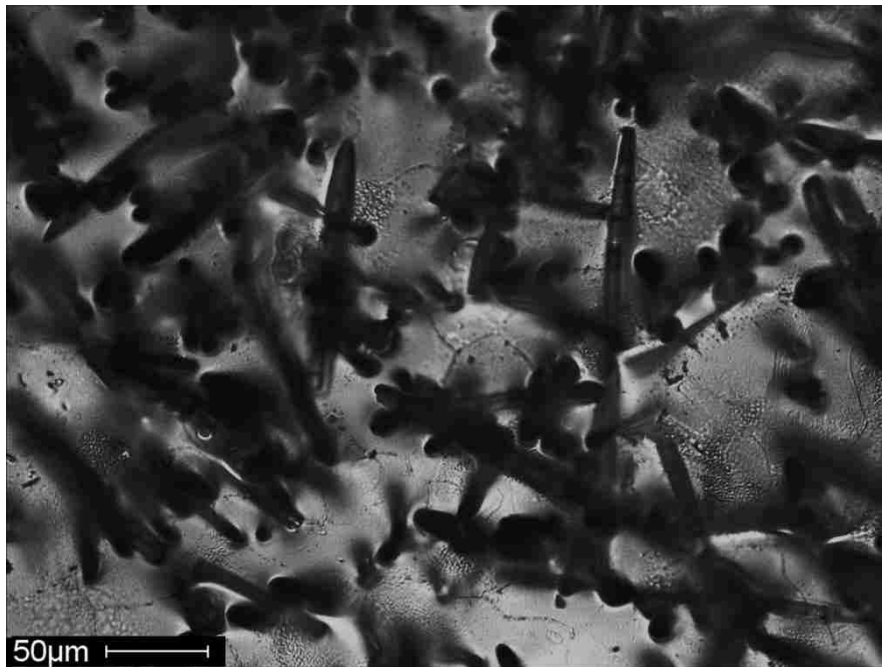
(b)



(c)



(d)



(e)

**Figure 4.10** Optical micrographs showing grain structure of, (a) unreinforced AM60 matrix alloy, (b) 7%, (c) 9%, (d) 11% and (e) 22% fiber reinforced composites (all are under T4 condition), respectively.

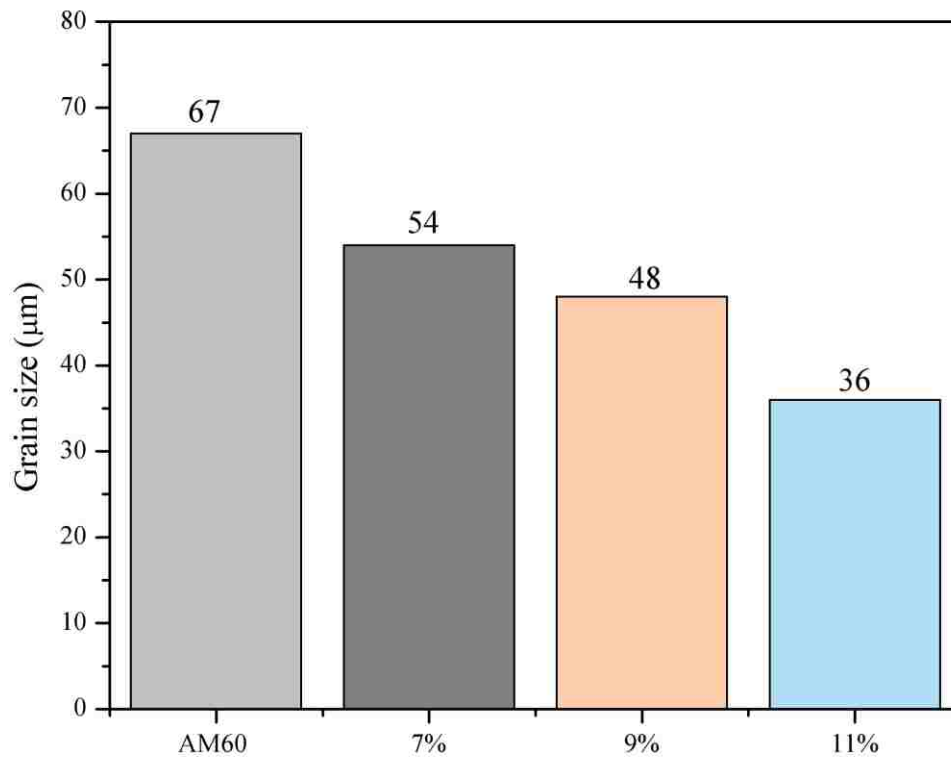


**Figure 4.11** Measured grain size of the matrix alloy AM60 and its composite with fiber volume fraction of 7%, 9% and 11%.

As can be seen from Figure 4.11, the grain size of the composites decreased significantly and the grain size distribution became more homogeneous after the addition of the fiber. The grain size decreased from 67 µm for matrix alloy AM60 to 36 µm for 11% fiber reinforced composite. It has been found [59] that the change in grain size can influence dislocation movement as well as the yield strength. As the grain size decreases, more grain boundaries become available to impede the further dislocation propagation, since more energy is required for a dislocation to change directions and move to the adjacent grain. As shown in Figure 4.11, the grain size of the matrix alloy decreased as the fiber volume fraction increased. It has been reported [60] that very small grain sizes might make the material brittle. The results relating to the mechanical properties will be discussed more in the succeeding sections.

#### 4.2.3.1 Grain refinement mechanisms

The microstructure observation has shown that the solidification behavior of matrix alloy AM60 was changed due to the presence of the reinforcing fiber. It can be seen from Figure 4.12 that most of the alumina fibers were located near the grain boundaries and some of them were present at the boundaries for the higher fiber volume fraction composites. The presence of the fibers around the boundaries may act as barriers to prevent the grains from growing further. As a result of the restriction of this growth, the primary phase would allow the melt to have enough time to form more nuclei, and then generate finer grain size in the solidified microstructure [61].

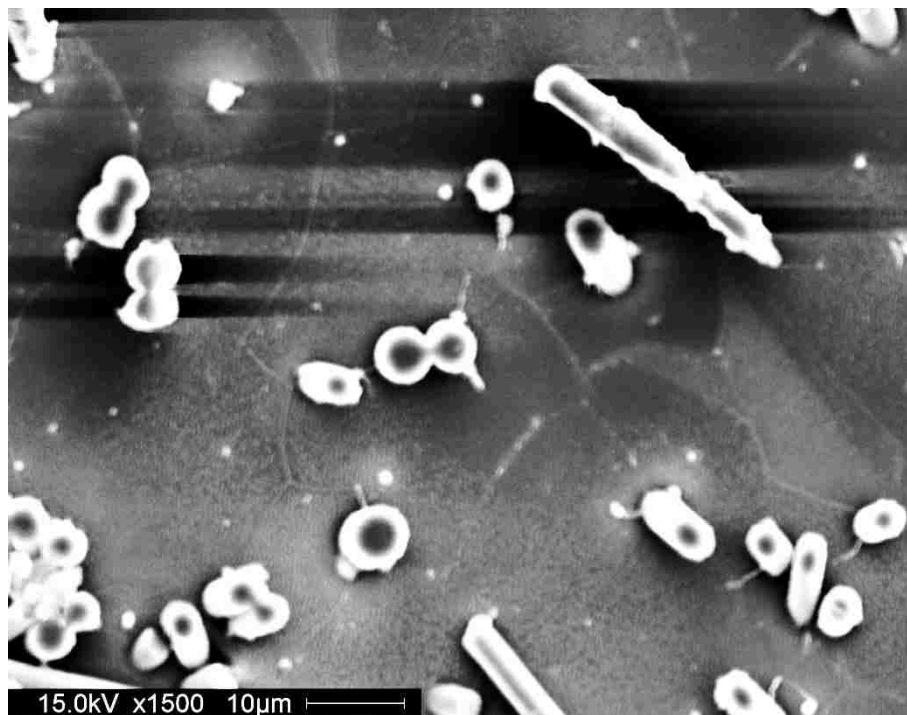


**Figure 4. 12** SEM micrograph showing the location of the alumina fibers for 11vol% composite. It is known that the alumina fiber has lower thermal conductivity and thermal expansion coefficient than the matrix alloy AM60. As a result, the magnesium melt near the alumina fiber would have lower cooling rate compared with the matrix alloy. And thus, the solidification of the



magnesium melt near the fiber could be retarded. The previous study [55] has shown that the fiber reinforced composite has higher liquidus temperature than the matrix alloy from re-melting the fiber reinforced composites. Then, the alumina fiber may not serve as a heterogeneous nucleation site for primary Mg. Nucleation of the primary Mg may take place in the space between the fibers. Table 4.1 lists the measured grain size of the fiber reinforced composites and the calculated average inter-fiber spacing based on Eq. 4.1. The comparison shows that the grains grew within the inter-fiber spacing. This indicates that the space between the fibers also can restrict the grain growth.

$$\lambda_f = \frac{(1-V_f)d_f}{V_f} \quad \text{Eq. 4.1}$$

Where  $\lambda_f$  is the inter-fiber spacing,  $V_f$  is the volume fraction of fiber and  $d_f$  is the diameter of the fiber.

**Table 4. 1** A comparison between the measured grain size of the composites and the calculated inter-fiber spacing

	Measure grain size ( $\mu\text{m}$ )	Calculated inter-fiber spacing ( $\mu\text{m}$ )
7%	54	66
9%	48	51
11%	36	40

#### 4.2.4 Solidification of magnesium matrix composites

Differential scanning calorimetry (DSC) analysis was carried out to measure the heat flows associated with transitions in the matrix alloy AM60 and its composites as a function of temperature in a controlled atmosphere. Figure 4.13 illustrates the typical heat flow curves for

the unreinforced matrix alloy AM60 and the composites with fiber volume fractions of 7% and 11%.

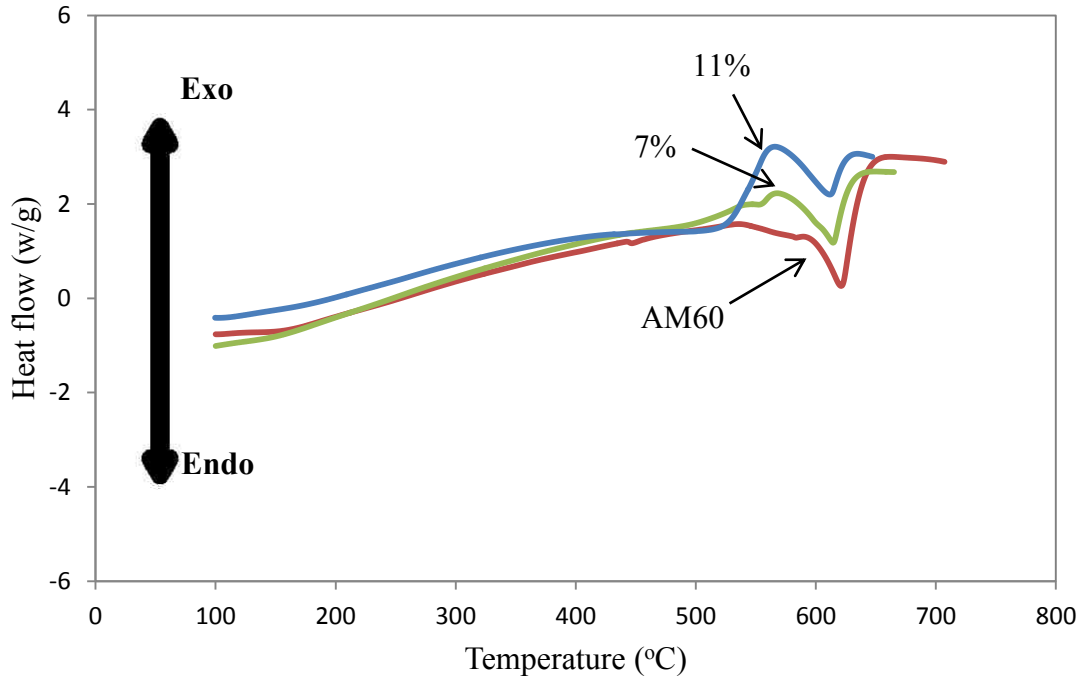


**Figure 4.13** DSC heat flow curves for magnesium matrix composite with fiber volume fraction of 7%, and 11% .

From Figure 4.13, the solidification temperatures of the matrix alloy AM60, the 7% and 11% fiber-reinforced composites were 617.1 °C, 608.4 °C and 601.4 °C, respectively. The peaks in Figure 4.13 generally describes the behaviours of the primary Mg phase in the matrix alloy AM60 and it composites. It is shown from Figure 4.13 that the peak shifted up as more fibers added to the matrix alloy. This observation indicates that less heat was needed to melt the magnesium in the composite of which more fibers and less magnesium were presented. Table 4.2 shows the calculated and measured results for the latent heat required to melt the Mg in the unreinforced AM60 alloy and the composites. The weight of the samples for calculation kept the same as the ones for DSC experiment. The heat absorbed by Mg and the latent heat to melt Mg

are decreased as the fiber volume fractions increased from 0% to 11%. The calculated results were basically agreed with the experimental results in the order of magnitude. The presence of the discrepancy should be at least attributed to the estimation of the reinforcement weight percentage for heat calculation.

**Table 4.2** Calculated and measured heat absorption and the heat needed for melting AM60 for unreinforced matrix alloy and composites with fiber volume fractions of 7%, and 11%

Fibre volume fraction	Sample weight (mg)	Fibre weight (mg)	AM60 weight (mg)	Heat absorbed by Fibre (J)	Heat absorbed by AM60 (J)	Total Specific Heat (J)	Latent heat for melting AM60 (J)	Measured Latent heat (J)
11%	18.7	3.55	15.14	0.00355	0.0189	0.0224	5.6505	1.1045
7%	20.3	2.53	17.76	0.00253	0.0222	0.0247	6.6260	3.0323
AM60	19.8	0	20	0	0.025	0.025	7.46	5.3598

### 4.3 Mechanical properties of the composites

#### 4.3.1 Hardness

Figure 4.14 illustrates the Rockwell hardness (HRB) as a function of fiber volume fraction for the unreinforced matrix alloy and the fiber reinforced composites. The preference of using Rockwell rather than Vickers hardness scale was due to the fact that the large indentation was capable of covering both the fiber and matrix alloy as one entire entity which ensures the consistency of the measurement. If the indent was too small, the areas were taken could be only either the reinforcements or the matrix alloy and consequently cause the large variation of the hardness values. From Figure 4.14, it is noted that the fiber reinforcement significantly increased the hardness as expected. The HRB hardness increased from 5.12 to 84.94 as the fiber volume fraction rose from 0% to 35%. This observation should be attributed to the presence of the

reinforcing fibers with their superior strength and stiffness. Besides, the reduced grain size also had contribution to the increase in hardness.

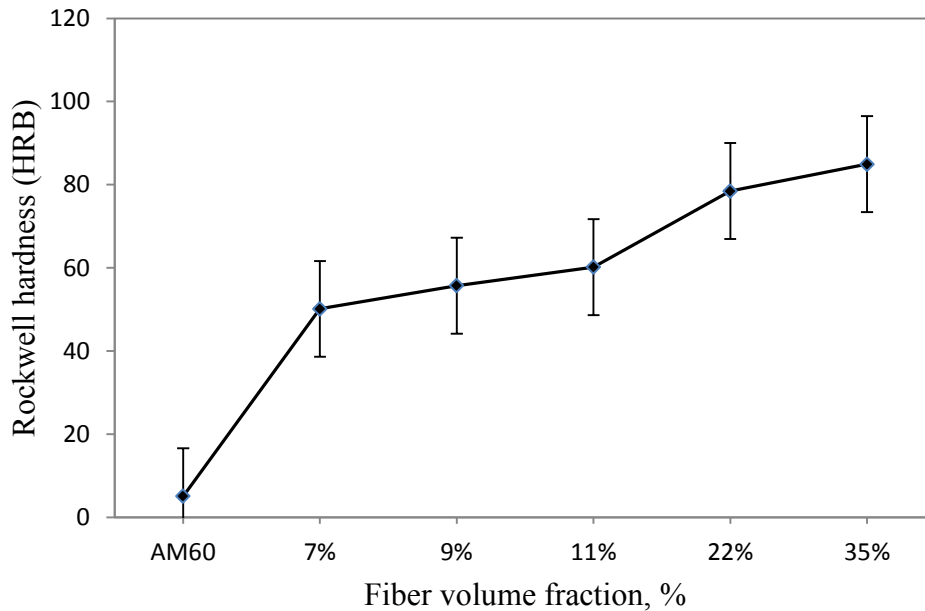


**Figure 4. 14** Hardness variation as a function of fiber volume fraction for the composites.

#### 4.3.2 Tensile properties

Figure 4.15 shows the typical engineering stress and strain curves for AM60 and its composite reinforced with  $\text{Al}_2\text{O}_3$  fiber of volume fraction of 7%, 9%, 11%, 22% and 35%. The corresponding properties such as ultimate tensile strength (UTS), yield strength (YS), elongation and Young's modulus are shown in Figures 4.16 and 4.17. It is evidently illustrated that the addition of the alumina fiber led to an increase in the strengths and Young's modulus, but there was a significant reduction in elongation. As the fiber volume fraction increased from 22% to 35%, the yield strength of the composite tended to disappear due to the depletion of plasticity in the material. The brittleness of the composites became very high as the amount of fiber reached to 22% and 35%.

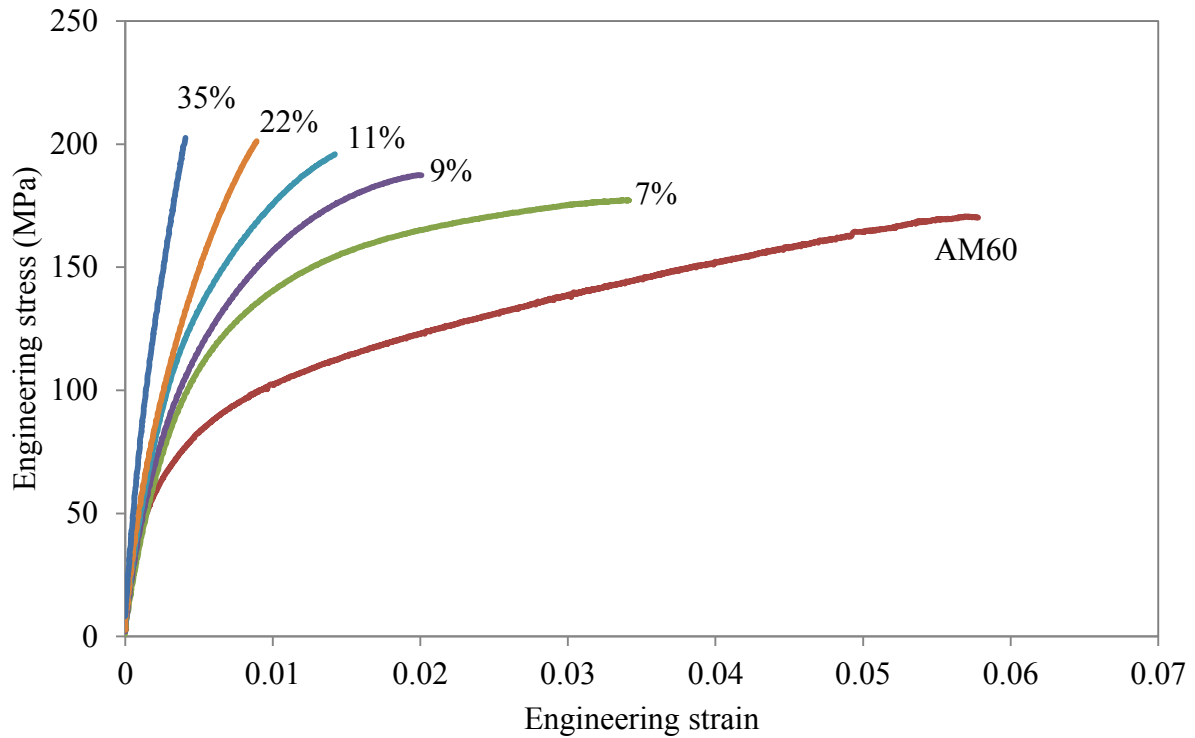


**Figure 4.15** Typical engineering stress vs. strain curves for AM60 alloy and 7%, 9%, 11%, 22% and 35% fiber reinforced composites.

**Table 4.3** Tensile properties of AM60 and composites with 7%, 9%, 11%, 22% and 35% of Al<sub>2</sub>O<sub>3</sub> fibers

	<b>YS (MPa)</b>	<b>UTS (MPa)</b>	<b>EI %</b>	<b>Young's Modulus (GPa)</b>
AM60	81.21	171.36	6.1	40
7%	124.74	177.28	3.4	45
9%	138.06	186.81	2.0	52
11%	156.27	189.24	1.5	58
22%	164.12	201.21	0.9	75
35%	-	202.56	0.4	116

From the tensile properties data listed in Table 4.3, it can be seen that the yield strength of the 22 % composite was improved by 102% over the unreinforced magnesium alloy AM60. They were 81.2 and 164.12 MPa for AM60 alloy and 22% composite, respectively. The UTS of AM60 was 171 MPa and 22% composite 201 MPa, which had almost 18% improvement. However, as the fiber volume fraction increased to 35%, there was a slight increment in UTS, only by 0.7%. Compared with the unreinforced AM60 alloy, the elongation dropped dramatically for the larger amount of fiber reinforced composite, i.e., 6.1% for the AM60 but 0.4% for 35% composite. It decreased almost 93%. The Young's modulus was measured from the linear portion of the engineering stress vs. strain curve. It is known that the higher the Young's modulus the higher the stiffness of the material. The Young's modulus for the 35% composite was 116 GPa, which was 190% higher than that of the AM60 alloy. It appears that with an increasing in fiber volume fraction, more loads are transferred to the reinforcement, which results in a higher tensile strength. The decreasing ductility of the composite could be attributed to the increased amount of fiber. The reasons might be that since the fiber was the final load barrier, the high stress concentration developed in cracked fibers prior to fracture embrittled the composite, and the probability of debonding between the reinforcement and matrix could be increased as the amount of fiber increased.

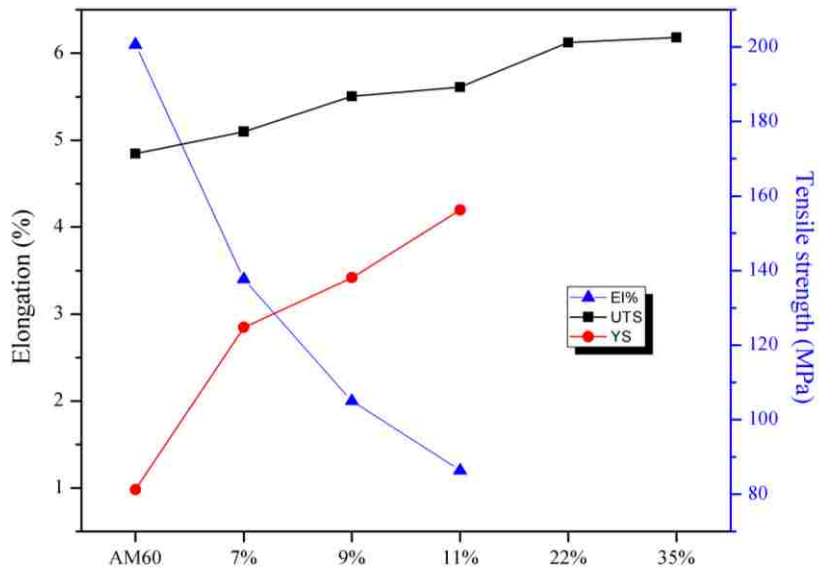


**Figure 4.16** UTS, YS and elongation of AM60 and its composites with fiber volume fraction of 7%, 9%, 11%, 22% and 35%.

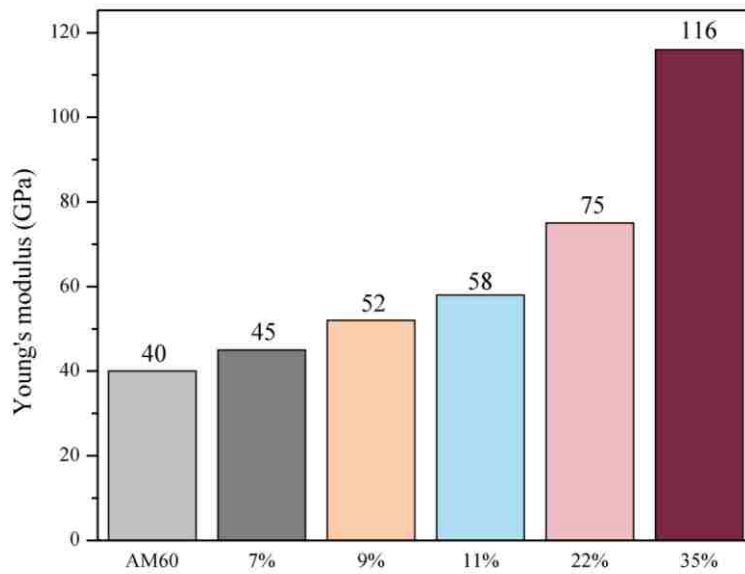


**Figure 4.17** Young's modulus of AM60 and its composites with fiber volume fraction of 7%, 9%, 11%, 22% and 35%.

The true stress-strain could be determined from the engineering stress-strain by applying the following equations:

$$\sigma_t = \sigma_e (1 + \epsilon_e) \quad \text{Eq. 4.2}$$

$$\epsilon_t = \ln (1 + \epsilon_e) \quad \text{Eq. 4.3}$$

where  $\sigma_t$  is the true stress,  $\epsilon_t$  is the true strain,  $\sigma_e$  is the engineering stress, and  $\epsilon_e$  is the engineering strain.

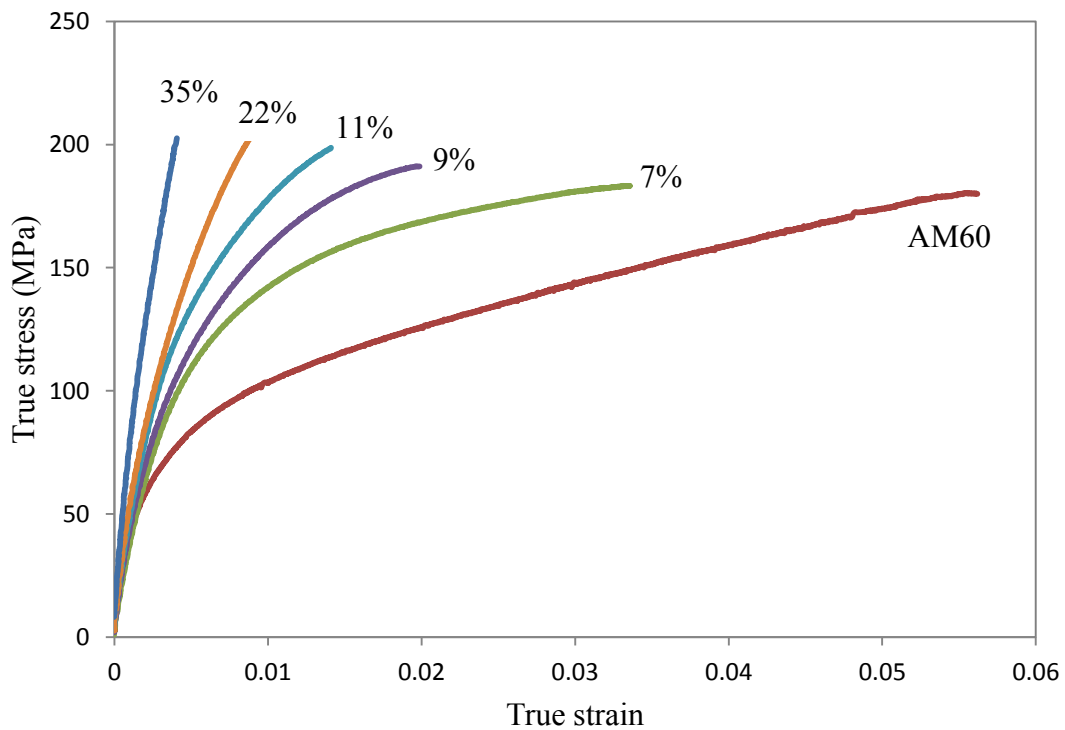


**Figure 4.18** Typical true stress vs. strain curves for AM60 alloy and composites with 7%, 9%, 11%, 22% and 35% fiber volume fractions.

Figure 4.18 shows the true stress and strain curves of AM60 alloy and composites with fiber volume fractions of 7%, 9%, 11%, 22% and 35%. All of the matrix alloy and composites revealed similar pattern, in which the materials deformed elastically first. Once the yield point



was reached, the plastic deformation took place. As the addition of fibers increased, the composites fractured at higher stress and lower strain levels than the matrix alloy AM60.

The stress-strain curve for metals is usually described by the power law relationship for plastic deformation [62]:

$$\sigma = K \varepsilon^n \quad \text{Eq. 4.4}$$

where  $K$  is the strength index,  $\varepsilon$  is the plastic strain and  $n$  is the strain hardening exponent.

**Table 4. 4** Best fit parameters of power equation.

Material type	K (MPa)	n	R <sup>2</sup>
AM60	552.6	0.3585	0.997
7%	1441.1	0.4914	0.9877
9%	1668.2	0.5037	0.996
11%	1754.1	0.4888	0.9919
22%	3309.8	0.5856	0.9984
35%	-	-	-

Table 4.4 lists the numerical values of the constants in Eq. 4.4 with the regression coefficients. The strain hardening rate can be obtained from the differentiation of the Eq. 4.4. The strain hardening behavior of the alloy and composites are shown in Figure 4.19, which was derived from Figure 4.18. As the fiber volume fraction increased, the strain hardening rate of the composite increased. The 22% fiber reinforced composite had a high strain hardening rate (25309 MPa) with respect to the AM60 alloy (10224 MPa) at the onset of plastic deformation. All materials revealed the similar trend, in which the strain hardening rates decreased with

increase in true strain. Composite with 22% fiber volume fraction had the highest strain hardening rate, which imply that the composite reinforced with more fibers were capable of spontaneously strengthening itself increasingly to a large extent, in response to lose a slight plastic deformation before the final fracture.

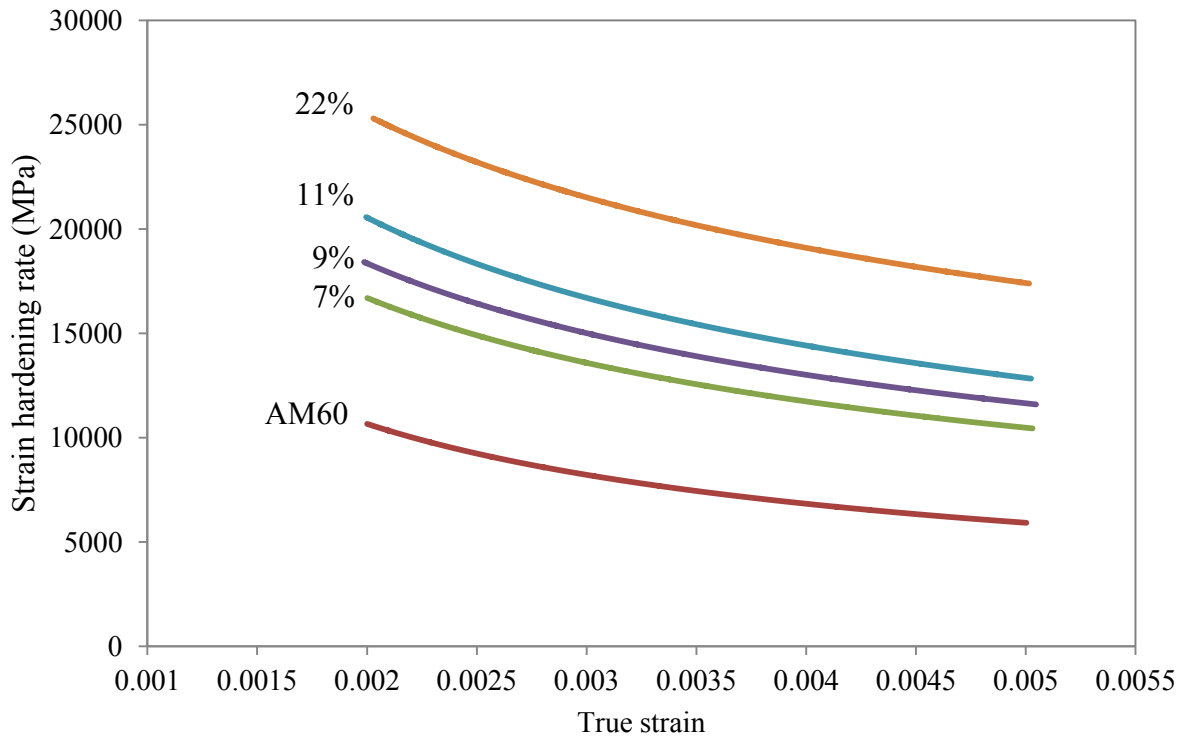


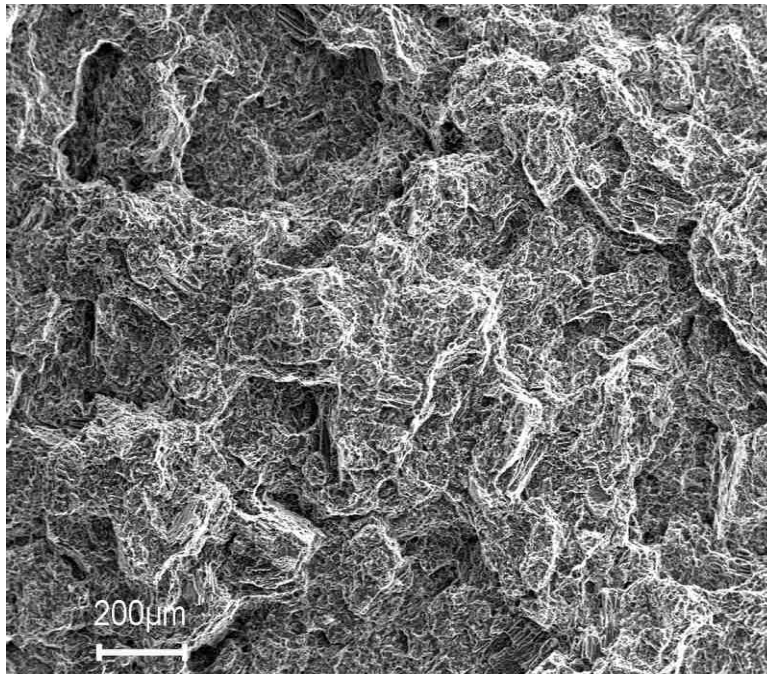
**Figure 4.19** Strain-hardening rate vs. true plastic strain curves for unreinforced AM60 matrix alloy and composites with fiber volume fractions of 7%, 9%, 11%, 22% and 35%.

#### 4.4 Fracture behavior

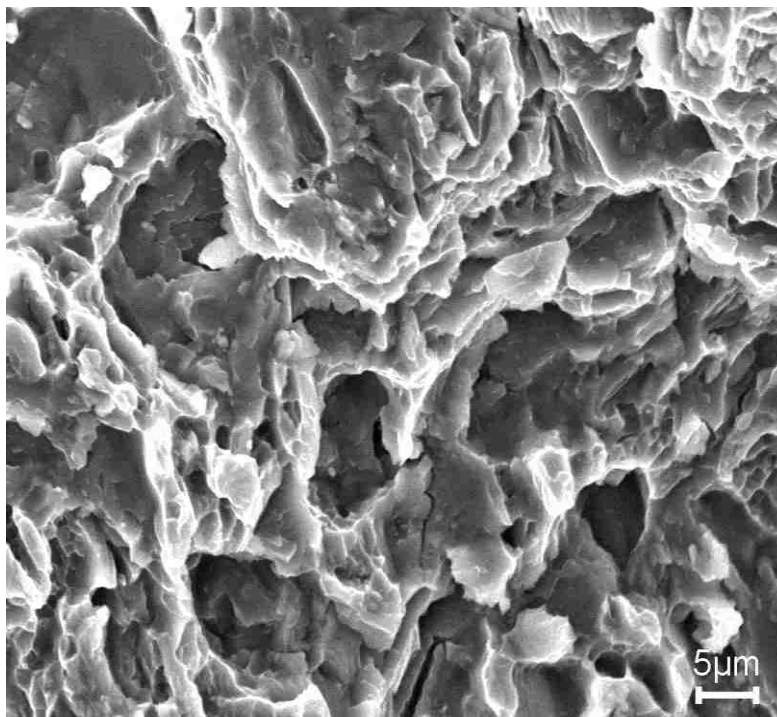
The fracture behavior of the unreinforced magnesium alloy AM60 and its composite with different fiber volume fractions were investigated using SEM. Figure 4.20 illustrates the typical fracture surface of the unreinforced alloy AM60 with low and high magnifications. There were shallow dimples on the surface and generally displays ductile behavior. It was well documented [35, 41, 54] that the fracture of unreinforced alloys was associated with the microscopic void

nucleation and growth. The voids nucleate at the locations with coarse intermetallic particles and other hard phases in the microstructure, which then grow and coalesce resulting in final fracture.

Figures 4.21 ~4.25 show the SEM fractographs of the composites with fiber volume fractions of 7%, 9%, 11%, 22% and 35%, respectively. However, composites fractured in a much different way in comparison with unreinforced alloy. Composites break in much brittle manner. There were no or fewer dimples found on the surfaces of the composites. During tensile testing, more loads were transferred to the fiber. The final fracture of the composite was initiated from the fiber cracking. Arrow 1 shown in Figures 4.21 ~ 4.23 indicated the fracture of fibers without being pulled out. For composites with higher fiber volume fractions, such as 22% and 35%, it was found that the fracture was mainly caused by the debonding between the fiber and the matrix alloy. High volume of fibers led to relatively poor infiltration of the molten metal into the close packed fiber network, while the fiber surfaces could not be fully covered by the matrix alloy. Figures 4.24 and 4.25 showed the fracture surfaces of the 22% and 35% fiber reinforced composite and Arrow 2 indicated the locations of pullout fibers. These fibers pullout might be the main mechanism of the failure for the composites with higher fiber volume fractions.

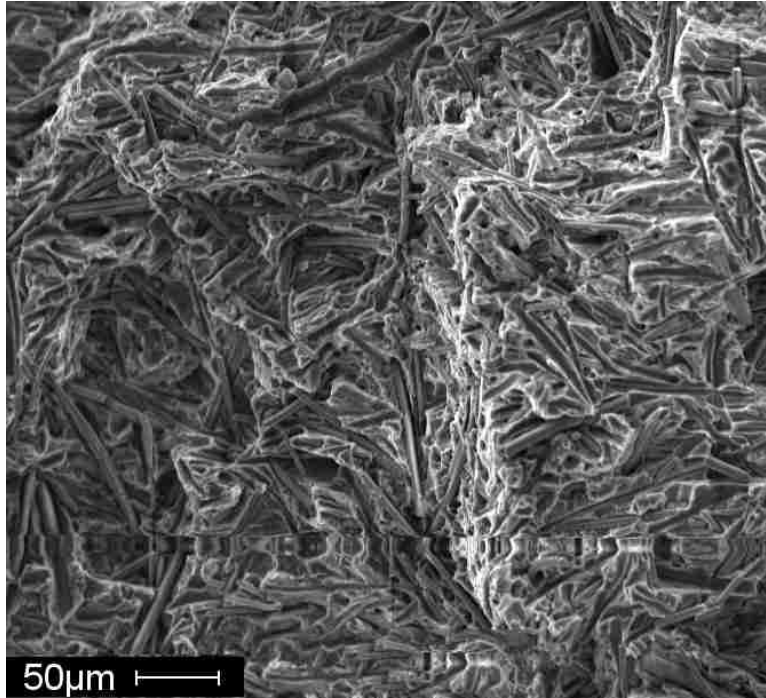


(a)

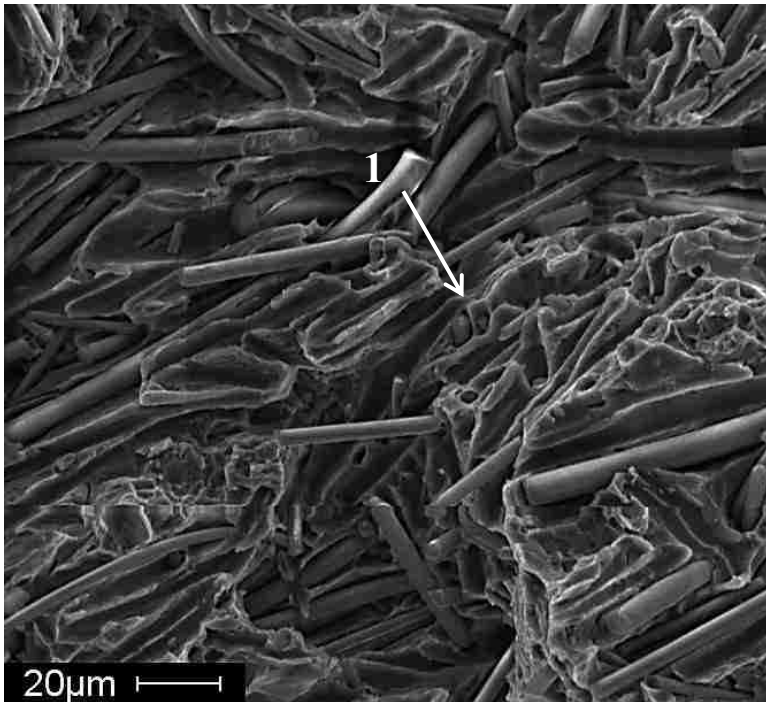


(b)

**Figure 4.20** SEM fractographs of the unreinforced magnesium alloy AM60, (a) low and (b) high magnification.

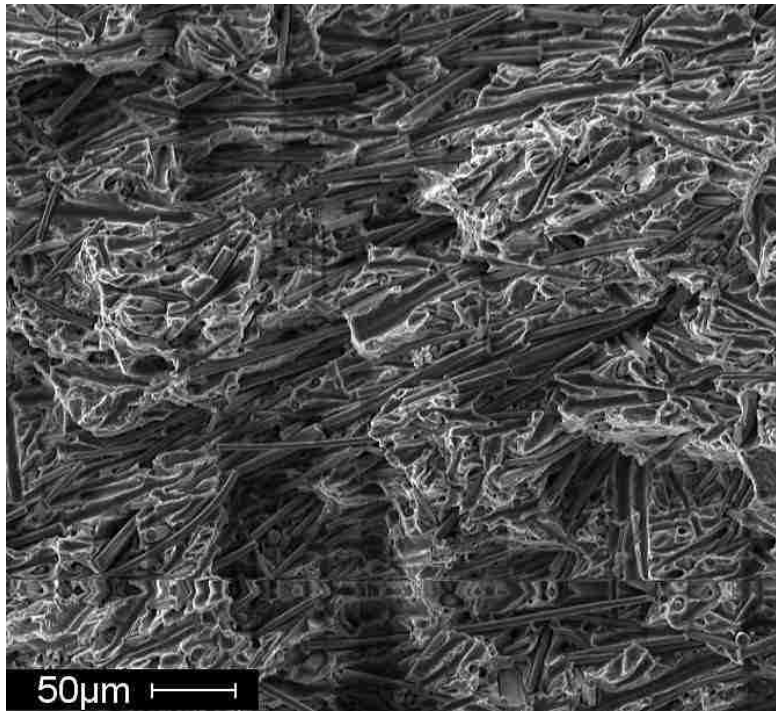


(a)

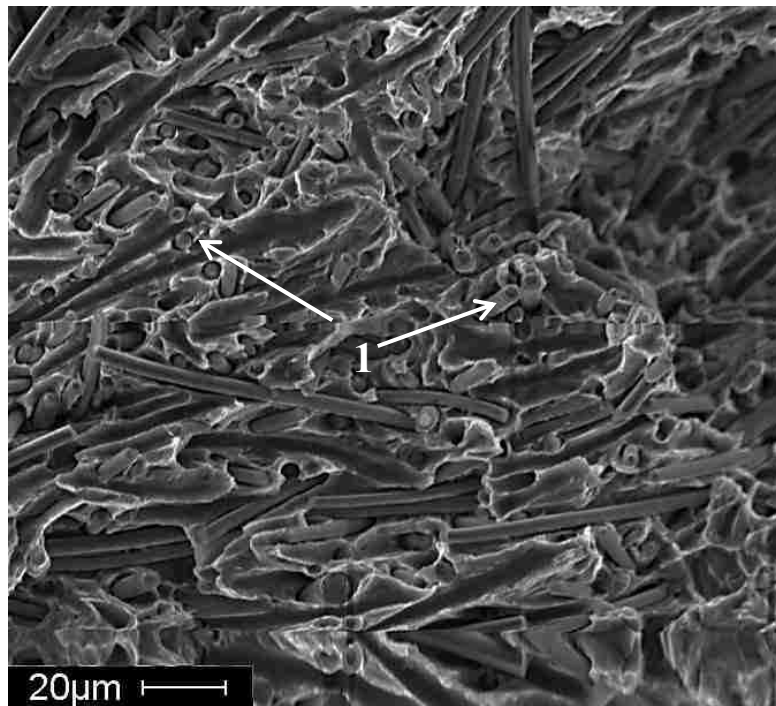


(b)

**Figure 4.21** SEM fractographs of the 7% fiber reinforced composite, (a) low and (b) high magnification.

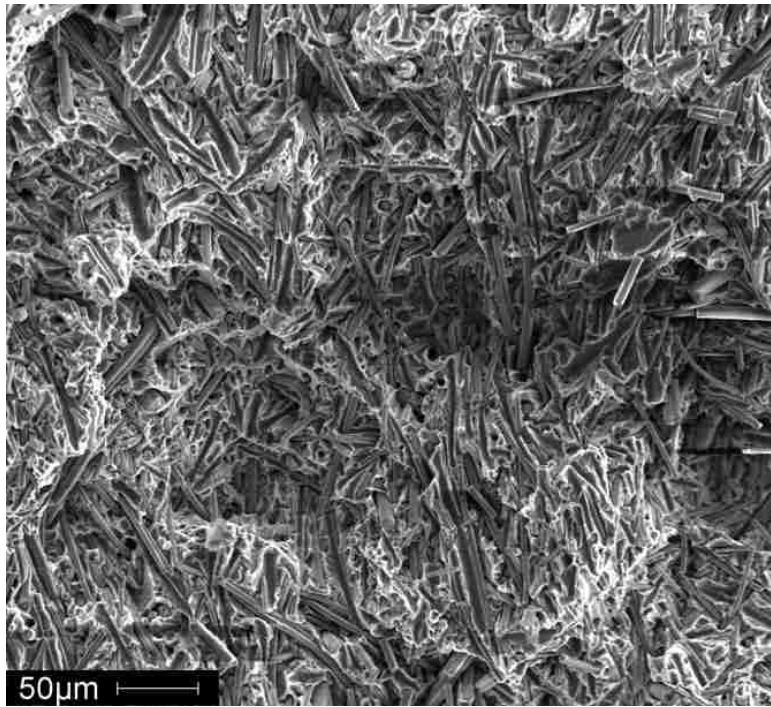


(a)

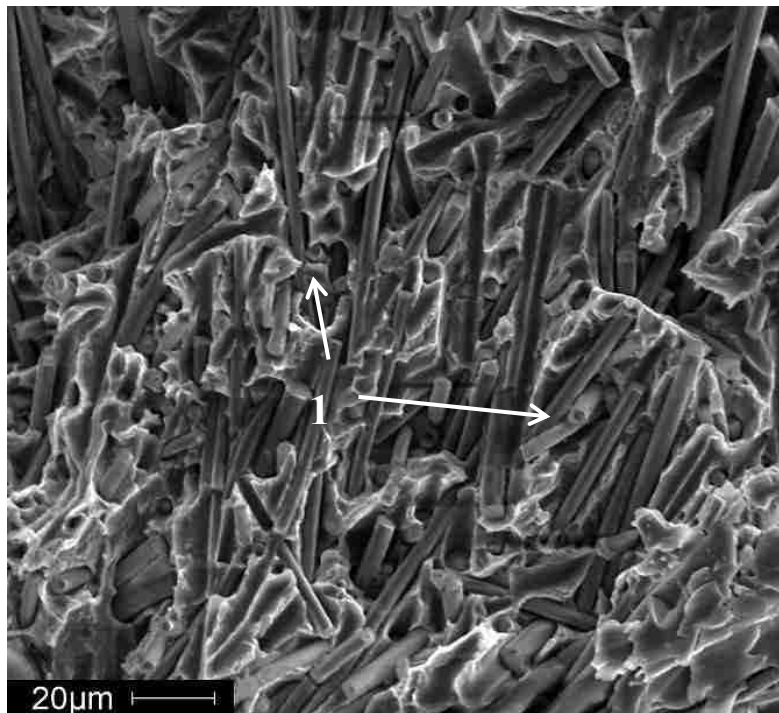


(b)

**Figure 4.22** Fractographs of the 9% fiber reinforced composite, (a) low and (b) high magnification.

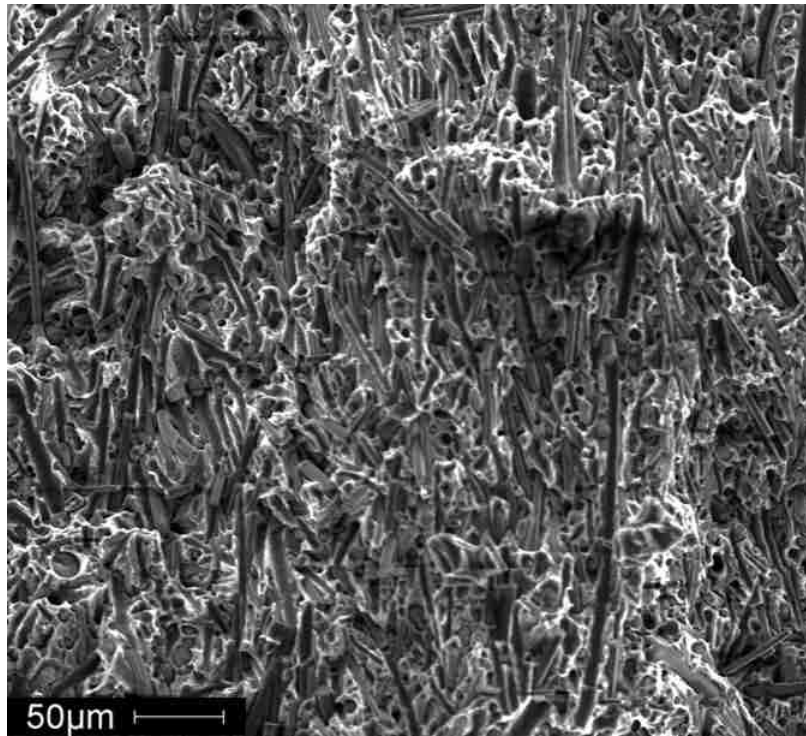


(a)

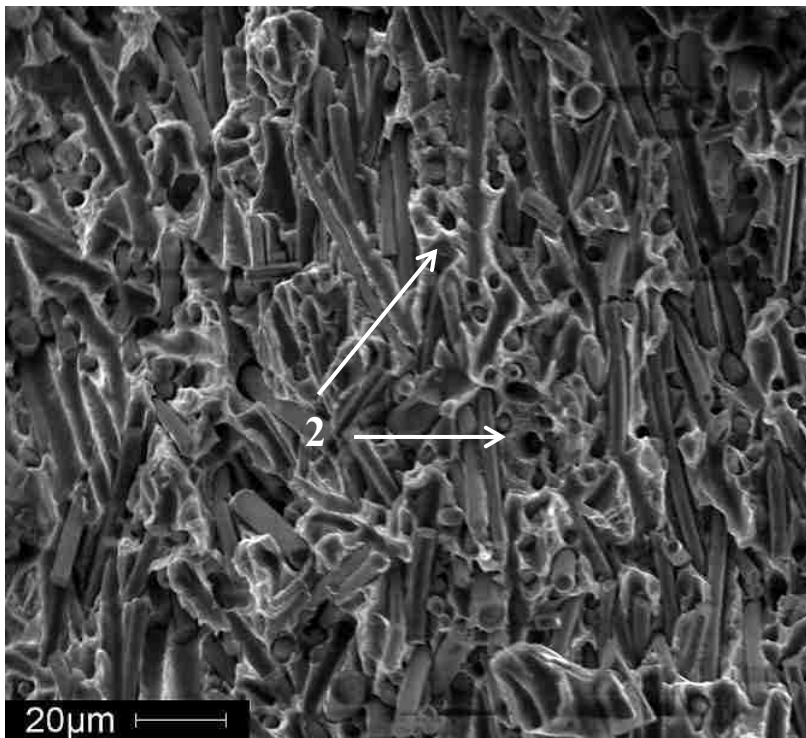


(b)

**Figure 4.23** SEM fractographs of 11% fiber reinforced composite, (a) low and (b) high magnification.



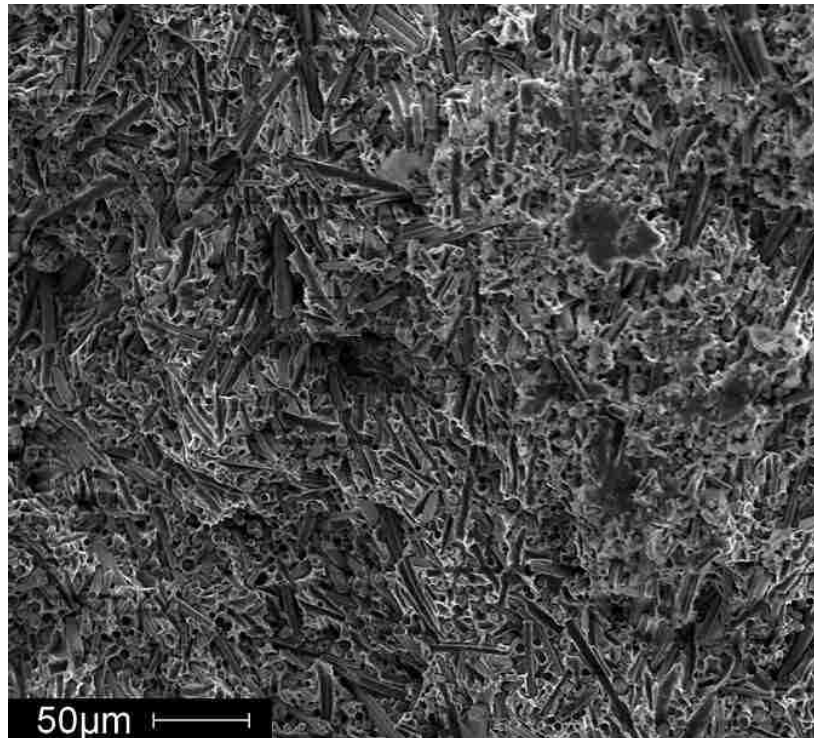
(a)



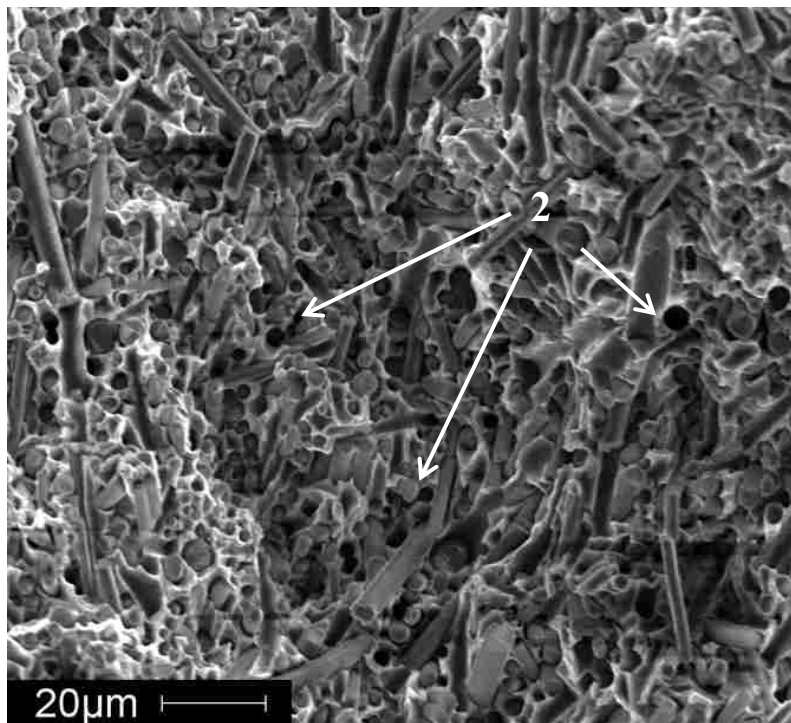
(b)

**Figure 4.24** Fractographs of 22% fiber reinforced composite, (a) low and (b) high magnification.





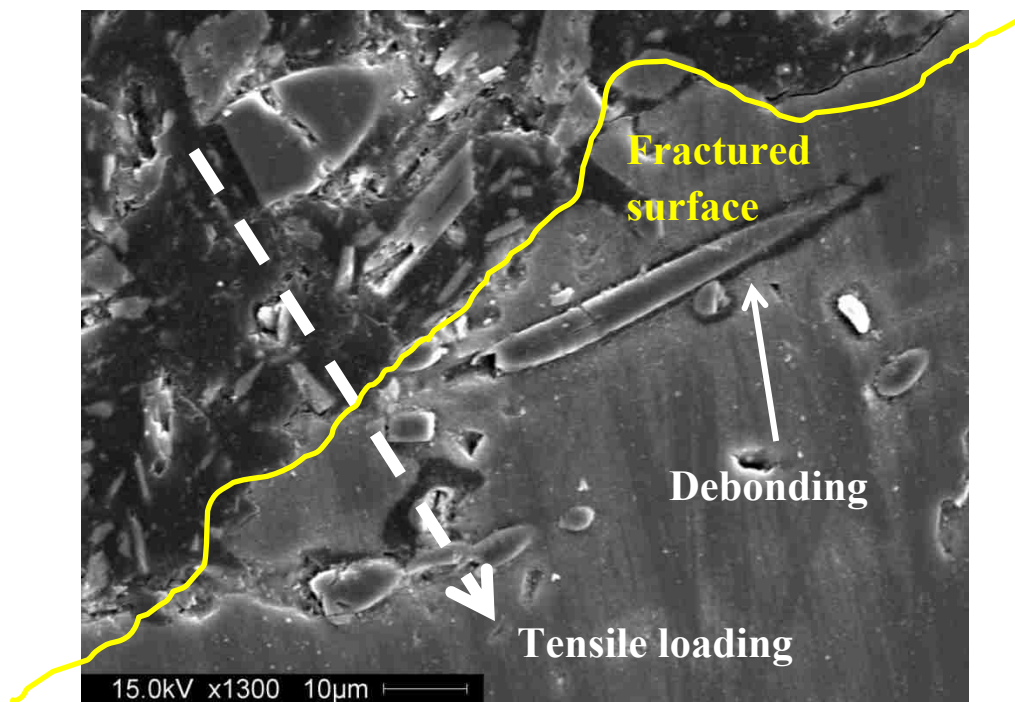
(a)



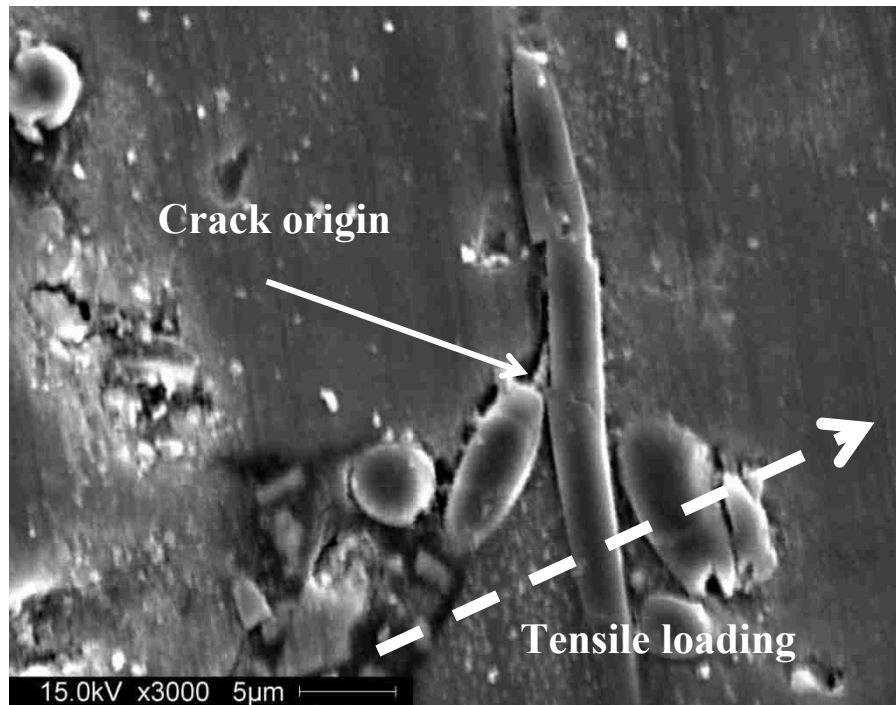
(b)

**Figure 4.25** Fractographs of 35% fiber reinforced composite, (a) low and (b) high magnification.

As mentioned above, the fiber pullout due to the segregation of the fiber and the matrix of the high fiber volume fraction composite might be the main cause of the final fracture. Figure 4.26 illustrate the damaged microstructures underneath the fractured surfaces, which supports the interpretation. Overall, the SEM fractographs show a good agreement with the tensile behaviours of the unreinforced alloy and the fiber reinforced composites presented in section 4.3.



(a)



(b)

**Figure 4.26** SEM micrographs showing the, (a) debonding of the fiber and (b) the crack origin in the composite with fiber volume fraction of 22%.

#### 4.5 Corrosion test

The differences in corrosion behavior between the composites with the variation in fiber volume fractions and the matrix alloy AM60 are illustrated in Figure 4.27. The current density ( $i_{\text{corr}}$ ) and polarization resistance ( $R_p$ ) obtained by Tafel calculations are listed in Table 4.5. Comparing the results between the composites and the matrix alloy, the polarization curves for the composites shifted to higher current densities. As the fiber volume fraction increased, the current density rose. On the other hand, the  $R_p$  decreased by the addition of the  $\text{Al}_2\text{O}_3$  fibers and the  $R_p$  values of the composites were much lower than that of the matrix alloy, as shown in Figure 4.26. By examining the values of the corrosion resistances listed in Table 4.5, the  $R_p$  of the 7% composite ( $3.995 \text{ k}\Omega \text{ cm}^2$ ) decreased by 73%, and the  $R_p$  of the 35% composite ( $0.321 \text{ k}\Omega \text{ cm}^2$ ) further decreased by 7 times in comparison with the matrix alloy ( $2.301 \text{ k}\Omega \text{ cm}^2$ ).

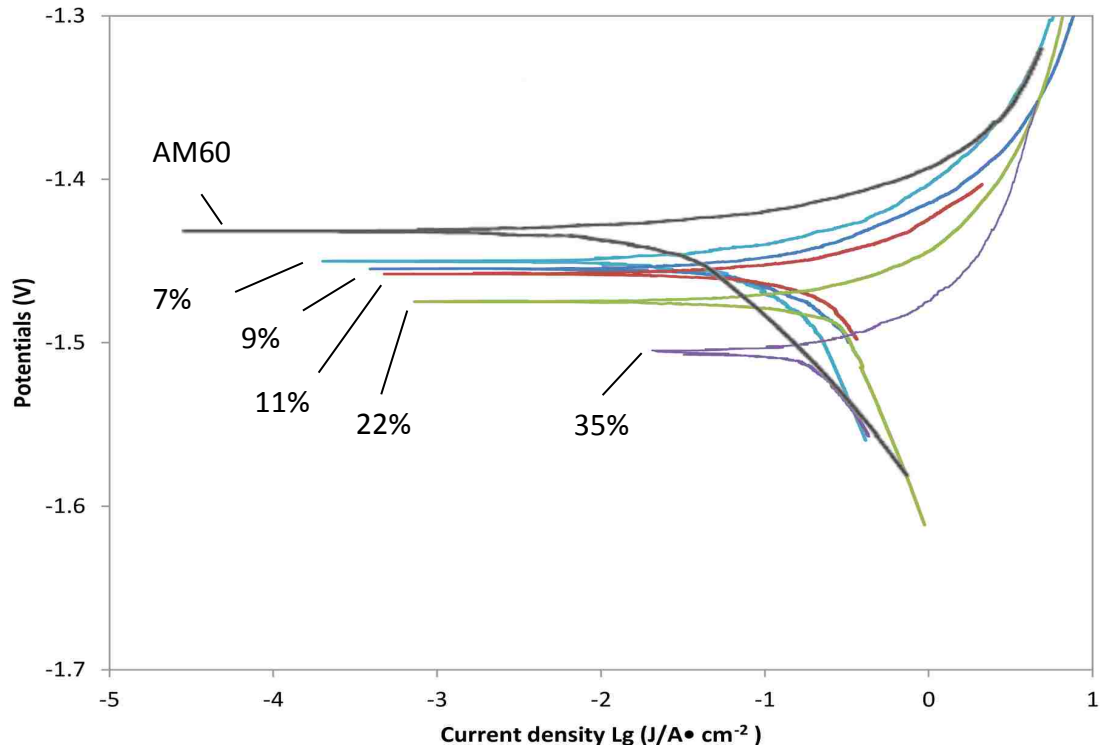


**Figure 4.27** Potentiodynamic polarization curves for the 7%, 9%, 11%, 22% and 35% Al<sub>2</sub>O<sub>3</sub> fiber reinforced composites in 3.5 wt% NaCl solution.

It is documented [47] that galvanic corrosion is the primary prospect when the magnesium is coupled with relatively noble materials. However, no evidence shows that there is galvanic interaction between the matrix alloy and the fiber since the alumina fiber acts as insulator in the composites. Hypothetically, the addition of alumina fiber could increase the corrosion resistance of the composite. However, the involvement of the alumina fiber in the matrix alloy AM60 indeed created excessive new interfaces between the matrix and the fiber. The generated interfaces could break the continuity of the Mg matrix and create preferential locations for corrosion taking place. As a result, the corrosion resistances of the composites decreased as fibers added.

**Table 4.5** Potentiodynamic polarization parameters of AM60 and composites with fiber volume fraction of 7%, 9%, 11%, 22% and 35%

Sample	$\beta_a$ (mV/dec)	$\beta_c$ (mV/dec)	$I_{corr}$ ( $\mu A/cm^2$ )	$R_p$ ( $k\Omega cm^2$ )
AM60	53.1	263.4	4.8	3.995
7%	31.5	189.1	5.7	2.301
9%	33.3	435.4	7.3	1.827
11%	41.9	567.1	10.5	1.583
22%	32.3	245.3	11.6	1.061
35%	12.6	189.4	15.3	0.321

#### 4.6 Summary

Excellent strengths and modulus of the composites were achieved by adding the  $Al_2O_3$  fiber into the matrix alloy AM60. These good results were accomplished by applying the combined preform and squeeze casting process, which was to infiltrate the liquid magnesium alloy AM60 into the preform under an applied pressure. The microstructure analyse revealed that the fibers were uniformly dispersed in the matrix alloy without any agglomeration. The property evaluation indicates that the fiber reinforced composite improved tensile strength and Young's modulus over the unreinforced alloy. As the fiber volume fraction increased from 7% to 22%, the strength (UTS and YS) of the composite increased rapidly. For the composite with 35% volume fraction of fibers, there was a slight increment in the UTS, but there was no result of YS due to the high brittleness of the composite with high volume fraction of  $Al_2O_3$  fiber. The elongation dropped dramatically for the fiber reinforced composite in comparison with the matrix alloy. The grain structure analysis indicated that an increase in the fiber volume fraction refined the grain. The

SEM micrographs showed that the fibers were mainly located near the grain boundaries, which implied that the fibers (inter-fiber spacing) could restrict the growth of the grain. The electrochemical testing results showed the presence of the alumina fibers deteriorated the corrosion resistance of the magnesium. The corrosion resistance kept decreasing as more fibers were added into the matrix alloy.

# CHAPTER 5:

## CONCLUSIONS AND FUTURE WORK

### 5.1 Conclusions

A process combining the preform preparation and squeeze casting has been developed to fabricate metal matrix composites with varying volume fractions of reinforcing fibers. It ensured the reinforcements evenly distributed in the composites and overcame the problems of the reinforcement deposition during solidification in stirring casting techniques. The experimental results showed that the current casting parameters satisfied the manufacturing of magnesium matrix composites with different fiber volume fractions up to 35%.

1. Preforms with fiber volume fractions of 7%, 9%, 11%, 22% and 35% were successfully fabricated. The 7% preform was made by using corn flour as an additive to reach a desired preform volume, which burned out in the following sintering process.
2. To ensure the fiber was uniformly distributed in the composites, SEM microstructure analysis on the etched specimens on time sequence was carried out. The observation revealed that the fibers were randomly dispersed and there was no fiber agglomerated for the various fiber volume fractions. No change in the orientation of the fibers was observed after the metal infiltration under the applied pressure of 90 MPa.

3. Preforms were fully infiltrated by molten magnesium alloy AM60 by applying squeeze casting technique. The casting conditions were set to be a preheated preform of 750 °C, preheated mold of 300 °C and squeeze casting pressure of 90 MPa.
4. With the variation in fiber volume fractions, the grains in the matrix alloy were refined as the amount of fiber increased. Fibers were most likely to freeze at grain boundaries; some of the fibers were located inside grains for higher fiber volume fractions, which indicated that the fiber could restrict the growth of the grains.
5. The MMCs tensile strengths increased with an increase in fiber volume fractions, which had superior improvement over the matrix alloy due to the high strength and stiffness of the Al<sub>2</sub>O<sub>3</sub> reinforcing fiber.
6. The tensile testing also showed a trend of decreasing ductility as the fiber volume fraction increased in comparison with that of the matrix alloy. The unreinforced AM60 alloy gave 6.1% elongation against 0.4% for the 35% fiber reinforced composite.
7. The examination of the fracture surfaces of the composites and the matrix alloy via SEM revealed that the composite fractured in somewhat brittle mode comparing with matrix alloy. The interface debonding and fiber cracking should be responsible for the final fracture of the MMCs.
8. The corrosion resistance of the composite decreased as the fiber volume fraction increased from 7% to 35%. The corrosion could be caused by the presence of excessive interfaces between the fiber and the matrix alloy. The interfaces could break the continuity of the matrix and thus created preferential locations for corrosion to take place.



## **5.2 Future work**

Magnesium matrix composited reinforced with higher fiber volume fractions, such as 22% and 35% showed a large amount of fiber debondings. This behavior significantly influenced the mechanical properties of the composites. To improve the bonding between the fiber and the matrix, the following work would be interesting to further study:

1. the bonding behavior by changing the types of the matrix alloys with high fluidity to obtain a better infiltration for high fiber volume fraction preforms;
2. the fiber/matrix interface behavior to have a better understanding of interfacial reactions in this region via TEM; and
3. solidification behaviours of the composites during squeeze casting by the direct measurement of temperature history in the preforms.

## REFERENCES

1. H. Z. Ye, X. Y. Liu, Review of recent studies in magnesium matrix composites, *Journal of Material Science*, 39 (2004) 6135-6171
2. K. U. Kainer, Influence of the production technique and type of reinforcement on the properties of magnesium-matrix composite, *Composite Material Technology*, ASME, 37 (1991) 191-197
3. M. Zhou, H. Hu, N. Li and J. Jo, Microstructure and tensile properties of squeeze cast magnesium alloy AM50, *Journal of Material Engineering and Performance*, 14 (2005) 539-545
4. *Magnesium-Alloys and Technologies*, Edited by K.U. Kainer, WILEY-VCH Gmb & Co. KGaA, (2003) 2-3
5. M. M. Avedesian and H. Baker, *Magnesium and Magnesium Alloys*, ASM Specialty Handbook, (1999) 50-51
6. W. S. Johnson, Fatigue Testing and Damage Development in Continuous Fiber Reinforced Metal Matrix Composites, the Symposium on Metal Matrix Composites: Testing, Analysis, and Failure Modes, Sparks, NV, 25-26 (April, 1988) 194-220
7. *Metal Handbook*, 9<sup>th</sup> edition, Volume 2, Properties and Selection: Nonferrous Alloys and Pure Metals, American Society for Metals, Metals Park, Ohio, (1978) 455-467
8. R. B. Ross, *Metallic Materials Specification Handbook*, 3<sup>rd</sup> edition, E. &F. Spon Ltd, London, (1997) 76-79
9. *Fine Ceramic Fibers*, edited by Anthony R. Bunsell, Marie-Helene Berger, Marcel Dekker, Inc., New York, (1999) 97

10. J. B. Donnet, T. K. Wang, S. Revouillat, and J. C. M. Peng, Carbon Fibers, Third Edition, Revised and Expanded, Marcel Dekker, Inc. New York, (1998) 36-38
11. S. Jayalakshmi, S. V. Kailas, S. Seshan, Properties of Squeeze Cast Mg- 10Al-Mn alloy and its Alumina Short Fiber Composites, Journal of Materials Science 38 (2003) 1383-1389
12. Y. Nishida, G. Ohira, Modelling of Infiltration of Molten in Fibrous Preform by Centrifugal Force, Acta mater, 47(1999) 841-852
13. H. X. Peng, Z. Fan, Cellular Arrays of Alumina Fibers, Journal of Materials Science, 36( 2001) 1007-1-13
14. N. W. Burningham, W. F. Rumpel, Properties of Boron Fibers and Composites, Polymer Engineering & Science, 7 (1967) 124-127
15. A. C. Reddy, E. Zitoun, Matrix Al-alloys for Silicon Carbide Particle Reinforced Metal Matrix Composites, Indian Journal of Science and Technology, 3 (2010) 1184-1187
16. S. Qu, L. Geng, J. Han, SiC/Al composites Fabricated by Modified Squeeze Casting Technique. J. Material Sci. Technology, 23 2007) 641-644
17. T.W. Clyne, M. G. Bader, G. R. Cappleman, P. A. Hubert, The Use of a  $\delta$ -alumina Fiber for Metal Matrix Composites, Journal of Material Science, 20 (1985) 85-96
18. Q. Jing, Solidification Microstructures in a Short Fiber Reinforced Alloy Composite Containing Different Fiber Fractions, China Foundry, 3 No.1 (2006)
19. H. Hu, Squeeze Casting of Magnesium Alloys and Their Composites, Journal of Material Science, 33 (1998) 1579-1589
20. J. Idris and J. Tan, Magnesium Technology; Minerals, Metal and Materials Society/AIME, Magnesium Technology, USA, (2000) 311

21. D. J. Lloyd, Particle Reinforced Aluminum and Magnesium Matrix Composites, *International Material Review*, 39 (1994) 1-23
22. D. Coupard, J. Goni, J. F. Sylvain, Fabrication and Squeeze Casting Infiltration of Graphite/ Aluminum Preforms, *J. Master. Sci.*, 34 (1993) 383-350
23. J. W. Kaczmar, K. Pietrzak, W. Wlosinski, The Production and Application of Metal Matrix Composite Materials, *Journal of Material Processing Technology*, 106 (2000) 58-67
24. T. W. Chou, A. Kelly and A. Okura, Fiber-Reinforced Metal Matrix Composites, *Composites*, 16, No.3 (1985) 187-206
25. J. Taftø, K. Kristiansen, H. Westengen, A. Nygard, J. B. Borradaile, and D. O. Karisen, *Proceedings of the International Symposium on Advances in Cast Reinforced Metal Composites*, ASM, 24 (1988) 71-75
26. M. Zhang, S. Xing, L. Xiao, P. Bao, W. Liu and Q. Xin, Design of Process Parameters for Direct Squeeze Casting, *Journal of University of Science and Technology Beijing, Mineral, Metallurgy, Material*, 15 (2008) 339-343
27. S. Y. Oh, J. A. Cornie, and K. C. Russell, Particulate Wetting and Metal: Ceramic Interface Phenomena, *Ceram. Eng. Sci. Proc.*, 8 (1987) 912-936
28. P. K. Rohatgi, *Interfacial Phenomenon in Cast Metal-Ceramic Particle Composites*, Metallurgical Society of AIME, Warrendale, PA, (1986) 185-202
29. W. Shi, M. Kobashi and T. Choh, Wettability of Molten Magnesium on Carbon and AlN, *J. Japan Inst. Metals*, 64, No. 5 (2000) 335-338

30. F. Delannay, L. Froyen, and A. Deruyttere, Review: The Wetting of Solids by Molten Metals and its Relation to the Preparation of Metal Matrix Composites, *J. Mater. Sci.* 22 (1987) 1-16
31. C. A. Leon, Infiltration Processing of Metal Matrix Composites using Coated Ceramic Particulates, Ph. D thesis, McGill University, (2000)
32. D. L. McDanel, Analysis of Stress-strain, Fracture, and Ductility Behavior of Aluminum Matrix Composites Containing Discontinuous Silicon Carbide Reinforcement, *Metal. Tran.*, 16A (1985) 1105-1115
33. J. Schroder, K. Kainera and B. Mordike, Developments in the Science and Technology of Composites Materials, ECCM 3, Bordeaux, France, (1989) 20-23
34. F. Rehman, S. Fox, H. M. Flower, D. R. F. West, Fiber/matrix Interactions in Magnesium-based Composites Containing Alumina Fibers, *Journal of Materials Science*, 29 (1994) 1636-1645
35. N. J. Musson, and T. M. Yue, The Effect of Matrix Composition on the Mechanical Properties of Squeeze Cast Aluminum Alloy- Saffil Metal Matrix Composites, *Mater. Sci. Engr. A*, 135 (1991) 237-242
36. M.S. Yong, and A. J. Clegg, Evaluation of Squeeze Cast Magnesium Alloy and Composites, *Foundryman*, (March ,1999) 71-75
37. M. M. Schwartz. *Composite Materials*, vol. 1: Properties, Nondestructive, Testing, and Repair, Prentice-Hall Inc., New Jersey, (1997) 44-45
38. K. U. Kainer, Influence of Heat Treatment on the Properties of Short-fiber- Reinforced Magnesium Composites, *Materials Science and Engineering*, A135 (1991) 243-246

39. B. L. Mordike and K. U. Kainer, Manufacture and Characterization of Magnesium Composite Materials, Trans. Indian Inst. Met., 50, No. 6(1997) 665-674
40. S. C. V. Lim, M. Gupta and L. Lu, Processing, Microstructure, and Properties of Mg-SiC Composites Synthesized Using Fluxless Casting Process, Material Science and Technology, 17 (2001) 823-832
41. S. Seshan, A. Guruprasad, M. Prabha and A. Sudhakar, Fiber- reinforced Metal Matrix Composites- A Review, J. Indian Inst. Sci. (1996) 1-14
42. M. G. Fontana, Corrosion Engineering, 3th ed., McGraw-Hill International Edition, (1996) 42
43. H. Umehara, M. Takaya, Corrosion Resistance of Die Casting AZ91D Magnesium Alloys in the Atmosphere, Magnesium Alloys and Their Applications, Wiley-Vch, Germany, (2000) 506-513
44. C. A. Walton, H. J. Martin, M. F. Horstemeyer, P. T. Wang, Quantification of Corrosion Mechanisms Under Immersion and Salt Spray Environments on an Extruded AZ31 Magnesium Alloy, Corrosion Science, 56 (201) 194-208
45. R. Lindstrom, L. G. Johansson, J. E. Svensson, The Influence of NaCl and CO<sub>2</sub> on the Atmospheric corrosion of Magnesium Alloy AZ91, Material and Corrosion, 54 (2003) 587-594
46. Q. Qu, J. Ma, L. Wang, L. Li, Z. Ding, Corrosion Behaviour of AZ31B Magnesium Alloy in NaCl Solutions Saturated with CO<sub>2</sub>, Corrosion Science, 53 ( 2011) 1186-1193

47. L. H. Hihara, Corrosion of Metal Matrix Composite, ASM Handbook Vol. 13B, Corrosion: Materials, S. D Craner and B. S., Covino Jr Ed., ASM International, (2005) 526-524
48. J. Zhu and L. H. Hihara, Corrosion of Continuous Alumina Fiber Reinforced AL2 wt% Cu-T6 Metal Matrix Composite in 3.15wt% NaCl Solution, Corrosion Science, 52 (2010) 406-415
49. Product Information, Saffil Alumina Fiber, Imperial Chemical Industries, PCL
50. Gibson, Sshby, Cellular Solids, Cambridge University Press; 1997
51. Y. S. Yang, K. Feng, W. X. Zhao, Fabrication and Properties of Al<sub>2</sub>O<sub>3</sub> Short Fiber Reinforced Aluminum Matrix Composite, Advanced Materials Research, 328-330 (2011) 1277-1280
52. ASTM Standard B557, Standard Test Methods for Tension Testing Wrought and Cast Aluminum and Magnesium Alloy Products
53. S. Guldberg, H. Westengen, and D. L. Albright, Properties of Squeeze Cast Magnesium-based Composites, SAE technical paper series, No. 910830 (SAE, Detroit, MI, 1991)
54. J. L. Song, Y. C. Yang, and K. S. Han, Squeeze Casting Conditions of Al/Al<sub>2</sub>O<sub>3</sub> Metal Matrix Composites with Variations of the Preform Drying Process, Journal of Materials Science, 31 (1996) 2615-2621
55. Q. Zhang, Development of Hybrid Mg-based composites, Master thesis, University of Windsor, 2009
56. T. Yamauchi and Y. Nishida, Infiltration Kinetics of Fibrous Preforms by Aluminum with Solidification, Acta metal. Mater, 43, No. 4 (1995) 1313-1321

57. T.P.D. Rajan, R. M. Pillai, B. C. Pai, Review: Reinforcement Coatings and Interface in Aluminum Metal Matrix Composites, *Journal of Materials Science*, 33 (1998) 3491-3503
58. G. R. Cappleman, J. F. Watts, T. W. Clyne, The Interface Region in Squeeze Infiltrated Composites Containing  $\delta$ -alumina Fiber in an Aluminum Matrix, *Journal of Materials Science*, 20 (1985) 2159-2168
59. T. M. Yue, H. U. Ha and N. J. Musson, Grain Size Effects on Mechanical Properties of Some Squeeze cast Light Alloys, *Journal of Materials Science*, 30 (1995) 2277-2283
60. Z. Drozd, Z. Trojanova, M. Pahutova, H. Ferkel, and W. Riehemann, Mechanical Properties of Mg and Mg Based Alloy Composites, *Advanced Light Alloys and Composites*, Proceeding of the NATO Advanced Study Inst., Zakopane, Poland, (1991) 5-15
61. H. Hu, Grain Microstructure Evolution of Mg(AM50A)/SiC<sub>p</sub> Metal Matrix Composites, *Scripta Materialia*, 39, No. 8(1998) 1015-1022
62. J. H. Hollomon, Tensile Deformation, *Transactions of the American Institute of Mining and Metallurgical Engineers*, 162 (1945) 268-275



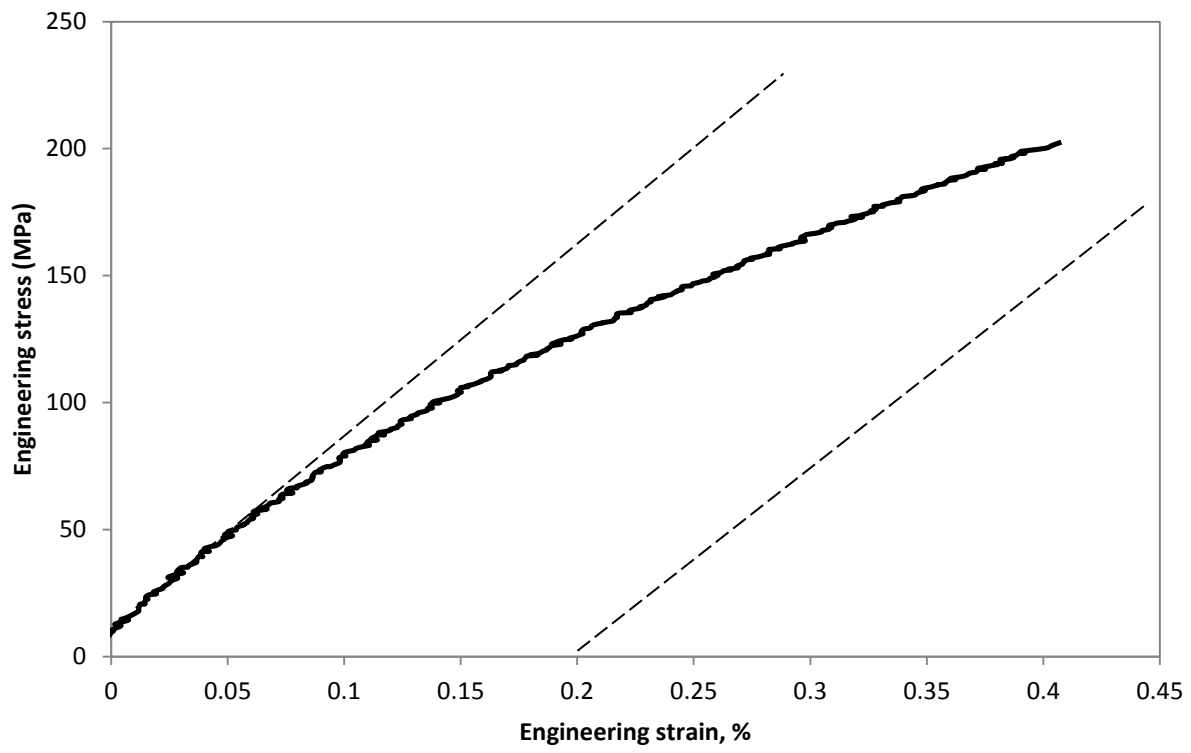
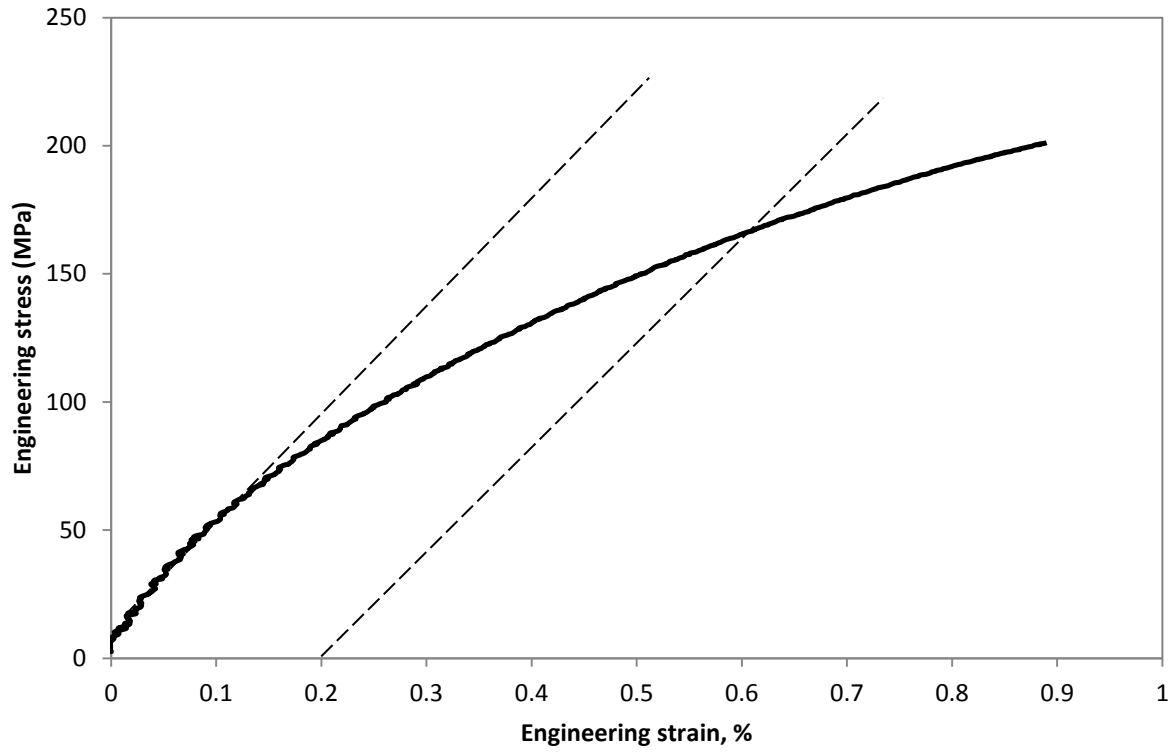
## **APPENDICES**

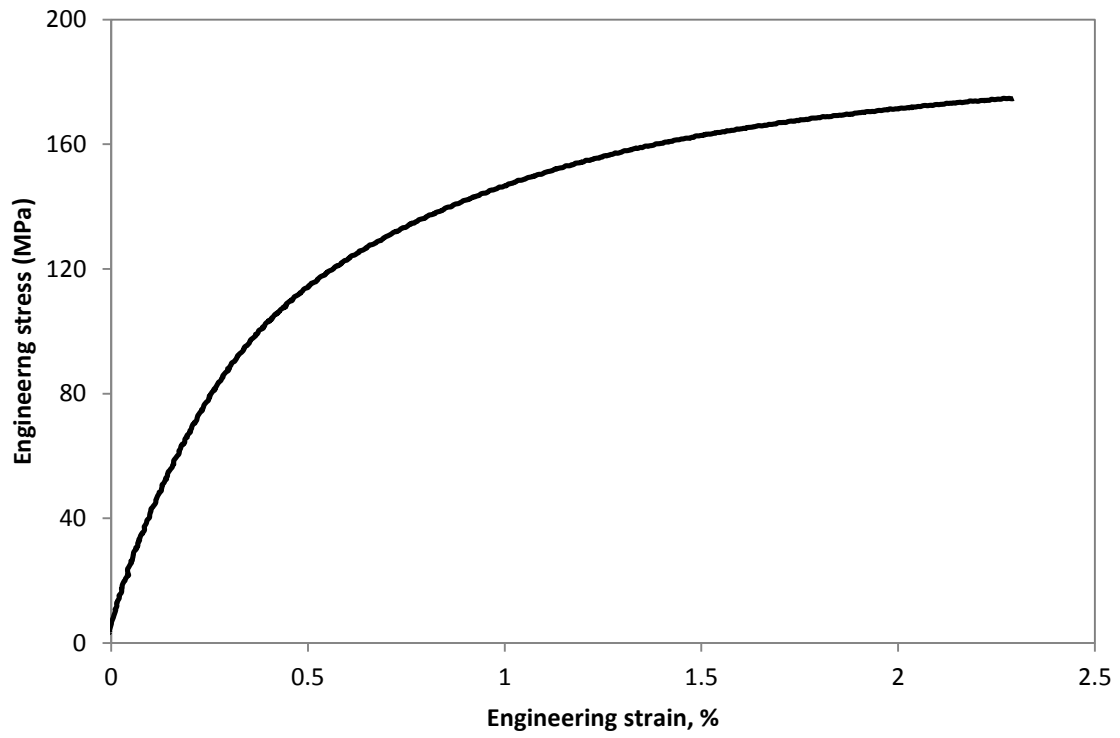
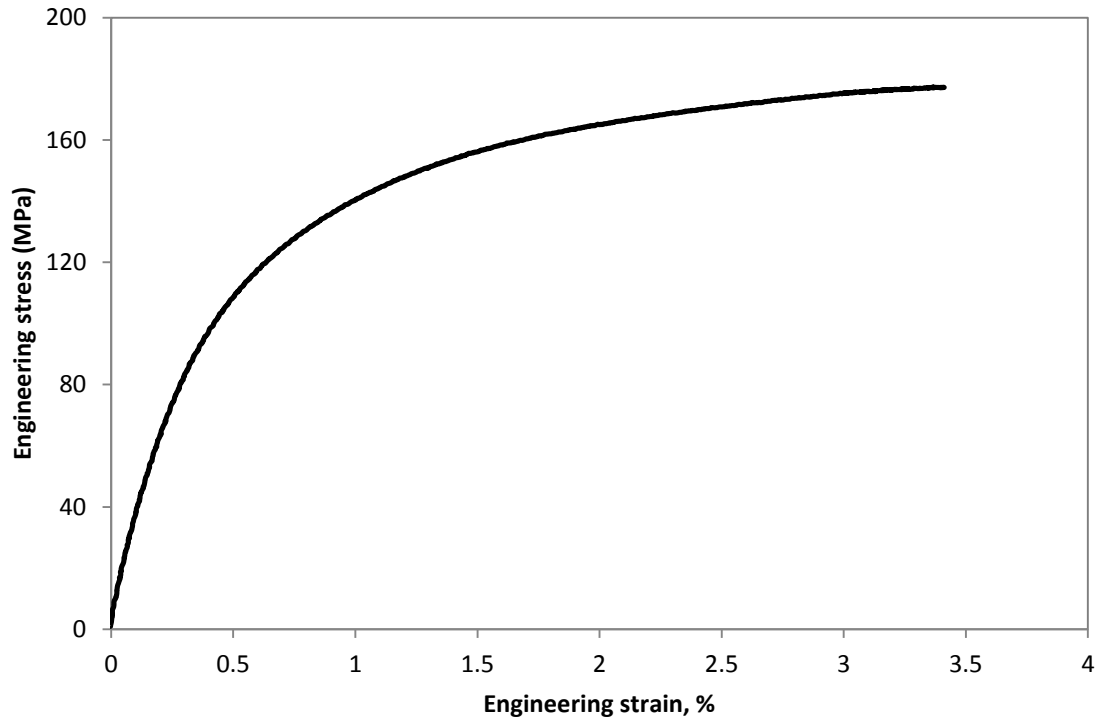
**Table Ap.1** Grain size measurement for matrix alloy and composites with different fiber volume fractions.

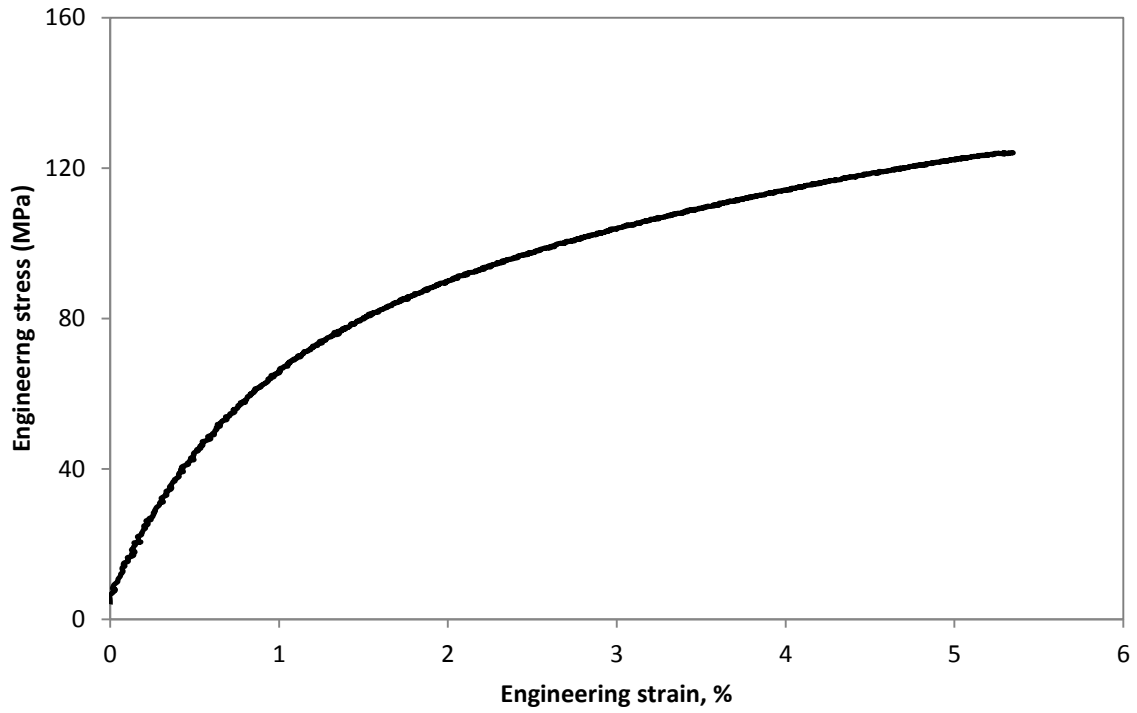
Number	Grain size			
	AM60	7%	9%	11%
1	78.4673	55.8473	44.9284	31.9432
2	46.6453	43.5568	51.3452	39.9023
3	72.6475	73.4756	59.3453	41.9483
4	78.4635	59.7564	63.3465	30.2312
5	55.748	43.5733	55.3453	22.0982
6	57.9483	31.8574	43.8864	29.5675
7	68.8944	67.9981	47.8473	43.3543
8	71.7585	83.0021	32.3487	32.2345
9	57.7465	61.5563	44.3422	30.2334
10	83.4857	43.1101	39.0987	20.1253
11	57.9982	59.4756	69.9323	30.0091
12	64.9684	42.7734	51.2342	35.9874
13	68.1298	60.1123	40.3456	33.9932
14	65.5833	49.8573	66.3453	41.9834
15	71.6745	71.8574	50.3452	53.4553
16	76.857	54.8593	41.3453	41.9483
17	67.8576	45.8801	46.3453	30.1983
18	54.8674	47.8593	32.0985	34.9025
19	67.8576	38.8872	42.2201	61.9583
20	79.3453	46.9244	46.3432	40.0114
<b>Average</b>	67.34721	54.11099	48.41945	36.30427
<b>Standard Deviation</b>	9.753321	13.07609	10.30577	9.806644

**Table Ap.2** Hardness measurement for matrix and composites with different fiber volume fractions.

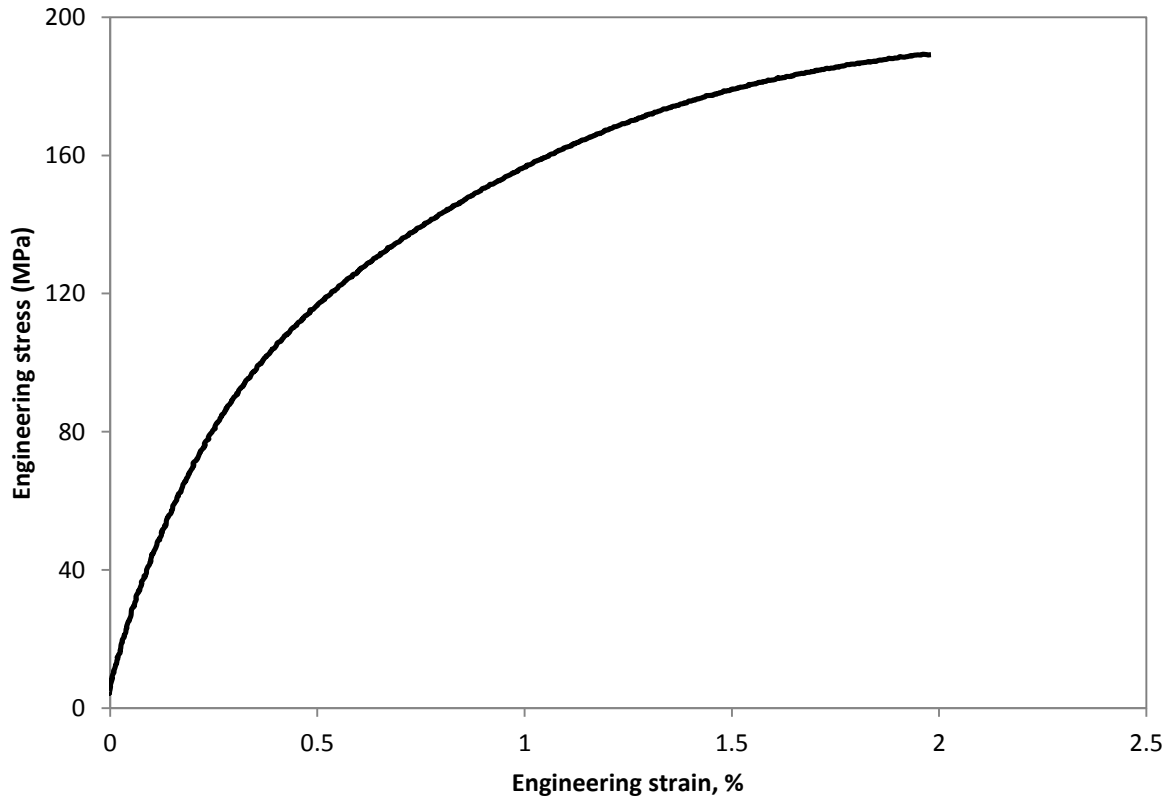
<b>Number</b>	<b>Hardness (HRB)</b>					
	<b>AM60</b>	<b>7%</b>	<b>9%</b>	<b>11%</b>	<b>22%</b>	<b>35%</b>
1	4.3	54.9	52.1	55.7	77.2	86.1
2	5.7	52.8	51.9	58.9	76.1	83.9
3	5.1	46.8	61	57.8	80	81
4	6.3	48.7	57.1	64.8	73.1	87.1
5	4.2	47.5	56.5	63.7	86	86.6
<b>Average</b>	5.12	50.14	55.72	60.18	78.48	84.94
<b>Standard Deviation</b>	0.90111	3.533129	3.810774	3.90858	4.876167	2.518531

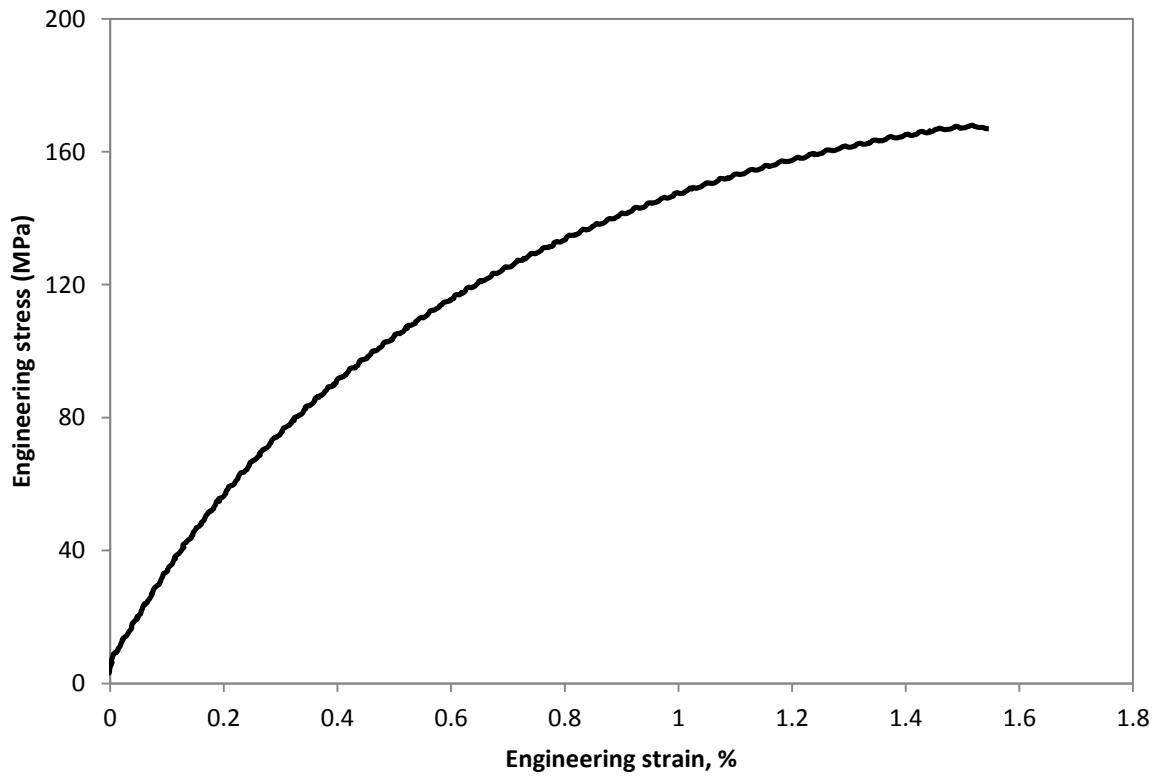
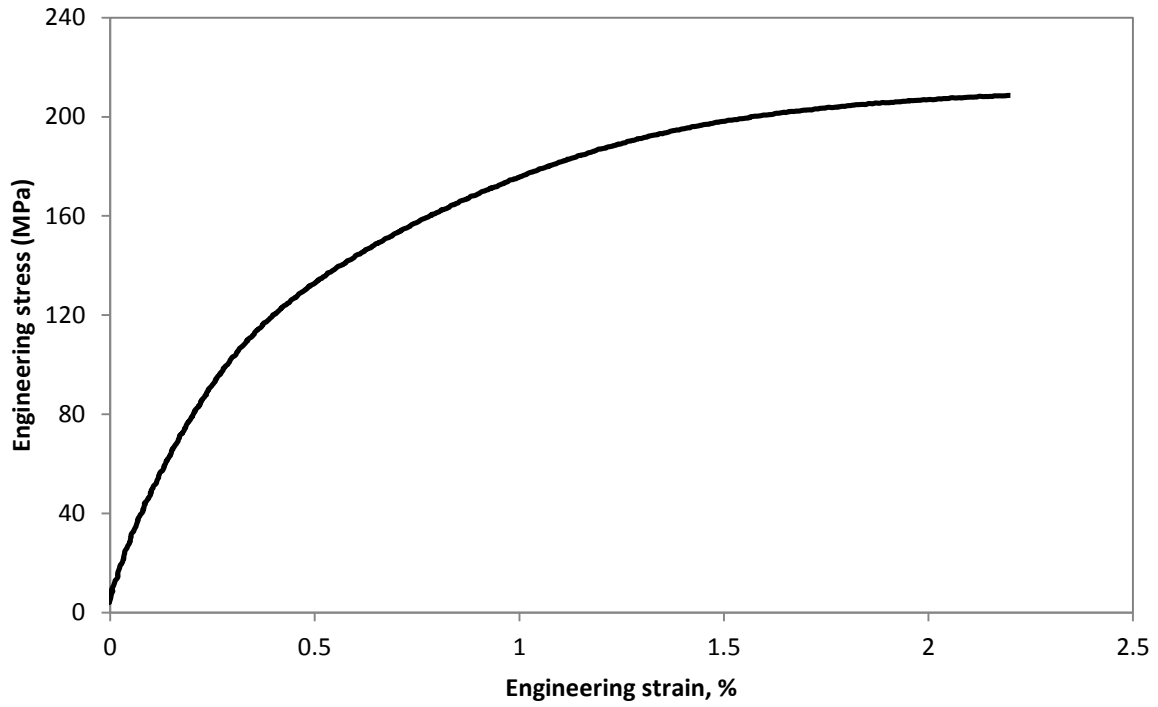




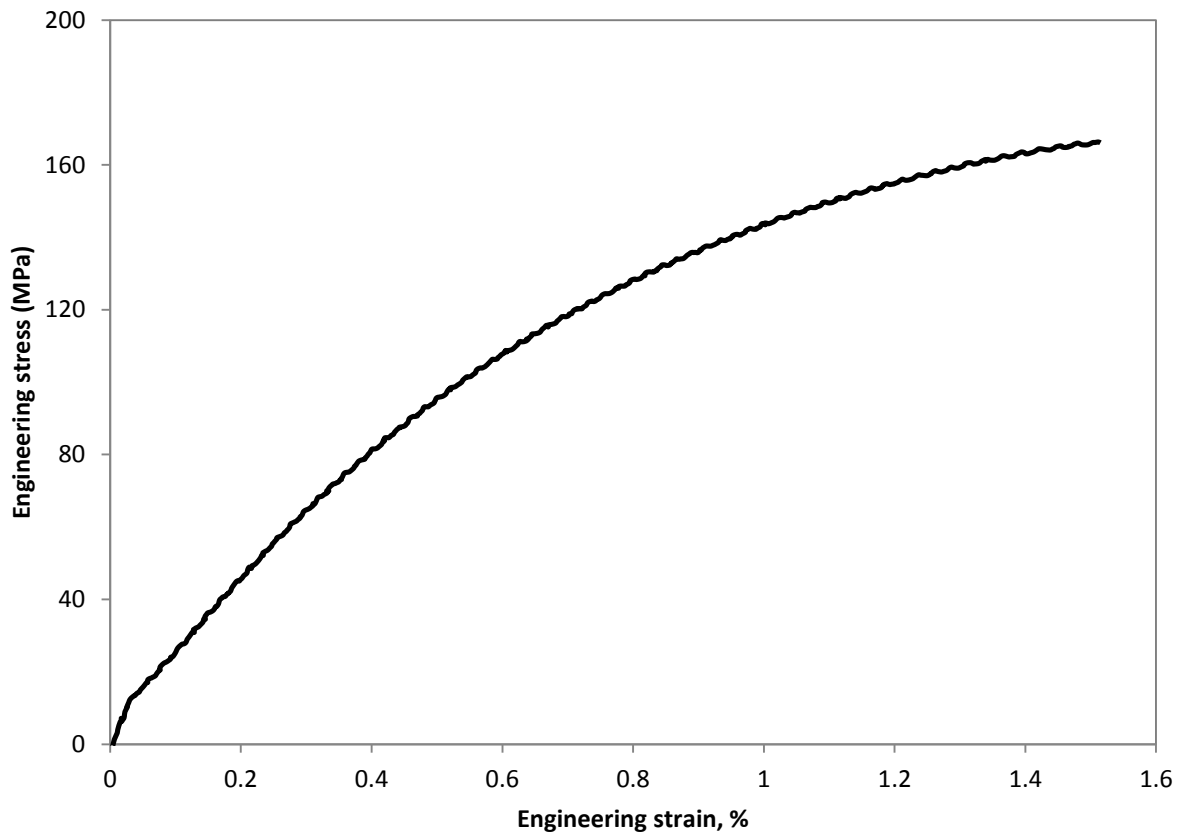
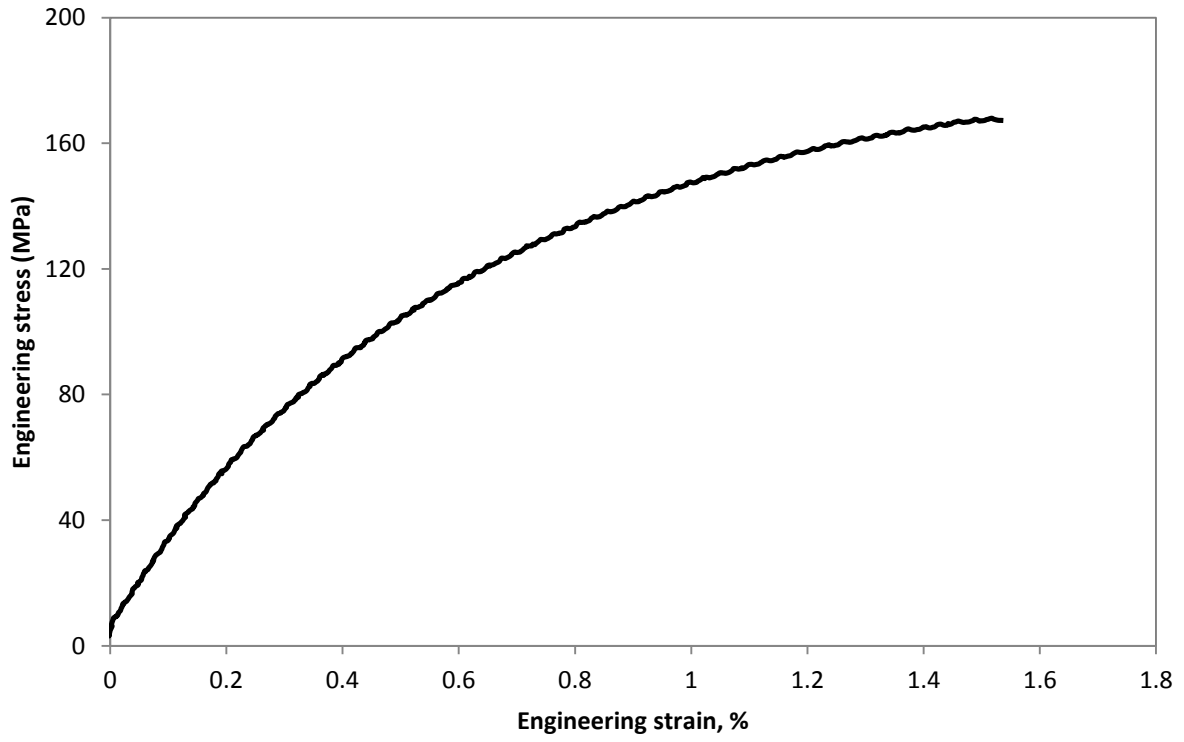


**Figure Ap.1** Engineering stress vs. strain curves for the 7% fiber reinforced composite.

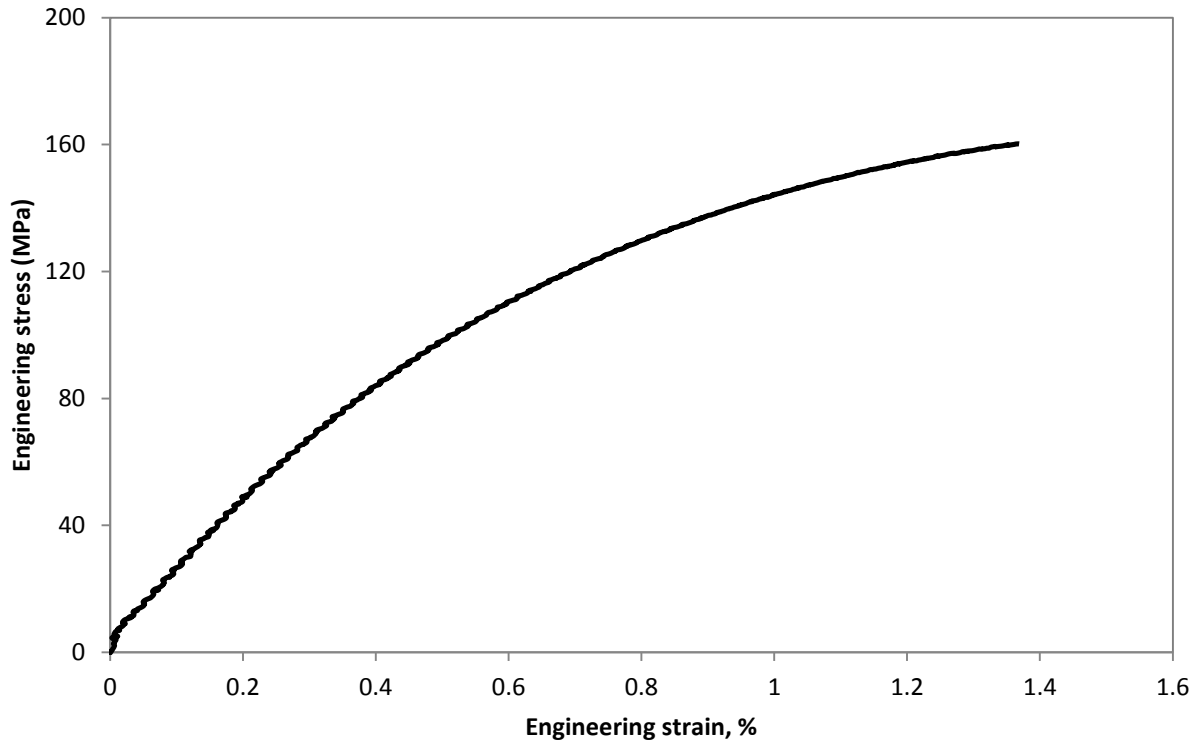




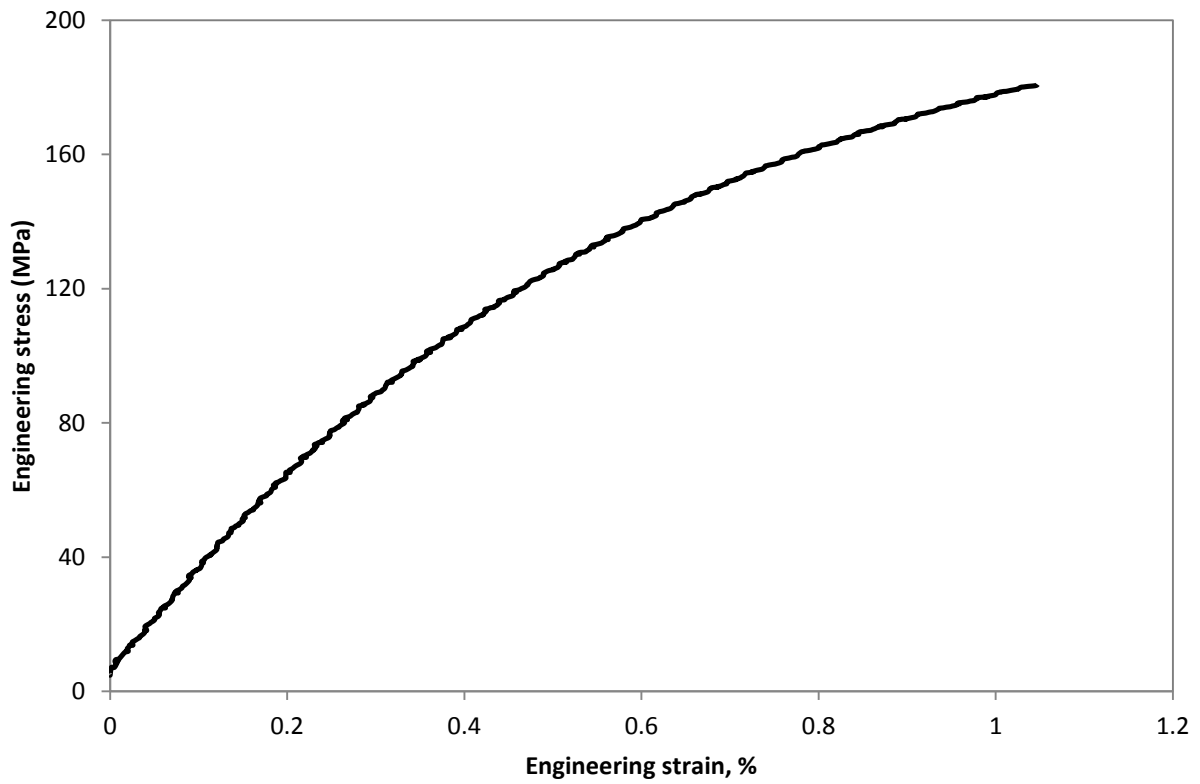
**Figure Ap.2** Engineering stress vs. strain curves for the 9% fiber reinforced composite.

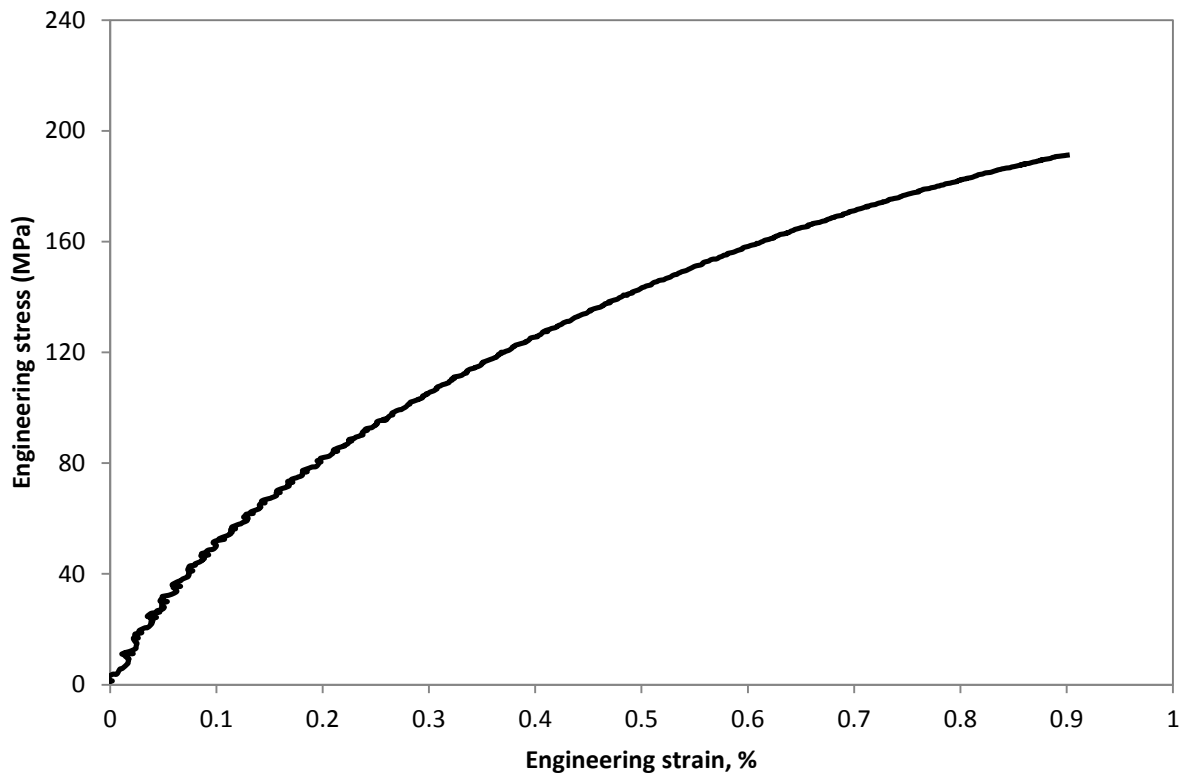
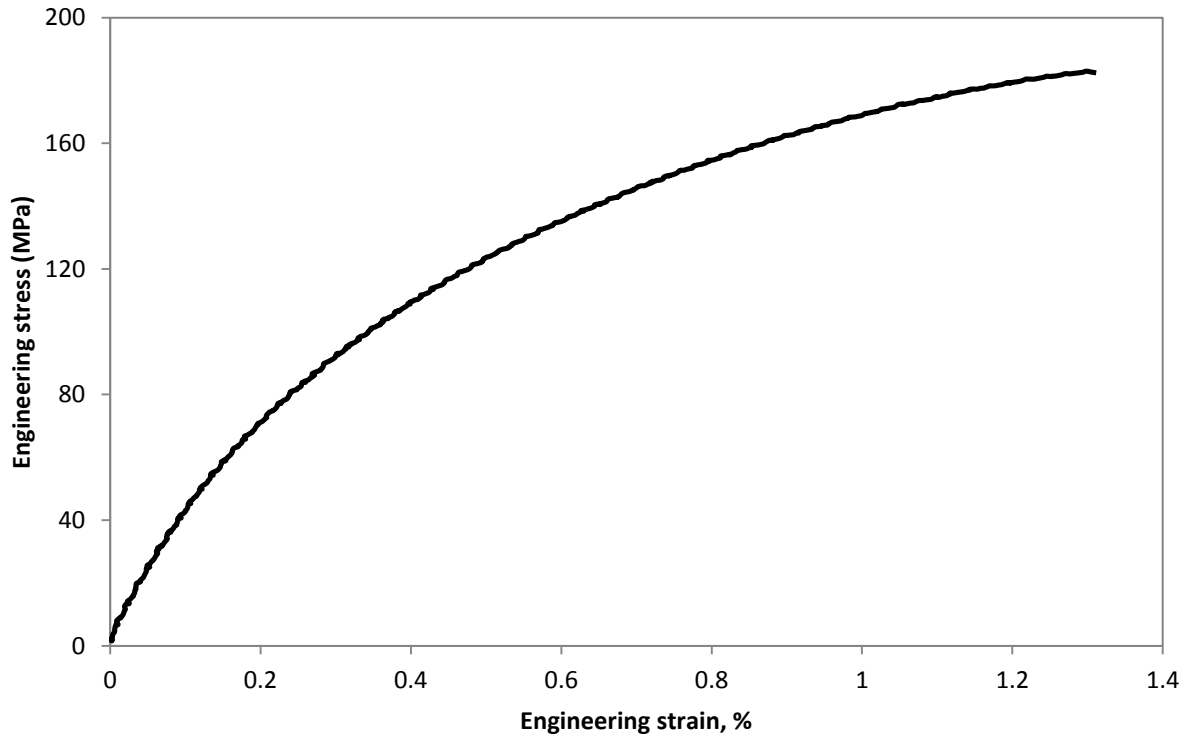




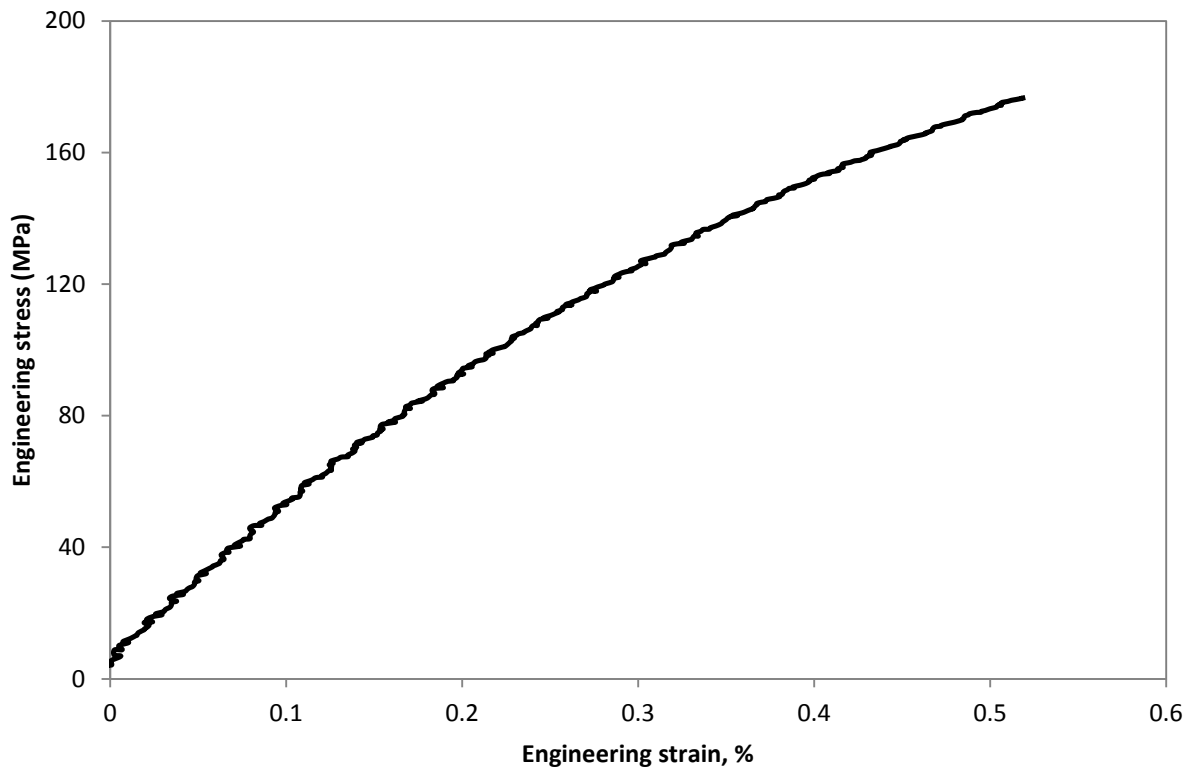
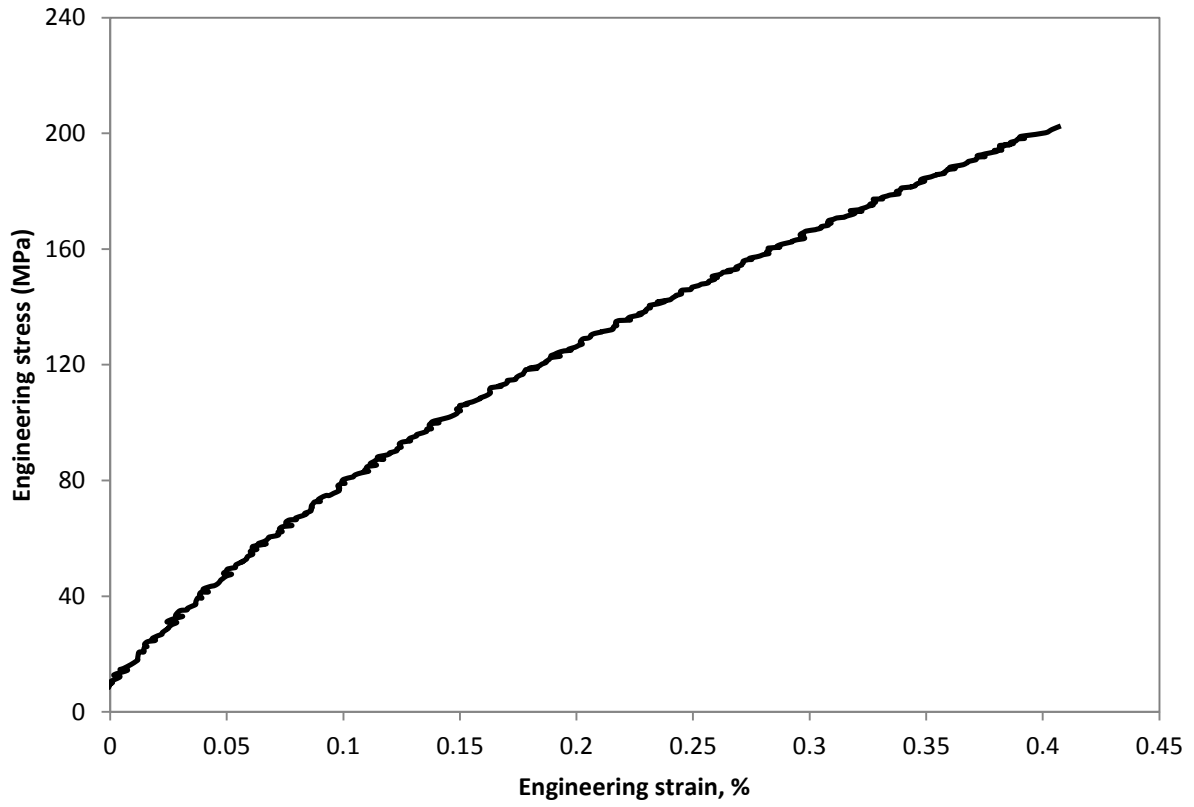


**Figure Ap.3** Engineering stress vs. strain curves for the 11% fiber reinforced composite.





**Figure Ap.4** Engineering stress vs. strain curves for the 22% fiber reinforced composite.



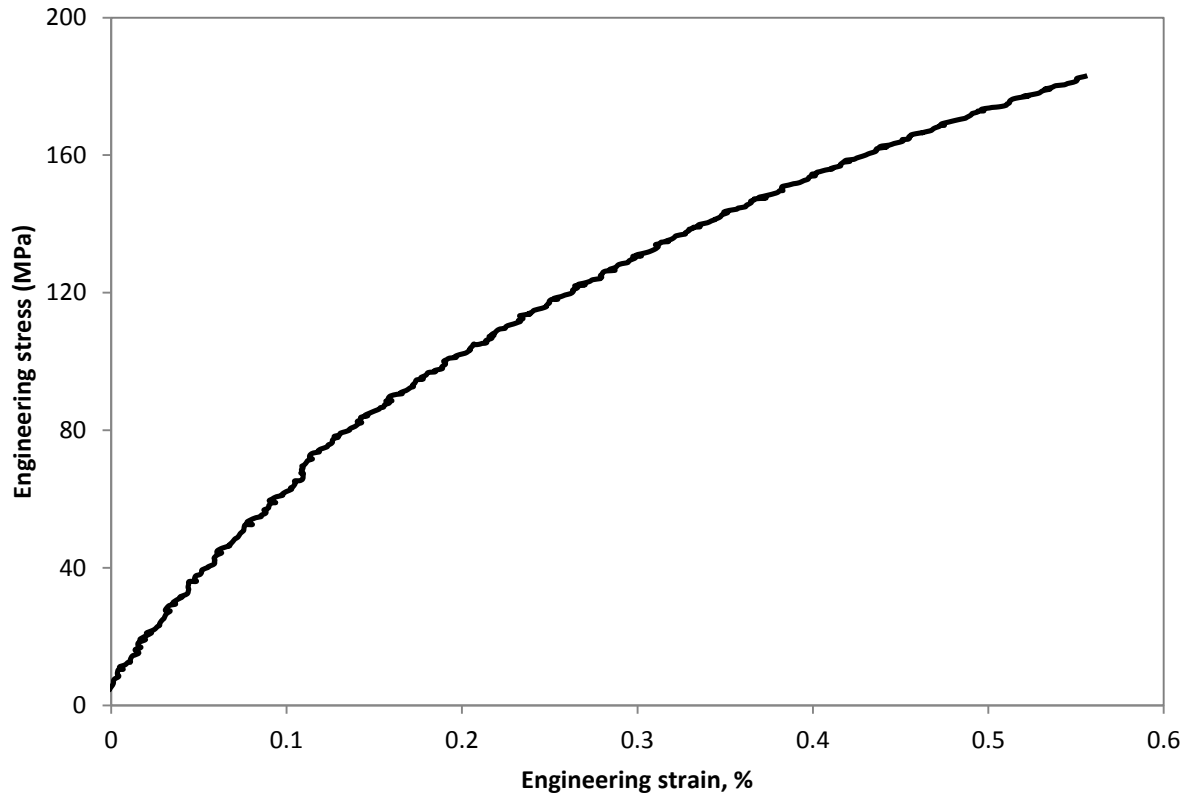
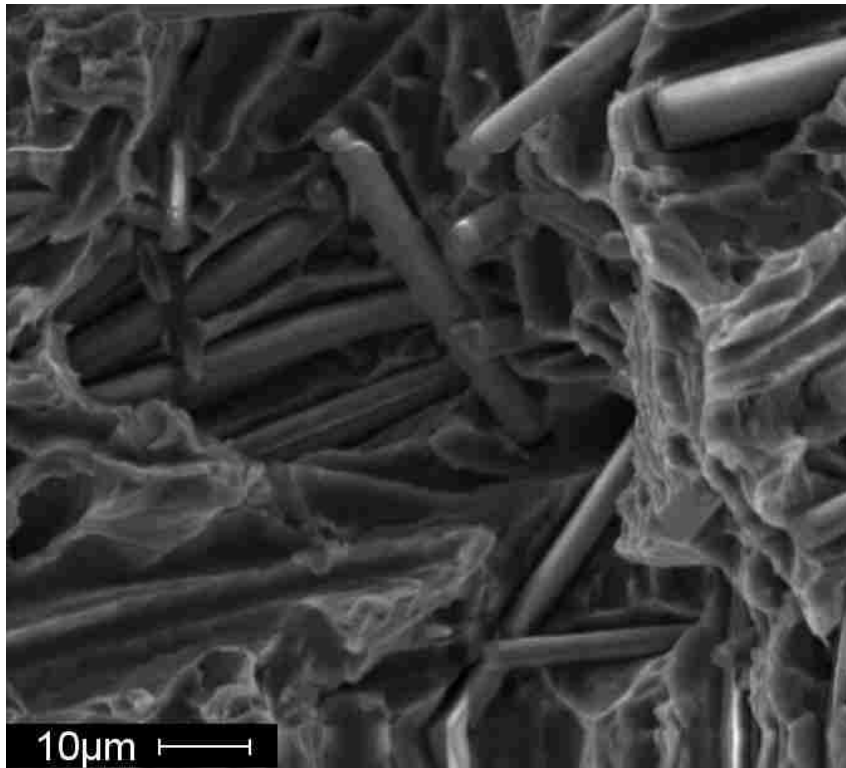
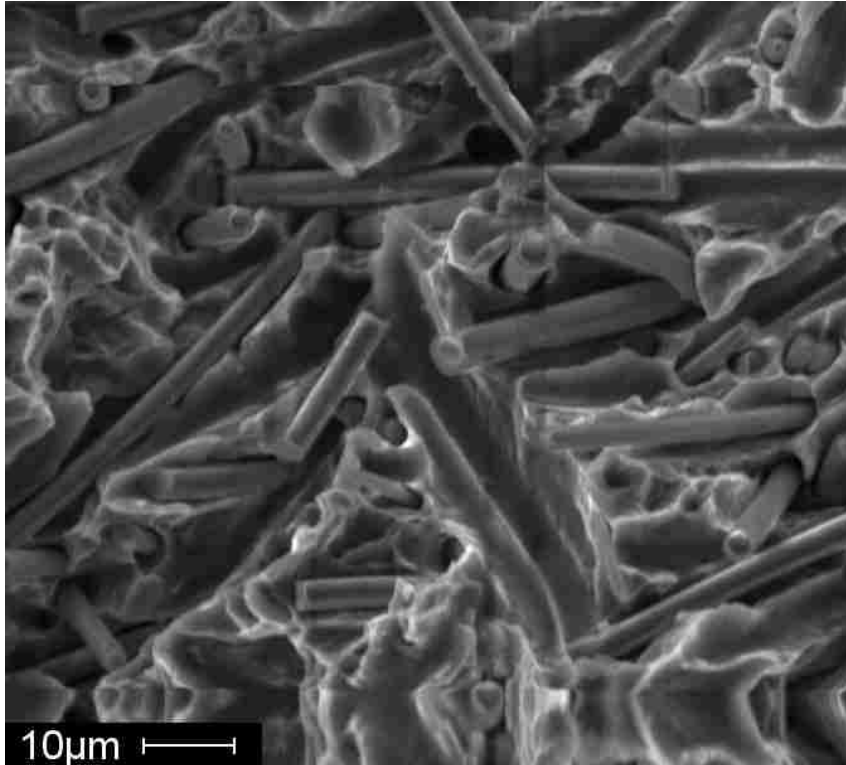


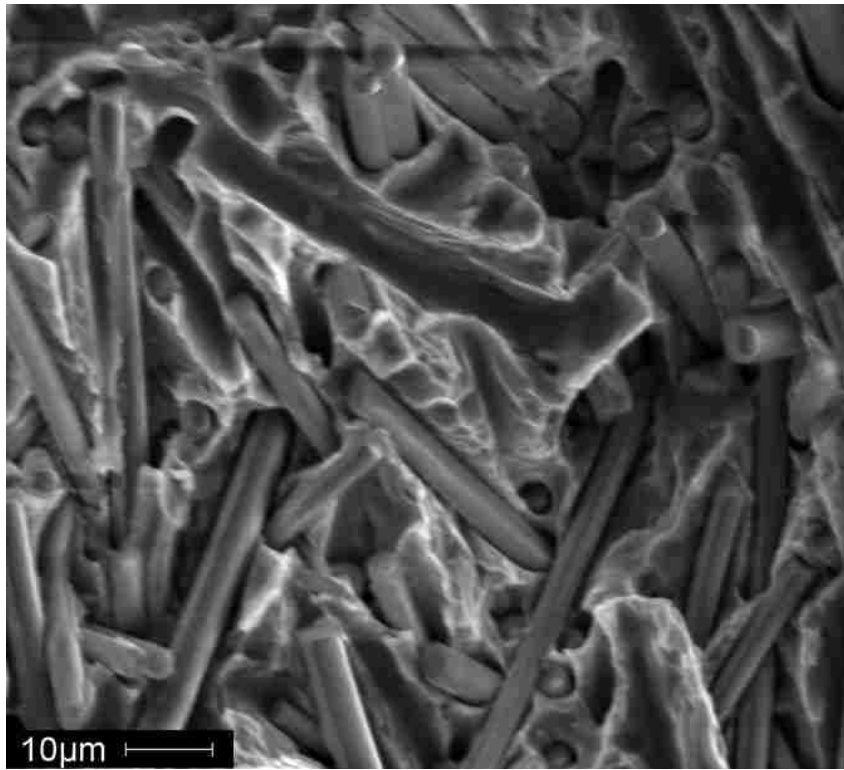
**Figure Ap.5** Engineering stress vs. strain curves for the 35% fiber reinforced composite.



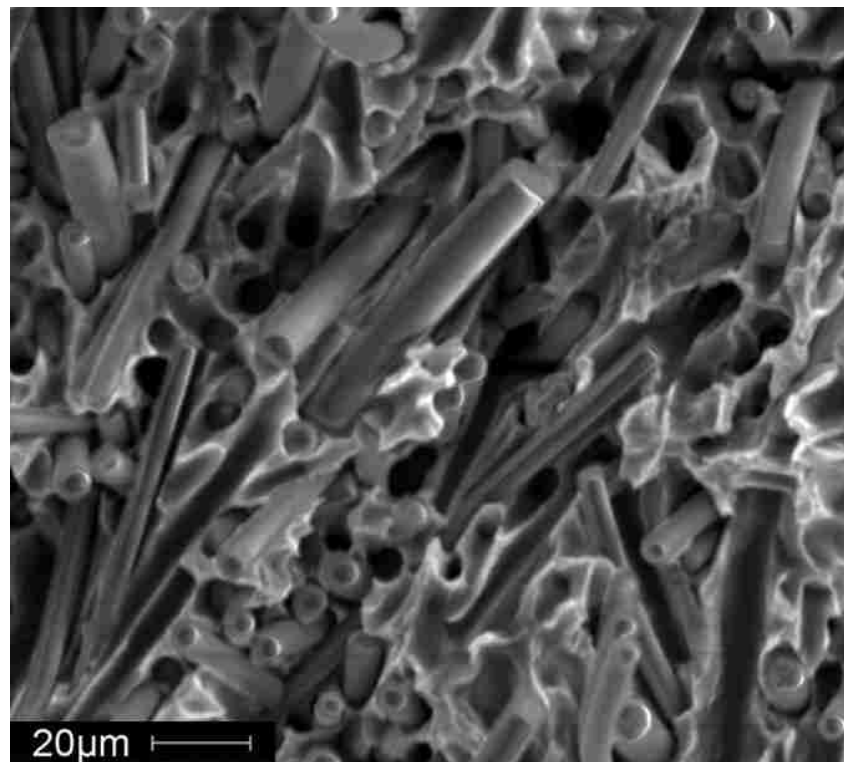
7%



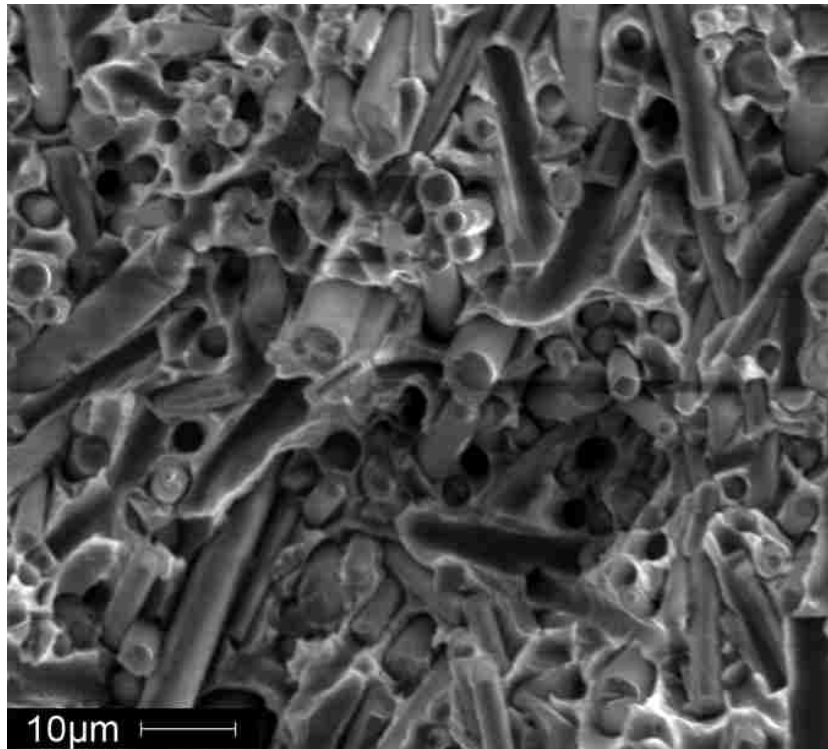
9%



11%

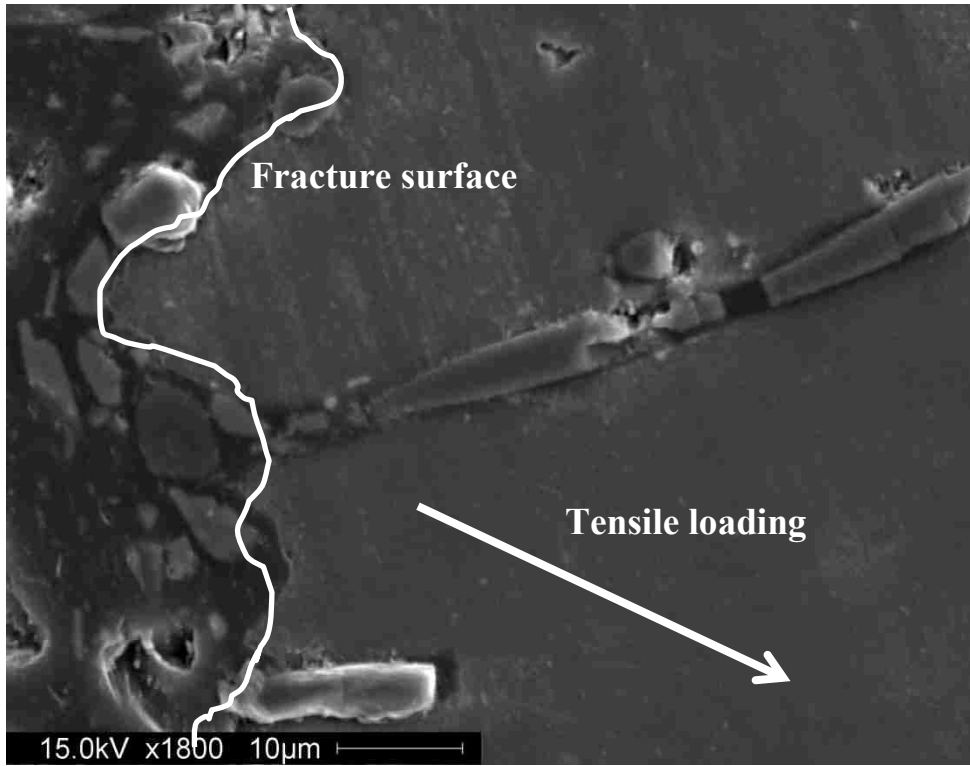


22%

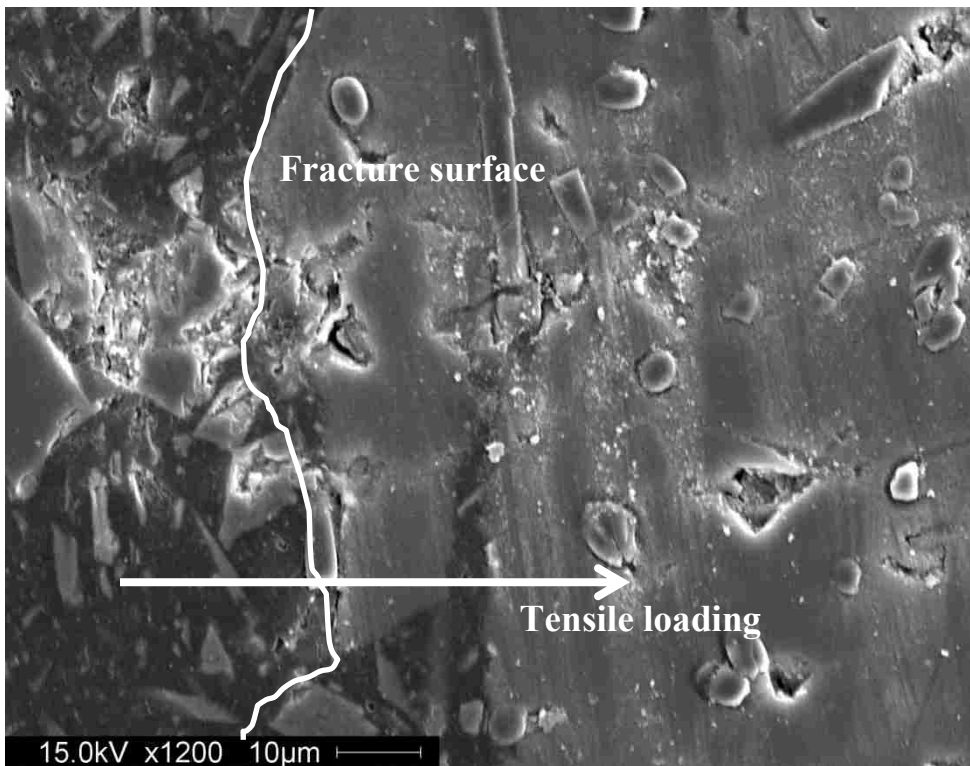


35%

**Figure Ap.6** SEM fractographs showing the fractured surfaces of composites with fiber volume fractions of 7%, 9%, 11%, 22% and 35% at the magnification of 1000X.

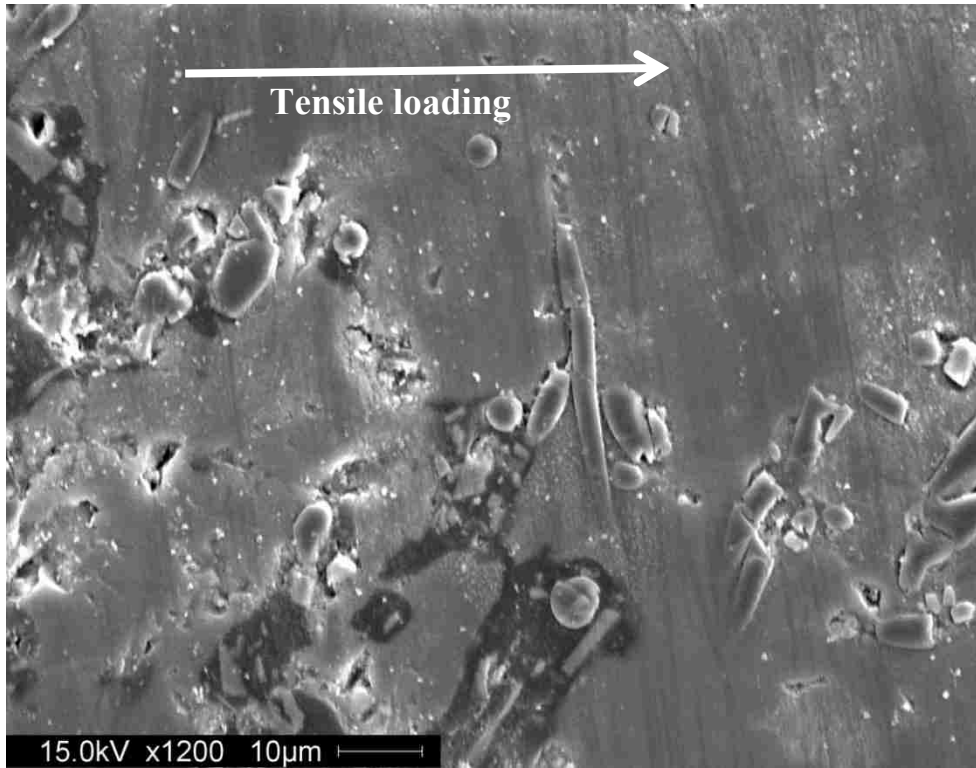


22%

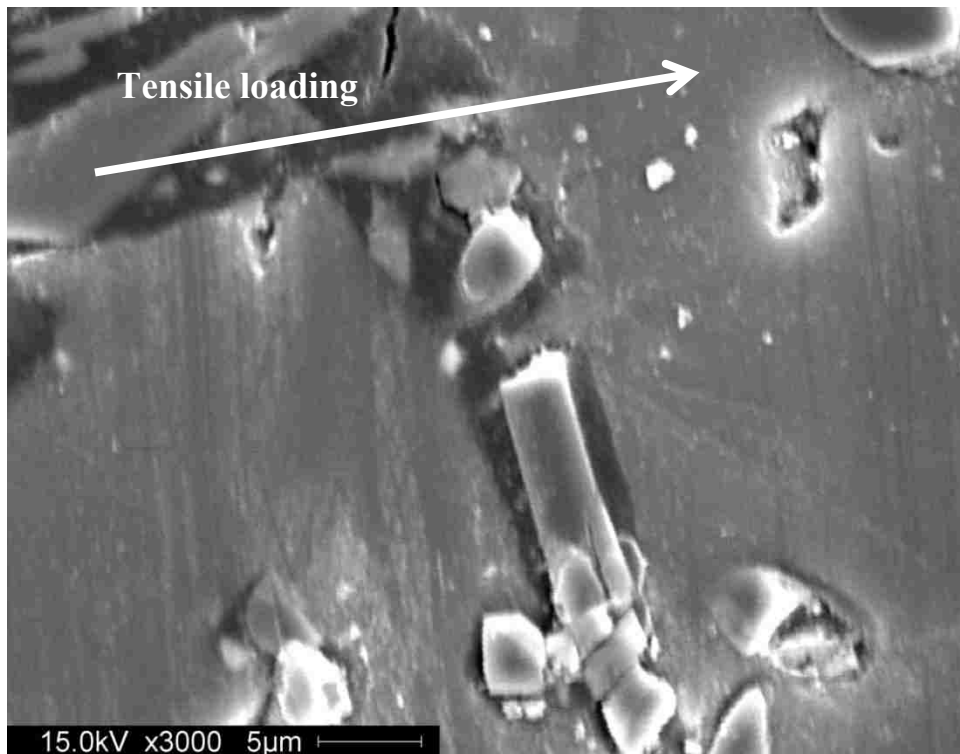


22%

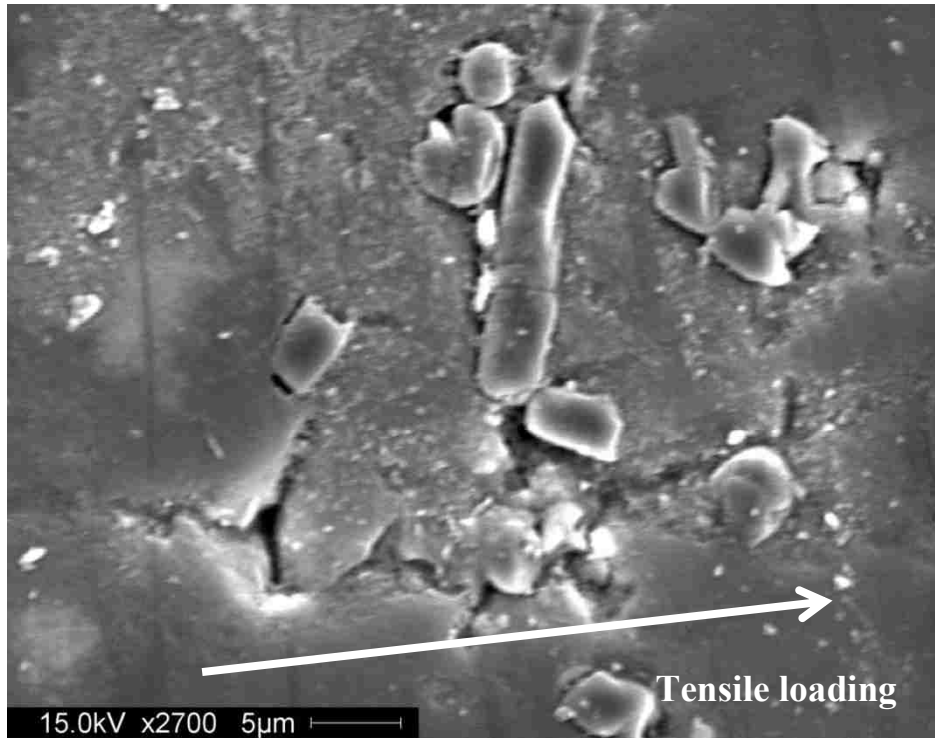




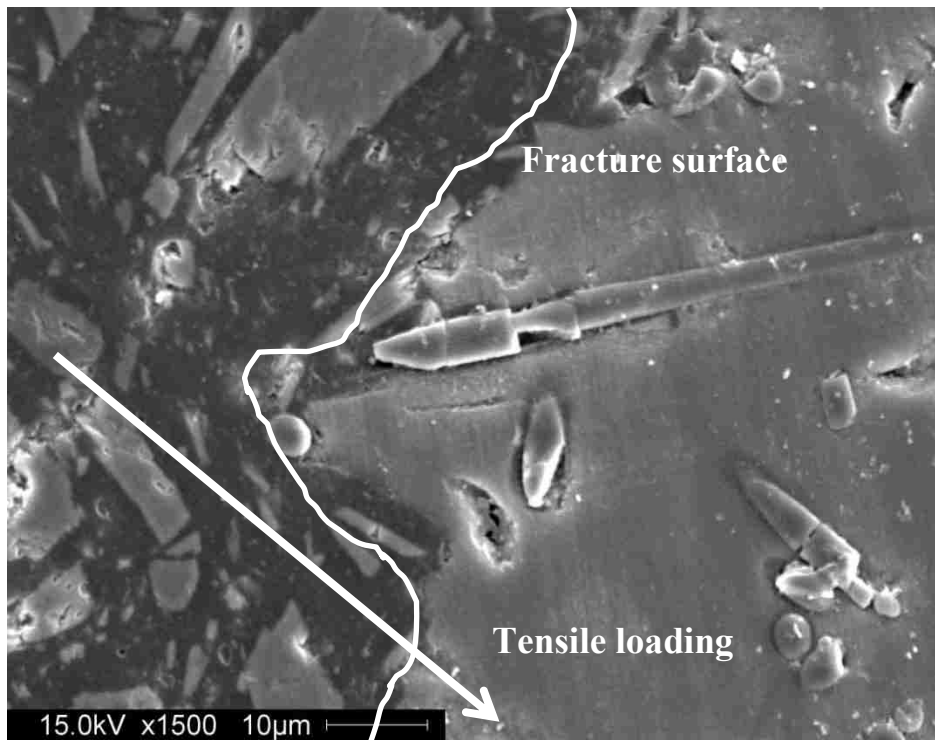
22%



35%



35%



35%

**Figure Ap.7** Fractured surfaces showing the fracture origin of 22% and 35% composites.

## Latent heat sample calculation

11% fiber reinforced composite:

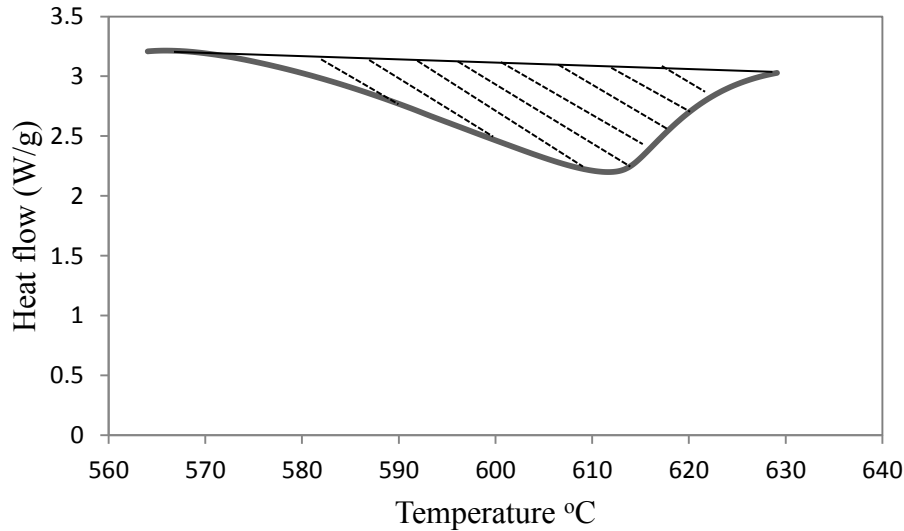


**Figure Ap.8** Enlarged heat flow cure for 11% composite.

Using EXCEL, the peak area of the curve was calculated to be 19.49 W °C/g .

The heating rate was set to be 20 °C/min, and the weight of the sample was 18.7mg.

$$\text{Latent heat} = \frac{19.49 \frac{\text{J}^\circ\text{C}}{\text{s g}}}{20 \frac{^\circ\text{C}}{\text{min}} \times \frac{\text{min}}{60\text{s}}} \times 0.0187\text{g} = 1.09\text{ J}$$

Theoretical calculation of the latent heat:

$$W_T = W_F + W_A$$

Where,  $W_T$  is the total sample weight,  $W_F$  is the weight of fiber and  $W_A$  is the weight of the alloy AM60.

The densities of the fiber and alloy AM60 are 3.3 g/cm<sup>3</sup> and 1.74 g/cm<sup>3</sup>, respectively.

Thus, the volume of fiber,  $V_F = W_F/3.3$ , and the volume of alloy AM60,  $V_A = W_A/1.74 = (W_T - W_F)/1.74$

$$\therefore \text{Vol}\% = \frac{\frac{W_F}{3.3}}{\frac{W_F}{3.3} + \frac{W_T - W_F}{1.74}} = \frac{1.74 W_F}{1.74 W_F + 3.3 (W_T - W_F)}$$

$$\therefore 1.74 W_F = Vol\% [1.74 W_F + 3.3 (W_T - W_F)]$$

$$1.74 (1 - Vol\%)W_F = 3.3 \cdot Vol\% \cdot W_T - 3.3 \cdot Vol\% \cdot W_F$$

$$1.74 W_F - 1.74 \cdot Vol\% \cdot W_F = 3.3 \cdot Vol\% \cdot W_T - 3.3 \cdot Vol\% \cdot W_F$$

$$(3.3 - 1.74) \cdot Vol\% \cdot W_F + 1.74 W_F = 3.3 \cdot Vol\% \cdot W_T$$

$$\therefore W_F = \frac{3.3 \cdot Vol\% \cdot W_T}{1.56 \cdot Vol\% + 1.74}$$

Thus, for an 11% composite with the sample weight of 18.7 mg, the weight of fiber in the sample is 3.55 mg, and the weight of the alloy AM60 is 15.14 mg.

The latent heat for alloy AM60 is 373000 J/kg,

$$\therefore \text{Latent heat for melting AM60} = 15.14 \text{ mg} \times \frac{373000 \text{ J}}{\text{kg}} \times 10^{-6} = 5.65 \text{ J}$$

## Preform Making Procedure

### Equipment:

Beaker (200ml)

Test tube (10ml)

Flat board

Sieve

### Chemicals:

Dispersant

Coagulant

Additive (Sodium Silicate Solution)

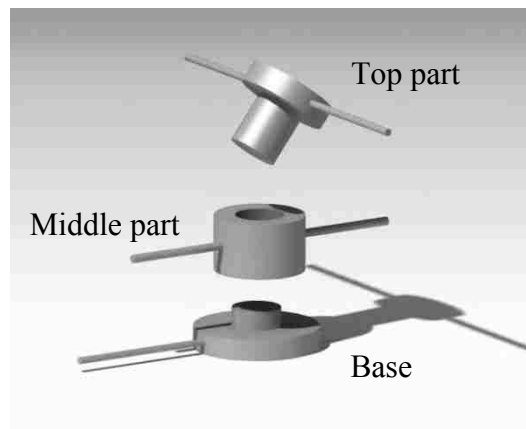
Fiber (Saffil<sup>TM</sup> Allumina Fiber)

### Experimental Procedures:

1. Wash all the equipments and dry them using paper towel
2. Preparing 2 grams dispersant
3. Grinding 100-120 grams fiber using the sieve
4. Using the 6 litre pail to prepare 40 °C water (fill to the fifth check line from the top of the pail)
5. Put the 2 grams dispersant into the pail with 40 °C water and stir for 5 minutes
6. Put the 100 grams fiber into the pail and stir for 5 minutes
7. Leave the mixture for at least one day
8. Pouring hot water (as hot as possible) into the beaker as long as the beaker is fulfilled
9. Put 9 grams coagulant into the hot water in the beaker and stir until the coagulant is dissolved
10. Preparing 8ml additive using the test tube
11. Pouring the 9 grams coagulant-water mixture into the pail and stir for 5 minutes
12. Put the 8ml additive into the pail and stir for another 5 minutes
13. Add the particles (based on desired volume fractions) into the pail synchronously with the additive and stir for 5 minutes (if perform with fiber and particle is desired)

14. Put the clean filter bag into another clean pail, and pouring the prepared mixture into the pail.
15. Fasten the bag and squeeze out the water as much as possible
16. Put the filter bag into the dryer and put a container under the water outlet of the dryer
17. Dry it until all the water is out of the filter bag
18. Get the sediment (fiber) out of the filter bag. If it is too dry, mix with same liquid (liquid that squeezed out from the filter bag)

19. As shown in the figure on right, place the base on a bath towel, make sure the surface is flat



20. Put the middle part on top of the base

21. Place the fiber into the hole (middle part)

22. Insert the top part into the hole of the middle part and squeeze using a jack (proper force)

23. Stop squeezing until the desired height (desired volume) is obtained

24. Bring the base, middle and top parts to the ground carefully

25. Push the two bars of the top part and pull the bars of the middle part using two hands simultaneously.

26. Pull the middle and top part up and flip it over carefully

27. Using a knife (box cutter) to move through the bottom of the product

28. Move the product onto a clean surface (desk)

29. Dry it for 3 days

### Heat Treatment

30. Power on the furnace

31. Press and hold the *select* button, until the screen is flashing with words

32. Change the option to LCL (bottom right corner)

33. Press *select* button to confirm

34. Adjust to the desired temperature by press the up & down button
35. If the furnace door needs to be opened during heat treatment, press and hold the *select* button, and change the option to RES (then Power Off if the heat treatments is finished)
36. Time period for heat treatment:

<i>Steps</i>	<i>Temperature</i>	<i>Time</i>
1	200 °C	3 hours
2	400 °C	15 minutes
3	750 °C	30 minutes
4	1000 °C	15 minutes
5	1100 °C	15 minutes
6	1200 °C	1.5 ~ 2 hours

\* *Start to count the time after the temperature reach to the specified value.*

**Preheating before squeeze casting**

<i>Steps</i>	<i>Temperature</i>	<i>Time</i>
1	200 °C	30 minutes
2	400 °C	15 ~30 minutes
3	750 °C	90 minutes

\* *Heat to 200°C one day before casting.*

# Metallographic Sample preparation

## Mounting

1. Open the 3 water valves
2. Turn on the Mounting Press machine
  - Holding time: 2 min. 30 sec.
  - Temperature: 150 °C
  - Pressure: 3000psi
3. Loose the top cap
4. Press and hold the button “ RAISE”
5. Place the sample (polishing side face down)
6. Press and hold “LOWER”
7. Put 3 spoon power (for sample <2cm)
8. Tight the top cap
9. Choose the “MOLD SIZE” to be 30mm (for sample <3cm)
10. When completed, open the top cap and press/hold “RAISE”
11. Turn off the machine
12. Close the water valve

## Polishing

1. Sand the edge of the mounted sample
2. 4 different size sand paper, polish the sample
3. Grinder (low speed), 2500C and 4000C sand paper
4. Using the GRINDER-POLISHER
  - Clean the surface
  - 1.0 micro-polish liquid for the left grinder
  - 0.05 micro-polish liquid for the right grinder
  - Add some liquid soap on the surface

## Etching

- Preparing 2% nitric acid
- Immerge the sample into the prepared acid for 30 seconds
- Clean with running water and ethanol
- Dry the sample using a hairdryer

Note: etch sample in a hood and wear gloves and goggles all the time.



## SDT Q600 Operation Procedures

1. Open the valve of Argon and Nitrogen, adjust the tuning valve to 20psi
2. Turn on the switch on the back of the SDT instrument
3. The computer should have a fixed IP address (not DHCP) of 172.23.188.11 and subnet 255.255.224.0 The DNS should be blank for both fields
4. Double click on the icon, *TA Instrument Explorer*, on the desktop of the computer and maximize the window
5. Make sure that the Sample Purge Flow is 100ml/min
6. On the SDT instrument, click on Control Menu → Furnace (open the furnace)
7. In the furnace, there are two crucibles (Al 960070. 901), the inner one is used as a reference (Do not touch)
8. Preparing the sample (20 ~ 40mg)
9. Cleaning and drying the sample
10. Preheat the crucible (remove the gas and impurity) by a hand held torch, then cool it down before putting into the furnace
11. Make sure that the two crucibles are not in touch
12. Click on Control Menu → Furnace (close the furnace) → Tare (zero the reference weight)  $\approx \pm 0.0076$
13. It is better for sample to have one flat surface
14. Click on Control Menu → Furnace (open the furnace)
15. Place the sample into the crucible (center)
16. Click on Control Menu → Furnace (close the furnace)
17. Click on *Experiment View* icon → Summary → Mode: SDT standard → Test: Custom → Sample (name) → Data file name (saving path)
18. Choose the date saving path, C: disk → TA → Data → SDT → *Name...*
19. Switch to Procedure → Test: Custom → Name → Ramp
20. Double click on *Editor* button
21. In the Segment Description section, double click on *Ramp: 20 – 800 °C*, to change the desired value (*heating rate 15 ~ 25 °C /min*)
22. Click on Note → change the Operator name → Mass Flow Control Settings (Sample: Argon, 100mL/min)
23. Make sure Air Cool is ON → OK
24. Click on the green start button (on top left corner of the window)
25. The test is finished until the sound of gas release can be heard

26. Cool the furnace down to 40 ~ 50 °C
27. Click Shut down button on the TA instrument, waiting for the message window appears (*The machine is safe to...*), then turn off the instrument.
28. Close the valve of the gas

## VITA AUCTORIS

NAME: Xuezhi Zhang

PLACE OF BIRTH: Shijiazhuang, Hebei Province, China

YEAR OF BIRTH: 1986

EDUCATION: Maple Leaf International School, Dalian, Liaoning Province, 2002

University of Windsor, B.A.Sc., Windsor, ON, 2006

University of Windsor, M.A.Sc., Windsor, ON, 2010